Title
Harmonic Oscillator Based Effective Theory, Connecting LQCD to Nuclear Structure

Author
McElvain, Kenneth Scott

Publication Date
2017

Peer reviewed|Thesis/dissertation

Harmonic Oscillator Based Effective Theory, Connecting LQCD to Nuclear Structure

by

Kenneth S. McElvain

A dissertation submitted in partial satisfaction of the

requirements for the degree of

Doctor of Philosophy

in

Physics

in the

Graduate Division

of the

University of California, Berkeley

Committee in charge:

Professor Wick Haxton, Chair
Professor Jeffrey Neaton
Professor Karl A. van Bibber

Fall 2017

Harmonic Oscillator Based Effective Theory,
Connecting LQCD to Nuclear Structure

Abstract

Harmonic Oscillator Based Effective Theory,
Connecting LQCD to Nuclear Structure

by

Kenneth S. McElvain

Doctor of Philosophy in Physics

University of California, Berkeley

Professor Wick Haxton, Chair

This work focuses on construction of a bridge from QCD (quantum chromodynamics), the theory of quarks, gluons, and their interactions, to nuclear structure, an obvious but unattained objective ever since the introduction of QCD in 1973. The bridge footing on one side of the chasm is QCD in the non-perturbative regime, only now beginning to yield to massively parallel computation in a Monte-Carlo space-time lattice formulation of QCD called LQCD (lattice quantum chromodynamics) that is our only tool for such problems. The resulting trickle of information about the nucleon interaction comes in the form of a fuzzy spectrum for two nucleons in a periodic box. It can be expected that the spectrum will sharpen and even eventually include a spectrum for three nucleons in a box with the introduction of larger and faster supercomputers as well as more clever algorithms. Fundamentally though, limits on what can be accomplished in LQCD are set by the famous fermion sign problem. Results in LQCD are produced as a small residual of the sum of large positive and negative contributions from the Monte-Carlo trials and accuracy only improves slowly with the number of expensive trials.

The bridge footing on the other side of the chasm is the configuration interaction shell model, which is commonly used for nuclear structure calculations from a microscopic Hamiltonian expressed in the colorless degrees of freedom of QCD we call nucleons. As currently executed, this method is a model, the two- and possibly three-body interaction in use lacking a rigorous connection to QCD or direct accounting for contributions from scattering outside the model space. Nucleons, like quarks, are fermions and a fermion sign like problem exists in these calculations as well. The configuration interaction shell model is formulated in an antisymmetrized harmonic oscillator basis that grows with the number of permutations of identical nucleons in the model space. However, fantastically efficient parallel sparse matrix techniques for finding low lying eigenstates exist, allowing quite large problems to be solved.

One footing of the bridge is solid and the other is nearing completion. Construction of the bridge itself then faces three major problems addressed in this dissertation, construction of the effective nuclear interaction from observables, finite volume effects associated with the

periodic volume in which LQCD results are calculated, and the construction of the A-body effective Hamiltonian from the two body effective interaction.

An effective theory is a organized and complete parameterized approximation limited to and preserving the known symmetries of an underlying theory (QCD in this case), constrained to some regime (energies below the mass of the pion in this case), and expressed in degrees of freedom suitable for solving the problem at hand (nucleons in a harmonic oscillator basis below an energy cutoff for the nuclear structure problem). An effective theory has a formal relationship to the underlying theory that a model does not. Unlike a model, a small number of observables may be used to fix the lowest order expansion parameters of the effective theory approximation with the expectation that the approximation remains valid in other situations for which observables are not available.

The first portion of this work focuses on the construction of a harmonic oscillator based effective theory (HOBET) from observables in a spherical harmonic oscillator basis. It builds on the prior work of Haxton, Song, and Luu in demonstrating the construction of an convergent effective theory from a known potential, establishing the form of the required effective theory expansion. The new work required the extension of HOBET to a theory no longer limited to bound states and with continuity in energy, enabling uniform treatment of bound and continuum states. Here the expansion parameters are instead derived from phase shift observables at continuum energies. A key insight developed during this work was the way in which the effective theory constructed at an energy is connected to the boundary constraints of the wave function. Using known techniques, Lüscher's method and the HAL QCD potential method, to transform the LQCD spectrum in periodic box to infinite volume phase shifts produces a successful mechanism for fitting the effective interaction without knowledge of the details of the potential.

The techniques for converting LQCD results to phase shifts have issues such as uncontrolled systematics related to the volume size and range of the interaction as well as suspect perturbative expansions. These issues motivated an investigation into the possibility of directly constructing the effective theory in a periodic volume. This new construction relies heavily on the previous insight about the connection of the effective theory to the wave function boundary constraints. A key result is that the kernel of the effective theory, which captures scattering through the excluded degrees of freedom, is in fact independent of the boundary conditions. It can be fit in the periodic volume context and then transplanted into an infinite volume spherical formulation of the effective theory by a straightforward basis transformation. Finite volume effects are automatically handled in the process. Of immediate interest to the LQCD community is that accurate phase shifts can be easily extracted from the effective theory, avoiding systematic and finite volume errors in existing methods.

With a two body effective interaction in hand the last step to a usable bridge is the construction of an A-body interaction in terms of the two body one. The exact form this construction is not settled yet, but one promising structure with leading contributions that can be calculated is explored.

The assembly of these three pieces completes the bridge, producing a way to perform nuclear structure calculations that is formally connected to the underlying theory of QCD.

To my wife Alisa Yaffa and our children Brian and Jodi.

Contents

List of Figures

List of Tables

Acknowledgments

I would like to thank my advisor Wick Haxton for guiding me to the intersection of lattice QCD, effective theory, and nuclear structure calculations. Thanks to him I have learned enough bits and pieces about the topics to make a serious contribution to tying them together. I also very much appreciated the help when I needed it and the freedom and time to figure things out in my own way. I was very lucky to have him as my advisor.

Thanks are also due to Calvin Johnson for including me in the BIGSTICK project, a configuration interaction code for nuclear structure, and trusting me to make significant contributions to the code. The parallel programming methods and techniques for solving large eigenvalue problems that I learned while working with Calvin all found a use in the software developed to support this dissertation.

I would also like to acknowledge members of the CalLat team with whom I had many discussions and derived an understanding and appreciation of lattice QCD from: André Walker-Loud, Thorsten Kurth, Amy Nicholson, Evan Berkowitz, Jason Chang and Pavlos Vranas. I look forward to spending more time with you all.

Finally I would like to thank the other members of my dissertation committee, Karl van Bibber and Jefferey Neaton, who both found time to review and comment while traveling in Asia.

Calculations supporting this work were performed on Vulcan through the Lawrence Livermore National Laboratory Institutional Computing Grand Challenge program and on Edison at NERSC, the National Energy Research Scientific Computing center (a DOE Office of Science User Facility supported by the Office of Science of the U.S. Department of Energy under Contract No. DE-AC02-05CH11231.)

Chapter 1

Introduction

The focus of this dissertation is to build an effective theory connection between nucleon scattering observables and nuclear structure for light nuclei. Once source of nucleon scattering observables is experimental data, another exciting one is the emerging ability of LQCD (Lattice Quantum Chromo Dynamics) computations to perform nucleon scattering simulations on the computer [1]. As LQCD nucleon scattering calculations become more mature and are done with pion masses near the physical values it should be possible to compute the spectra of light nuclei, say up to ^{16}O, in an A-body effective theory that is directly connected to QCD using the techniques found here.

Ever since the development in 1973 of QCD, the theory of quarks and gluons that produces nucleons and their interactions, there has been a desire to directly derive nuclear structure from QCD [2]. QED (Quantum Electro Dynamics) is QCD's simpler cousin and is characterized by a $U(1)$ gauge group and importantly a coupling parameter $\alpha \approx 1/137$ at low energy scales and higher values at higher energy scales. A perturbative expansion, expressed in Feynman diagrams of QED interactions and organized by the number of times photons interact with charged particles, converges rapidly as α^n suppresses diagrams with n photons coupling to charged particles at emission and absorption. QCD on the other hand has a more complex $SU(3)$ color gauge structure and a coupling parameter α_s that runs to larger values at the lower energy scales associated with nucleons and nuclear structure. The more complex non-abelian gauge structure results in gluon-gluon interactions that are missing with the photon. One effect of the large coupling parameter and gluon-gluon interactions is that at modest energies all particles are colorless combinations of valence quarks. The effective theory of QCD at these scales includes the colorless nucleons and mesons with the nucleon interaction as a residual effect of QCD. The large value of α_s sabotages the use of a perturbative expansion as contributions from higher order diagrams do not reduce quickly enough for convergence, long delaying the direct use of QCD in producing an interaction.

Advances in LQCD with clever algorithms and compounding improvements in the performance of supercomputers have now reached the point that the two-body QCD nuclear

[1] An attempt has been made to be consistent with respect to conventions and the usage of symbols. The choices made are documented in Appendix E.

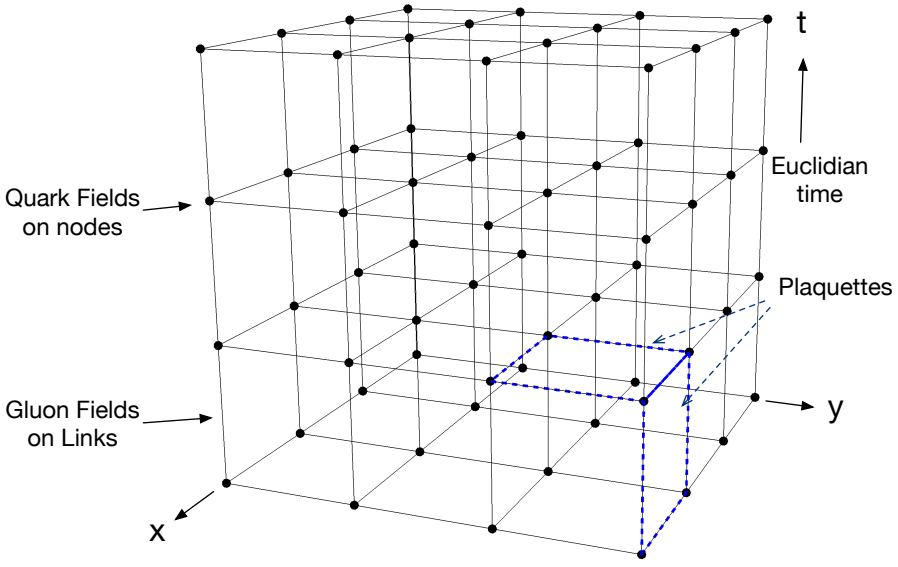

Figure 1.1: The representation of lattice fields in LQCD: quarks fields are placed on the nodes of lattice and gluon fields on the links. Space and time are periodic and time is Euclidian. The z direction has been suppressed due to the limitations of paper.

problem is nonperturbatively solvable. A good introduction to the topic by Creutz is found in [3]. The procedure is to make space and Euclidian time discrete with quark fields described on the points of a space-time lattice and gluon fields on the links between the lattice points where the gluon fields describe the color space transform between adjacent lattice points as is shown in Figure (1.1). The QCD action, normally expressed as an integral over space and time, becomes a sum over the lattice points for quark contributions and over plaquettes, small loops along the links in the lattice, for the gluon contribution.

Euclidian time is essential for the Monte-Carlo sampling used to evaluate the path integral. With Euclidian time comes the problem of separating the contributions from the ground and excited states. In quantum mechanics if the state of a system is a equal superposition of eigenstates $|a\rangle$ and $|b\rangle$ with energies E_a and E_b, then under time evolution the two eigenstates pick up an oscillating phase with the fastest oscillation associated with the largest energy.

$$|\psi\rangle = \frac{1}{\sqrt{2}}\,|a\rangle\, e^{-iE_a t} + \frac{1}{\sqrt{2}}\,|b\rangle\, e^{-iE_b t} \tag{1.0.1}$$

Both states persist with constant amplitude. Now suppose that the substitution $t \to -i\tau$, also known as a Wick rotation to Euclidian time, is made.

$$|\psi\rangle = \frac{1}{\sqrt{2}}\,|a\rangle\, e^{-E_a \tau} + \frac{1}{\sqrt{2}}\,|b\rangle\, e^{-E_b \tau} \tag{1.0.2}$$

Now as time passes, the amplitudes of both states decline, but the highest energy state declines faster, eventually leaving the lowest energy state to dominate the wave function. In LQCD the same principle applies, enabling one to tease out the lowest energy contributions to a measurement such as a propagator for a pair of nucleons.

The lattice is made finite and periodic so that the size of the computation is suitable for a super-computer. Samples of the vacuum state, called configurations, are generated following a probability density implied by the QCD Lagrangian and statistical measurements of the effective mass of a two nucleon propagator can be made by measuring the decay rate with Euclidian time on those samples via Monte-Carlo integration. Unfortunately, the propagator for two nucleons written in terms of quark fields also contains the physics describing 6 pions. The two nucleon state being measured decays rapidly as $\exp(-2m_N\tau)$ while the six pion state decays as $\exp(-6m_\pi\tau)$ yielding an exponentially increasing introduction of noise with time from pion states that is only eliminated by a delicate cancelation in the sum over configurations. The statistical quality of results only improves slowly with the square root of the number of expensive to compute configurations, yielding an overall signal to noise ratio $\sim \sqrt{N}\exp\left(-(2m_N - 3m_\pi)\tau\right)$. This is an example of the famous fermion sign problem, producing a small result from cancelations in a large sum of large positive and negative contributions. The problem worsens rapidly with the introduction of additional nucleons, making it unlikely that calculations with more than a few nucleons can be done. Despite these obstacles, credible LQCD calculations can now be performed on super-computers – though often, to improve the convergence, unphysically large pion masses must be introduced through fictitious quark masses.

As is usual in such problems part of the progress is simply faster/bigger computers, but even more important are physics motivated strategies to make the measurements with less statistical noise and to get more data per sample, yielding orders of magnitude improvements. For example, if the nucleon operators used in propagators have less contamination with excited states, then the state corresponding to nucleon propagation will emerge sooner before noise from pion contributions becomes large, yielding a dramatic reduction in the number of measurements required [4]. Even with such an improvement there is a strong motivation to connect LQCD calculations to effective theory for nuclear structure calculations.

Long before the development of QCD, nuclear physics was described in terms of interacting protons and neutrons, bound by potentials that were initially derived phenomenologically, later determined from careful analyses of NN phase shifts, and in recent years further constrained by chiral EFTs that take into account the special role of the pion in mediating long-distance interactions. In retrospect, the existence of a rather precise treatment of QCD at low energy in terms of composite fermions – bound states of the quarks – and potentials that make no reference to gluons, is remarkable.

This starting point for nuclear physics was initially executed in simple models – e.g., collective models of Bohr and Mottelson and of Goldhaber and Teller, noninteracting shell models that built on the notion of nuclear mean fields, later embellished by Goeppert-Mayer with spin-orbit corrections that altered shell closures [5]. Often the connection to the underlying NN potential was vague. Over the years such models became more elaborate and

more closely coupled to the underlying NN interaction. Perhaps the best modern example is the configuration-interaction shell model, employing very large bases of Slater determinants that are allowed to interact through a potential that is rooted in measured NN interactions. Typically that potential is softened – beginning with the G-matrix that sums an infinite set of ladder diagrams, taking into account the very strong repulsion that operates between nucleons at short range. It is also often modified in ad hoc ways, such as adjusting S-wave interaction strengths to better match data. Calculations also show that three-body forces are needed, if the goal is to predict binding energies to better than 10%. An intuitive understanding of potentials has also been gained: how they are connect to pion and vector-meson exchange via modern chiral EFT approaches.

With the exception of light nuclei where effectively exact calculations can be done in very large nucleon Hilbert spaces, the model spaces used are effective – limited to momenta that prevent one from constructing in detail the consequences of strong repulsion on the NN correlation function at long distances. Although it is often forgotten by practitioners, such treatments do not then produce true wave functions, but rather some low-momentum projection of that wave function. Because large parts of the Hilbert space have been omitted, it will fail in this task (and in the associated task of finding eigenvalues) unless the interaction used is modified from the bare one, to take into account the parts of the Hilbert space that have been excluded. The process of adjusting the interaction as the size of the Hilbert space is reduced is called renormalization. This renormalization in principle can be done from the starting point of the true (or "bare") interaction – though an exact solution of the renormalization problem is equivalent to solving the original problem in the full Hilbert space. Alternatively, the effective interaction can be done empirically, by introducing corrections to the bare interaction that are fit to observables. While the term is frequently misused, the latter approach is an effective theory if the parameters introduced and new interactions added are part of a systematic scheme, based on some power counting that organizes the needed corrections in some kind of hierarchy. The development of an ET for the Slater determinant basis most commonly used in nuclear physics, the harmonic oscillator, is a guiding motivation of this dissertation.

In particular, one can envision reformulating the shell model as such an effective theory: the model can be employed in a way that preserves important symmetries, like translational and rotational invariance. Historically, the transition from the naive shell model to an effective theory occurred in steps, and is arguably still incomplete. Initially there were important conceptual hurdles: how can a low-momentum basis, which seems like a mean field, be compatible with a potential with a GeV hard core? But the concept of the healing distance, described in reference [6], seemed to reconcile these two pictures. A nucleus may be roughly modeled as a Fermi gas with all states up to the Fermi surface occupied. The healing distance can be understood as a consequence of nucleons scattering in that Fermi gas instead of freely. Free nucleons scatter with a phase shift, meaning that the free wave function is perturbed out to infinite distance. The perturbed state is a mix of other states of the same energy. In a Fermi gas other states of the same energy are are already occupied and the scattering result must quickly settle back into the same set of states, "healing" the

wave function and limiting the size of the wound in the wave function. Qualitatively then, one can appreciate that a renormalized interaction can reproduce long-range behaviors and wave function features, even though the short range part of the interaction continues to exist only in its indirect contributions to interactions of low energy states. In the harmonic oscillator based effective theory described here the produced wave functions are precisely the projections of the true wave function to the soft restricted Slater determinant basis of the effective theory.

More microscopic calculations begin with a bare interaction that one hopes to renormalize into a soft effective interaction in a modest sized discrete basis for the shell model. Unfortunately, the bare interaction combines a very short range hard core at GeV scales, a medium range attractive component attributable to pion exchange between nucleons and long range scattering by the kinetic energy operator. The disparate length scales embedded in the bare interaction are a strong hint of renormalization problems. Despite this, great efforts were made to diagrammatically construct the effective interaction as a perturbative sum, exploring many different ways to organize the sum of terms with the hope that cancellations within each group would lead to a convergent sum. In the early 1970's the diagrammatic effective interaction methods were analyzed more deeply and found to fail to converge independent of organization of the sum. In 1970 Barrett and Kirson [7] calculated the effective interaction for two valance nucleons above a ^{16}O core up to selected N4LO terms, discovering that there was no grouping of terms that yielded convergence. The concluding line of their abstract "... and that the success of first- plus second-order perturbation theory in fitting experimental spectra for these nuclei is unexplained" reveals the state of the art at that time. In 1972 and 1973 Shucan and Weidenmüller wrote two papers [8][9] showing that the convergence failure is related to the overlap of the spectrum of the bare interaction in the excluded space with the spectrum of the effective interaction. This overlap is a consequence of the lack of a separation of scales between the excluded and included degrees of freedom.

More recently progress has been made with a combination of novel techniques such as SRG (similarity renormalization group), introduced as a general technique by Glazek and Wilson in [10] and applied to the nuclear interaction by Bogner et al. in [11] to soften the interaction in a momentum basis with a cutoff. Softening of the interaction combined with the advance of computing power enabling the use of much larger effective Hilbert spaces has produced an improved match of calculation and experiment [12] . SRG finds a parameterized unitary transform that both preserves the kinetic energy contribution and reduces the strength of off diagonal elements of the potential, reducing the coupling of low and high momentum states. Eigenvalues in the Born series expansion of the T matrix are seen to reduce in magnitude indicating perturbative improvement, but inducing 3 and higher body contributions. A lucky coincidence is that the initial evolution of the SRG unitary transform induces 3-body terms that partially cancel with known 3-body potentials, improving the spectral match to experiment of calculations based on the evolved two body interaction. The initial evolution comes with reduced coupling of low and high momentum states and a slowly improving prediction of the binding energy of the triton, followed by rapid deterioration as the higher body contributions grow strongly. In contrast, in the HOBET approach we discuss, the

effective interaction will be extended to the shell-model scale where many-body calculations are performed.

Regardless of the source of the potential, the standard next step is to take matrix elements in a large harmonic oscillator basis. For the two body deuteron one can then directly solve for the ground state, finding that the basis must be quite large, over $\Lambda = 100$, to accurately reproduce the experimental binding energy. For potentials produced with a such momentum cutoff this raises a question about the overlap of the harmonic oscillator states, each of which covers a distribution of momentum states, with the excluded momentum region. Pushing on, the next step is to integrate out all but low lying states in the harmonic oscillator basis and resulting in two cutoffs in two different bases, one at some high momentum and a second at the energy of the highest included harmonic oscillator states. The argument is that the momentum cutoff is well above the eventual harmonic oscillator cutoff even accounting for the momentum spread of each state, so how could it matter? The problem with this argument is that the incorrect information in the high excitation harmonic oscillator states flowed down into the interaction specified in the small state space. Even more important, the mismatch between the momentum basis and harmonic oscillator basis will result in violation of important symmetries such as translation invariance. Preservation of translation invariance in a truncated harmonic oscillator basis depends on a clean energy cutoff of the basis.

To those used to applying effective theory in other domains the two step process from QCD or observables to a UV potential to an effective interaction is strange. The usual process directly connects observables to the parameters of the effective theory expansion. In a momentum basis one can follow Weinberg's prescription, writing down a complete set of operators consistent with the symmetries of the UV theory. The operators are organized according to the size of their contribution as controlled by a hopefully small expansion parameter [13]. The parameters are then fit to reproduce observables. There is no reason to create dubious UV detail in a potential, if in the end all that detail is integrated out in the final effective interaction.

One advantage Weinberg had is that the kinetic energy operator is diagonal in a momentum basis, so it won't connect the included P states to the excluded Q states across the momentum cutoff. The extension to a harmonic oscillator basis is not obvious because the kinetic energy operator T changes to a tri-diagonal form, strongly connecting states of the highest nodal number in P to Q. In connection with the hard core of realistic interactions this leads to the poisoning of the effective theory described by Shucan and Weidenmüller. The HOBET (Harmonic Oscillator Based Effective Theory) program began with an attempt to understand this problem. Song [14] and then Luu [15] studied the problem by tediously integrating out Q with a known potential in simple 2 and 3 body cases with the goal of understanding the mechanism that prevented convergence. Their antidote was to find a decomposition of the effective interaction in which troublesome parts involving repeated scattering by T through Q can be analytically summed, leaving a remainder for which a short range expansion is suitable. It is remarkable and not at all foreordained that such a decomposition was found. The work here builds on this foundation.

The success of shell model calculations in reproducing spectra with 2 body interactions strongly suggests rapid convergence in n-body interactions with $n = 3$ or possibly 4 being sufficient for most calculations. The hope is that a rigorous A-body effective Hamiltonian can be constructed from the 2 and 3 body effective interactions which shows the same rapid convergence in the number of interacting nucleons. A key element enhancing convergence in the HOBET approach is that the contributions of the kinetic energy operator are summed to all orders restricting the convergence requirement to strong interactions occurring at short distances. In contrast, all other nuclear effective interactions approaches of which we are aware require the stronger condition that the entire effective interaction has a converging few-body expansion. Coupled with the demonstration that the 2-body interaction is analytic in E, meaning that the interaction is continuous in E and valid for both continuum and bound states, the A-body effective Hamiltonian can be fit to observables and continued to bound states at negative energy yielding a rigorous effective theory for nuclei. The definition of rigor here includes knowing in advance the form of the effective Hamiltonian that preserves the symmetries of the underlying theory. There is also no need for an intermediate high momentum potential in Q that must be renormalized to determine LECs, a process that defeated people in the 1970's.

1.1 What is an Effective Theory?

As this dissertation is about a harmonic oscillator based effective theory, it seems appropriate to more precisely define what is meant by an effective theory. A nice pedagogical introduction can be found in lectures on the topic by Daniel Phillips [16]. Sometimes the phrase effective theory has been applied to hybrids influenced by effective theory thinking but lacking some of the attributes and are more properly called models. Models have their own important role in physics, but are not the topic here.

An effective theory is defined with respect to a regime of interest, normally chosen to be suitable for solving some class of problems. The regime is usually specified as a bounded part of the Hilbert space for the underlying and unknown full theory. For example, it may be defined as momentum states under a cutoff or as is done here as an energy cutoff in a harmonic oscillator basis. Degrees of freedom associated with particles only accessible at high energy may be integrated out and replaced with composites as happens when constructing an effective theory of QCD in terms of nucleons and pions.

The effective theory is a systematic parameterized expansion or approximation that is consistent with the underlying symmetries of the underlying theory and otherwise complete. Systematic means that the form of the expansion is known and that the pieces of the expansion can be organized by the size of their contributions so that controlled approximations can be made by truncating the expansion. A common phrase used to describe this is power counting because the terms of the specific expansion are controlled and grouped by powers of an expansion parameter. In principle, arbitrarily good accuracy can be attained by evaluating the expansion to sufficient order.

With a known underlying theory the the parameters associated with the pieces of the expansion can in principle be determined if one's computational ability is strong enough. This process is referred to as integrating out the degrees of freedom beyond the effective theory regime. If the calculation is too hard, or the full underlying theory is not known, then the expansion parameters may be fit to reproduce observables, yielding the same effective theory.

This last statement very importantly applies to the problem of constructing an effective theory for QCD. We have no way to directly compute the expansion parameters of an effective theory directly from QCD, but with LQCD the values of observables can be computed and used to fit the effective theory.

Because of the systematic expansion, once the expansion parameters have been fixed to reproduce observables, one can expect to correctly predict observables that weren't used in the fitting process but are in the regime the effective theory is designed for. This is a strength of effective theories relative to models.

1.2 Alternate Effective Theory Strategies

There are several alternative effective theory strategies for nucleon many body approaches: the Lee-Suzuki approach, Chiral EFT, and. lattice EFT. The key difference to look for is how they define the portion of the Hilbert space and the basis that it is expressed in, determining what types of the problems the effective theory is suitable for.

An effective theory approach that leads to an energy independent Hermitian form in a harmonic oscillator basis is that of Lee and Suzuki [17]. It can be used to take a hard interaction – such as the phenomenological Av_{18} fitted to NN scattering and characterized by hard cores in excess of a GeV – and explicitly renormalize it. The Lee-Suzuki effective interaction is structurally compared to the Bloch-Horowitz effective interaction by Jennings [18]. The essential difference in construction is that instead of the eigenstates of the effective Hamiltonian being taken from all states which overlap P, the model space, one also divides the original eigenstates into two parts $|k\rangle$ and excluded part $|k'\rangle$ with a requirement that $P|k\rangle$ forms a complete and independent basis for P. The key step is to produce an orthonormal basis for $P|k\rangle$. The result is that each basis member corresponds to a linear combination of elements from $|k\rangle$ in the full Hilbert space. A similar equation to the Bloch-Horowitz equation can be used to compute the effect of scattering through $|k'\rangle$. A good attribute is that the effective theory result is directly expressed in a harmonic oscillator basis, the basis of choice for nuclear structure calculations. As mentioned earlier, the result is energy independent and Hermitian, which means that the eigenstates in the model space will be orthogonal, which can't be the case with the restriction of the full wave function - consequentially the interpretation of the eigenstates is unclear as is their use in evaluating observables. An additional downside of this approach is that the resulting effective Hamiltonian is restricted to the original eigenstate set $|k\rangle$, so the constructed H_{eff} can't be used to make predictions outside of the subspace spanned by $|k\rangle$.

Chiral EFT is a way to construct a nuclear potential with a more direct connection to QCD. Quarks and gluons lose their independent existence and are always hidden in "colorless" bound states such as nucleons, pions, and heavier mesons which become the relevant degrees of freedom of the theory. A review can be found in [19]. The effective theory is formulated in a cut off momentum basis with degrees of freedom consisting of the colorless bound states of quarks: pions, and nucleons. In this theory the effective Lagrangian consists of all terms consistent with the symmetries of the underlying theory of QCD. The terms carry LECs (low energy constants) that must be fit to observables and are organized according to an expansion parameter (Q/Λ_χ) where Q represents the pion mass/momentum and Λ_χ is a cutoff momentum roughly associated with the next meson mass above the pion. Potentials derived via perturbation theory through N^3LO have been constructed and their LECs fit to observables with great success.

To this point all the elements of an effective theory have been met. The usual next step is to take matrix elements of the potential in a large harmonic oscillator basis. The change of basis immediately creates a problem because harmonic oscillator states can be represented as a sum over a momentum basis and high n states will have substantial overlap with momentum states above the cutoff, resulting in missing contributions to large n matrix elements. Integrating out these high n states to reduce the dimension of the effective Hamiltonian will then propagate these missing contributions. Even worse, the mismatch in basis will violate translation invariance, breaking the clean separation of relative and center of mass modes in the harmonic oscillator basis.

The essential point is that for a consistent effective theory, the basis in which the cutoff is taken should be the one the theory is constructed in. A two step process with a basis change in the middle does not cleanly separate the included P space from the excluded Q space.

The closest in spirit to HOBET is an EFT formulated on a Lattice [20]. The lattice is a periodic space time lattice with nucleon fields on the lattice cites. Differential operators are implemented as difference operators over neighboring sites in much the same way as LQCD. The effective theory can be formulated as a pionless theory valid up to momentum scales on the order of m_π or even a formulation of Chiral effective field theory valid to higher momenta. Unlike the path taking a Chiral effective theory into a harmonic oscillator basis described above, the effective theory is constructed directly in the calculation basis, avoiding the previous basis incompatibility. Rotational symmetry is a challenge to maintain because the lattice structure and the volume both break it, though improved operators involving more neighbor points can mitigate part of the problem. This impacts the factorization of the Hilbert space into angular momentum channels, impacting calculation costs for systems of more nucleons. Continuum extrapolation of results will also be required. The basis should be very suitable for nuclear matter calculations and study of bound states of small number of nucleons.

This work relies on the Bloch-Horowitz equation [21], to be reviewed in Chapter 2, which constructs an effective Hamiltonian in a restricted space defined by projection operator P. All eigenstates where $P|\psi_i\rangle \neq 0$ are eigenstates of the effective Hamiltonian. This is

attractive because after H_{eff} is determined by fitting a perturbative expansion to data in one energy range, one can expect that H_{eff} can be applied to other states outside that range. A common objection to the Bloch-Horowitz equation is that it is energy dependent. For purposes herein, this will be seen to be a virtue, providing a key part of dealing with the mixed scales of the kinetic energy operator and the short range nuclear potential.

Chapter 2

The Bloch-Horowitz Equation

The Bloch-Horowitz equation is central to this thesis, so a substantial review is appropriate.

In many contexts one would like to reduce the physics of a system to a subset of states relevant to the quantities being calculated. The full basis could be a continuous basis like a momentum or position basis, or a discrete basis such as a set of harmonic oscillator states. The complete set of states form a Hilbert space in which the Hamiltonian can be expressed. Reducing the physics to low energy or momentum states states means partitioning the Hilbert space into an included set of states which are defined with a projection operator P, and an excluded set of states with projection operator Q with $P + Q = 1$. P and Q will be used as projection operators and as the names of the corresponding sets of states. The important question is, how close can one get to writing a Hamiltonian that operates on the restricted basis P with the same eigenvalues. Such a Hamiltonian is called an effective Hamiltonian.

The development begins with the time independent Schrödinger equation, which describes the stationary states of the system.

$$H\left|\psi_i\right\rangle = E_i\left|\psi_i\right\rangle \tag{2.0.1}$$

$P + Q = 1$ may be inserted freely.

$$(P+Q)\,H\,(P+Q)\left|\psi_i\right\rangle = E_i\,(P+Q)\left|\psi_i\right\rangle \tag{2.0.2}$$

The projection operators split this equation into two.

$$\begin{aligned} PH\,(P+Q)\left|\psi_i\right\rangle &= E_i P\left|\psi_i\right\rangle \\ QH\,(P+Q)\left|\psi_i\right\rangle &= E_i Q\left|\psi_i\right\rangle \end{aligned} \tag{2.0.3}$$

The first equation is close to the desired form, but still has a reference to $Q\left|\psi_i\right\rangle$. The second equation can be used to eliminate it.

$$\begin{aligned} (E_i - QH)\,Q\left|\psi_i\right\rangle &= QHP\left|\psi_i\right\rangle \\ Q\left|\psi_i\right\rangle &= \frac{1}{E_i - QH} QHP\left|\psi_i\right\rangle \end{aligned} \tag{2.0.4}$$

Substituting into the first equation of Eq.(2.0.3) yields the Bloch-Horowitz equation for an effective Hamiltonian

$$\begin{aligned} P\left(H + H\frac{1}{E_i - QH}QH\right)P\left|\psi_i\right\rangle &= E_i P\left|\psi_i\right\rangle \\ H_{eff}\left(E_i\right) &= P\left(H + H\frac{1}{E_i - QH}QH\right)P \end{aligned} \tag{2.0.5}$$

One way to think about this equation is in terms of an expansion of $1/\left(E - QH\right) = \left(1/E\right)\left(1 + QH/E + \left(QH/E\right)^2 + \cdots\right)$. In this form the terms represent longer and longer sequences of scattering by H through the Q space before returning to the included P space.

There are a number of important observations about this equation. First, the eigenstates of H_{eff} are the projections of the eigenstates of the full theory described by H, except for a special case where a state has 0 overlap with P. Second, the eigenvalues are the same eigenvalues. This may come as a surprise because P may consist of a finite number of basis states where the full theory has a continuum of eigenstates. How can such an $H_{eff}\left(E\right)$ reproduce all the eigenvalues of the full theory? The answer is in the energy dependence. The matrix elements in the finite basis change with energy.

A third important observation is that the eigenstates of $H_{eff}\left(E\right)$ are not orthogonal. This is a consequence of projecting the orthogonal eigenstates of H into P. A set of 3 orthonormal 3D vectors projected onto a table top will not remain orthogonal and the same happens to $\left|\psi_i\right\rangle$. In addition, the projected vectors will not be of unit length or normalized. In fact, it is possible to get 0 length, and the same can happen with $H_{eff}\left(E\right)$ eigenstates.

A fourth observation is that $H_{eff}\left(E\right)$ depends on the energy, the same energy that appears as the eigenvalue on the right. The Bloch-Horowitz equation must be solved self consistently. For bound states a strategy of iterative resubstitution (also known as fixed-point iteration) starting with an initial guess works well. Every energy in the continuum must be an eigenvalue, so iteration is not required and as will be later exploited, self-consistency of continuum states places constraints on the effective theory expansion.

Once the eigenstates of $H_{eff}\left(E\right)$ have been found an obvious use is to compute matrix elements of operators. The spectrum will match the spectrum of H, but the states themselves are projections and the normalization is unknown. Formally one can reconstruct the full wave function from the projection, as long as it is not 0, in the following way.

$$\begin{aligned} \left(E_i - \left(P + Q\right)H\right)\psi_i &= 0 \\ \left(E_i - QH\right)\psi_i &= PH\psi_i = E_i P\psi_i \\ \psi_i &= \frac{E_i}{E_i - QH}P\psi_i \end{aligned}$$

For bound states this operation is well defined because the Green's function for $E/(E-QH)$ must go to 0 at infinity, but for continuum states the operator $E/(E-QH)$ needs a boundary condition. The boundary condition is given by the phase shift, or in coupled channel cases the S-matrix.

If one knows the complete H, then it is at least formally possible to evaluate H_{eff}. In practice it is common to express part of Eq.(2.0.5) as an expansion respecting the underlying symmetries of H. Then coefficients in the expansion are fit to reproduce experimental data. Returning to the case of continuum states, every positive energy is an eigenvalue and $H_{eff}(E)$ should have an eigenvalue matching E. Any failure to obtain a match must therefore come from errors in the expansion constants. Fitting the expansion constants to minimize such errors is a good way to determine their values.

Other useful formulations of the Bloch-Horowitz equation can be obtained via the operator equation

$$\frac{1}{A-B} = \frac{1}{A} + \frac{1}{A}B\frac{1}{A-B} = \frac{1}{A} + \frac{1}{A-B}B\frac{1}{A} \tag{2.0.6}$$

These formula may be easily verified.

$$\frac{1}{A} + \frac{1}{A-B}B\frac{1}{A} = \frac{1}{A} + \frac{1}{A-B}(B-A)\frac{1}{A} + \frac{1}{A-B}A\frac{1}{A} = \frac{1}{A-B} \tag{2.0.7}$$

As an example use of the operator equation, a shorter form of the Bloch-Horowitz equation can be transformed into the standard form Eq.(2.0.5).

$$H\frac{E_i}{E_i - QH} = HE_i\left(\frac{1}{E_i} + \frac{1}{E_i}QH\frac{1}{E_i - QH}\right) = H + H\frac{1}{E_i - QH}QH \tag{2.0.8}$$

Continuing to expand the resolvent results in the following expansion.

$$\begin{aligned} H_{eff}(E_i) &= P\left(H + H\left(\frac{1}{E_i} + \frac{1}{E_i}QH\frac{1}{E_i - QH}\right)QH\right)P \\ &= P\left(H + \frac{1}{E_i}HQH + \frac{1}{E_i^2}HQHQH + \ldots\right)P \end{aligned} \tag{2.0.9}$$

This defines a nice perturbation expansion for H_{eff} with the small requirement that H is well behaved. The definition of well behaved comes down to the eigenvalues of HQ/E_i. If any eigenvalue has a magnitude larger than or equal to 1, then the series will not converge. In nuclear physics $H = T + V$ does not meet this small requirement. Part of the reason is a mixing of energy scales. A realistic nuclear potential such as Argonne v_{18}, shown in Figure (3.1), has a hard core with energy in the GeV range. Despite this, the deuteron is bound by ≈ -2.22 MeV, implying that the wave function is spread out over a large range, well outside of the range of the potential. In a harmonic oscillator basis long range corresponds to a high nodal quantum number. The connection to these states is not primarily through the potential, it is instead through the kinetic energy operator T. This is why the IR part of H is associated with T and the UV with the potential V. T is a hopping operator in a harmonic oscillator basis, see Eq.(A.4.1), which also has the effect of coupling the highest state in in each angular momentum channel of P to the lowest state in Q with the same angular momentum. Strong coupling between included states and excluded states poses a challenge for effective theories that will have to be dealt with.

2.1 Reformulation of the Bloch-Horowitz Equation

Haxton, Song, and Luu studied the convergence of a perturbative expansion of the Bloch-Horowitz propagator in a harmonic oscillator basis [22].

$$\frac{1}{E-QH} = \frac{1}{E-H_{ho}} + \frac{1}{E-H_{ho}} Q(V-V_{ho}) \frac{1}{E-H_{ho}} + \cdots \tag{2.1.1}$$

In the included space defined by $\Lambda_\infty > 70$ they found that matrix elements $\langle \alpha \left| H_{eff} \right| \beta \rangle$ with α and β well away from the boundary converged rapidly. On the other hand matrix elements with either α or β in the last included shell converged poorly, requiring ~ 1000 orders of perturbation theory to converge. The poor convergence was traced to the strong coupling across the boundary of P by the QT part of QH in the propagator and between adjacent states in Q. Powers of QT/E in the expansion of the propagator for weakly bound systems with small E then connect the edge of P to a cascade of harmonic oscillator states higher in Q with longer and longer range and therefore corresponding to IR physics.

The hard core of the nuclear potential had it's own convergence problems and a modified contact gradient expansion was found that was able to represent it accurately. The combination of simultaneous IR and UV contributions in H is responsible for convergence problems. These observations motivated the search for a reorganization of the Bloch-Horowitz equation that separated the short range physics in V from the long range effect of T, enabling an analytic calculation to all orders of the contribution of the well understood T operator and leaving short range physics to an effective theory expansion.

The organization that Haxton and Luu found did not completely separate T and V, but trapped the remaining combined contribution between copies of the QV operator, resulting in a short range operator, the fourth in brackets below, that is well modeled by an effective theory expansion.

$$H_{eff}(E) = P \frac{E}{E-TQ} \left[T - T\frac{Q}{E}T + V + V\frac{1}{E-QH}QV \right] \frac{E}{E-QT} P \tag{2.1.2}$$

The effective theory expansion of the fourth term will be in terms of a set of operators multiplied by associated LECs (low energy constants). If one can argue that the fourth term has little energy dependence, then the LECs will also be nearly energy independent. Energy independence in the LECs will be very useful in fitting the expansion to observables which are taken at a substantial spread in energy. The argument begins with an expansion of the term with the operator equation Eq.(2.0.6).

$$V\frac{1}{E-QH}QV = -V\left(\frac{1}{QH} + \frac{1}{E-QH}\,\frac{E}{QH} \right) QV \tag{2.1.3}$$

The first term is energy independent. The second term will be small if $\left\langle (QH)^{-1} QV \right\rangle >> \langle E \rangle$. A way see this is to work in terms of the spectrum of H, which consists of continuum states and possibly some bound states. Working from the right in the above equation, V is

short range, connecting low and high momentum states and will produce a wide distribution in an expansion over the spectrum of H, but Q will eliminate the parts of wave functions about the length scale b of the harmonic oscillator, strongly suppressing overlap with bound states of H and the lower energy continuum spectrum of H having significant overlap with P. The result is that the remaining part of the spectrum to be acted on by H will be in the higher energy part of the spectrum where H will produce large eigenvalues, dominating E in the region of interest which includes bound states and moderate continuum energies. This argument suggests that increasing the overlap of P with eigenstates of H in the energy range of interest will decrease energy dependence. The overlap can be increased trivially by making P larger and more interestingly by tuning the harmonic oscillator length scale so that a larger fraction of bound state wave functions and lower energy members of the continuum can be represented in P. There is a Goldilocks b for the problem that minimizes energy dependence.

Returning to Eq.(2.1.2) a derivation can be found in [15]. A shorter derivation will be included here with some explanation because the techniques will be useful later in the A-body extension of HOBET. Liberal use of the operator equation Eq.(2.0.6) will be used in the derivation which begins with the shorter form of the Bloch-Horowitz equation Eq.(2.0.8).

$$\begin{aligned} H\frac{E}{E-QH} &= (T+V)\left[\frac{E}{E-QT}+\frac{E}{E-QT}QV\frac{1}{E-QH}\right] \\ &= \left\{T\frac{E}{E-QT}\right\}_1+\left\{V\frac{E}{E-QT}\right\}_2+\left\{V\frac{1}{E-QH}QV\frac{E}{E-QT}\right\}_3+\left\{T\frac{E}{E-QT}QV\frac{1}{E-QH}\right\}_4 \end{aligned}$$

The pieces have been grouped and labeled so they can be individually worked on. Note that in portion 3 above that the order of the operators are reversed as allowed by Eq.(2.0.6).

$$\begin{aligned} \{\}_1 &= \frac{1}{E-TQ}\,(E-TQ)\,T\frac{E}{E-QT} = \frac{E}{E-TQ}\left[T-T\frac{Q}{E}T\right]\frac{E}{E-QT} \\ \{\}_4 &= T\frac{1}{E-QT}QV\frac{E}{E-QT}+T\frac{1}{E-QT}QV\frac{1}{E-QH}QV\frac{E}{E-QT} \\ &= \left(\frac{E}{E-TQ}-1\right)V\frac{E}{E-QT}+\left(\frac{E}{E-TQ}-1\right)V\frac{1}{E-QH}QV\frac{E}{E-QT} \end{aligned}$$

In recombining the pieces portions 2 and 3 will cancel with the negative parts of portion 4, yielding the desired form, also shown diagrammatically in Figure (2.1).

$$H\frac{1}{E-QH} = \frac{E}{E-TQ}\left[T-T\frac{Q}{E}T+V+V\frac{1}{E-QH}QV\right]\frac{E}{E-QT} \tag{2.1.4}$$

Note that this equivalence did not depend on the P-space projectors that are part of Eq.(2.1.2), so the alternate expansion is actually more general.

An intuitive explanation of the roles of the components of this expression will be useful. First, Green's functions for the resolvents on either end will reconstruct a long range wave

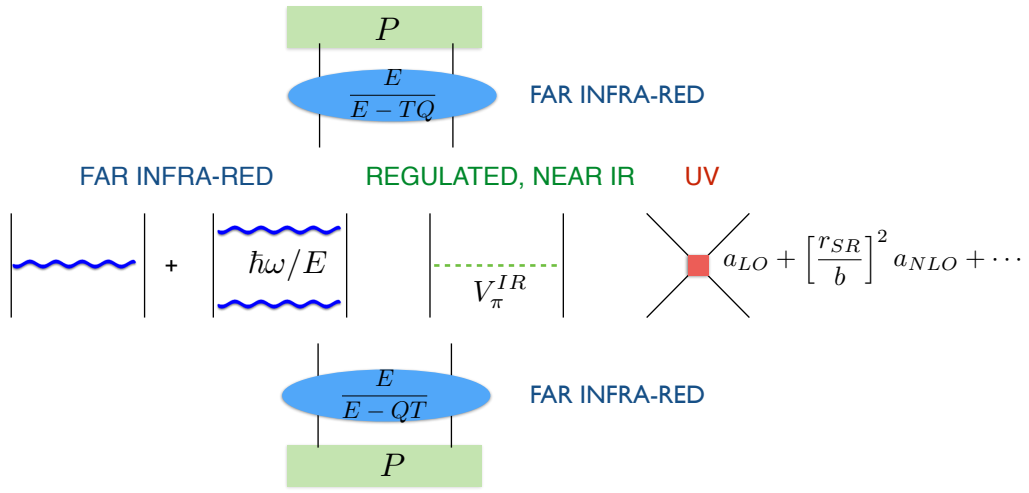

Figure 2.1: HOBET's effective interaction, appropriate for a harmonic oscillator basis where translational invariance requires P to be cut off in total quanta. This is in contrast to chiral EFT interactions which employ a momentum cutoff. The colors blue, green, red indicate far-IR, near-IR, and UV corrections.

function with the same exponential decay as is expected for negative energy states or oscillatory behavior as a scattering state for positive energy states. Specifically, in a harmonic oscillator basis it will be seen that the Green's functions are the identity except for states at the edge of the P space, states for which the kinetic energy operator T couples to states in Q. When the first two terms in brackets are evaluated in the context of the Green's functions they will account for all the repeated scattering by purely by T through the Q space. This result is extremely important for weakly bound states of short range potentials where the wave function is extended far beyond the potential. The kinetic energy operator T is a hopping operator in the harmonic oscillator basis and plays a major role in coupling lower energy states to high energy states that have long range. The last two terms in brackets are the potential and a term that involves repeated scattering by H through Q, but capped on each end by the presumed short range V. This short range operator contains the result of integrating out repeated scattering by H that begins and ends with scattering by V to connect to the P space. In HOBET, this short range operator is the focus of the effective theory expansion as the T pieces can be evaluated to all orders. The Haxton-Luu form of the Bloch-Horowitz equation achieves a separation of scales that was not obvious in the original form.

Chapter 3

Realistic Nuclear Potentials

Modern realistic nuclear potentials accurately reproduce observables such as phase shifts, the deuteron bound states and magnetic moment with amazing accuracy.

In experiments one can send beams of neutrons or protons, which have better data, at specific energies into hydrogen and observe the angular distributions of outgoing particles. Initial polarizations of the nucleon spins can be controlled by strong magnetic fields coupled to the magnetic moments of the nucleons. From those spin polarizations and angular distributions one can compute a set of scattering parameters at each energy, relative angular momentum and relative spin state. The usual parameters are known as phase shifts and mixing angles, or they may be encoded into an S-matrix, which relates the amplitudes of incoming states to outgoing states. A large database of phase shift and mixing angle results for both experiments and various realistic potentials is available at NN-Online [23].

Realistic nuclear potentials were constructed by making educated guesses as to the forms of the contributions based on meson exchange models. The terms were parameterized and then fit to reproduce the phase shift and mixing angles. Failures to reproduce phase shifts at higher energies were observed and new terms were added. For example, a coupling between angular momentum and spin was added to reproduce proton-proton phase shifts at higher energies [24].

An example realistic nuclear potential used in this dissertation is the Argonne v_{18} potential [25], with channels relevant to the deuteron shown in Figure (3.1). Of note is the very large potential values at $r < 0.25$ fm, reaching ≈ 2 GeV. This "hard core" is a feature of other realistic potentials as well. The wave function of the deuteron is concentrated around the shallow wells near 1 fm and the long range potential contributions decay as a one pion exchange potential.

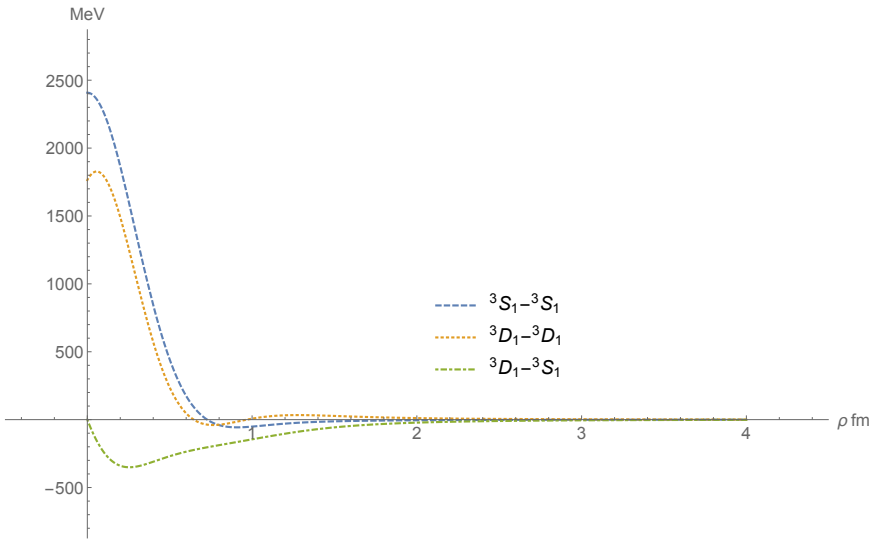

Figure 3.1: The three parts of the Argonne v_{18} potential coupling the $^3S_1$ and $^3D_1$ channels.

Chapter 4

The Configuration Interaction Shell Model

As was seen in the introduction, LQCD suffers from the fermion sign problem, preventing it's application to any substantial number of nucleons. The configuration interaction shell model for A nucleons partially avoids the issues associated with the fermion sign problem by working in an explicitly anti-symmetric basis, but suffers from what is essentially the same computational complexity due to the growth of the basis with A. However, computational techniques for finding low lying eigenstates of very large sparse matrices are incredibly efficient, allowing many nucleon systems to be solved. In a practical sense this is the answer that is needed. If one replaces the usual Hamiltonian model with an effective theory matched to LQCD calculations, then nuclear structure can be faithfully computed from QCD. The properties of the configuration interaction method therefore informs the parameters of the effective theory, and motivates the review here.

Suppose one wants to compute the nuclear spectra of a light element like ^{6}Li. In the configuration interaction shell model one first picks a single particle basis. This basis is much like the familiar set of states of an electron about a proton. The states are parameterized by angular momentum quantum numbers J and j_z. There is also a radial wave function parameterized by a nodal quantum number n. The basis of choice in these calculations is the harmonic oscillator basis for several reasons. First, the basis is complete as will be seen later when a free wave of angular momentum ℓ is represented as a sum over the harmonic oscillator basis. Second, the basis is appropriate for representing confined wave functions such as bound states with a modest number of terms. Third, the basis is easy to calculate with. Fourth, and probably not last, the harmonic oscillator basis is the only such basis in which translation invariance in a truncated basis can be maintained, which is required to avoid contaminating the spectrum with oscillations of the center of mass.

Neutrons and protons are fermions, so overall anti-symmetry of the wave function must be maintained. Take an example consisting of two neutrons and two single particle states ϕ_a and ϕ_b. A properly anti-symmetrized wave function of two spin up neutrons in those states

will have the form

$$\psi(\vec{r}_1, \vec{r}_2) = \left(1/\sqrt{2}\right) \left(\phi_a(\vec{r}_1)\phi_b(\vec{r}_2) - \phi_a(\vec{r}_2)\phi_b(\vec{r}_1)\right) \tag{4.0.1}$$

For three particles, there would be 6 terms, for n particles $n!$ terms. The general expression for A particles is the Slater determinant, abbreviated as SD.

$$\psi\left(\vec{r}_1, \vec{r}_2, \ldots, \vec{r}_n\right) = \frac{1}{\sqrt{n!}} \begin{vmatrix} \phi_1\left(\vec{r}_1\right) & \phi_2\left(\vec{r}_1\right) & \cdots & \phi_n\left(\vec{r}_1\right) \\ \phi_1\left(\vec{r}_2\right) & \phi_2\left(\vec{r}_2\right) & \cdots & \phi_n\left(\vec{r}_2\right) \\ \vdots & \vdots & \ddots & \vdots \\ \phi_1\left(\vec{r}_n\right) & \phi_2\left(\vec{r}_n\right) & \cdots & \phi_n\left(\vec{r}_n\right) \end{vmatrix} \tag{4.0.2}$$

Slater determinants can be compactly represented in second quantization as an ordered set of fermion creation operators acting on the vacuum. Other orders produce the same SD up to a phase of -1 for odd permutations.

$$\hat{a}_1^\dagger \hat{a}_5^\dagger \hat{a}_7^\dagger \left|0\right\rangle \tag{4.0.3}$$

The above expression describes a 3 particle SD. The number of such SDs is a function of the number of single particle states and the number of particles. In a typical ^6Li calculation there are 112 single particle states, yielding $\binom{112}{3} = 227920$ SDs for the protons and the same amount for the neutrons. The selected single particle states range up to $n = 1, L = 5$ and $n = 3, L = 0$ with a cutoff energy over the ground state of $5\,(\hbar\omega/2)$. Most of these SDs will have energies well above the cutoff for single particle states. This will turn out to cause a problem with translation invariance.

Naively, the total number of states in the calculation basis would the be product of the number of proton and neutron SDs, but various ways of reducing the basis are possible. First, the system has rotational invariance and it is therefore possible to fix $J_z = 0$ for analysis. Each SD has a well defined J_z of it's own and the sum of the proton SD J_z and the neutron SD J_z must be 0, greatly reducing the basis size. One can also introduce an energy cutoff on the basis, limiting the number of quanta of excitation energy. Limiting the excitation quanta to 4 in this case yields 2392 SDs for each species and a total basis size of 17040, which is much more reasonable for calculation.

The described basis is called an M-scheme basis in which the basis members do not have good total angular momentum but J_z is well defined. An alternate basis formulation called J-scheme has basis members that are linear combination of M-scheme basis elements which do have well defined J. The J-scheme basis will normally have a smaller dimension than an M-scheme basis, but the evaluation of the Hamiltonian is more complex. In practice, simplicity has led to higher performance in highly parallel implementations. For the remaining discussion on the topic, the basis will be assumed to be M-scheme.

Once the Hamiltonian is expressed in the basis above the problem is to find the low lying eigenvalues and states of the system. A good introduction to the required techniques may be found in Whitehead et al. [26] and in a description of a more modern and complex program

called BIGSTICK described by Johnson et al. in [27]. With enhancements to BIGSTICK described in [28] it is capable of solving for the low lying states in systems with larger than 10^9 states. Despite this, the rapid explosion in the number of states with the energy cutoff means that the energy cutoff must be modest even for light nuclei like ^{12}C.

The downside of limiting the excitation quanta is that now the Hilbert space has been divided into an excluded space and an included space, but no attempt has been made to capture the effect of the Hamiltonian scattering from the included space to the excluded space and back as would be done in an effective theory. The induced error can be large. An initial effort towards modifying the shell model into an effective theory was made by Haxton and Song in [29]. Section 12.1 shows how to use a 2-body effective interaction in an A-body effective theory shell model calculation.

The only real way to keep the A-body basis size in a range possible to compute with is to begin with an accurate two or three body effective interaction in a small basis. Effective theory A-body calculations provide a strong motivation for directly constructing the effective interaction in a harmonic oscillator basis instead of the more usual two step process of constructing a momentum cutoff based effective theory followed by taking harmonic oscillator matrix elements. In the second step a large number of states must be retained because the two bases do not have a consistent separation of P and Q.

The A body system has translation invariance. A way to separate the center of mass motion in our calculations is needed or it will contaminate the spectrum. The key is that one can transform from an independent particle basis to a relative basis based on Jacobi coordinates. To accomplish this requires Moshinsky brackets

$$\langle n_a, \ell_a, n_b, \ell_b : \Lambda |\, n_{rel}, \ell_{rel}, N_{cm}, \ell_{cm} : \Lambda \rangle \tag{4.0.4}$$

which couple independent to relative and center of mass oscillator states where both sides are coupled to total angular momentum Λ. The brackets are defined by Moshinsky in [30] and summarized Appendix A.7. Energy conservation tells us that $2n_a + \ell_a + 2n_b + \ell_b = 2n_{rel}+\ell_{rel}+2N_{cm}+\ell_{cm}$, which in turn tells us that the unitary transform from a product single particle states to a product of relative states will not mix energies. Parity and total angular momentum are also conserved. Moshinsky brackets can be repeatedly applied with Jacobi coordinates to transform an A-body system to $A-1$ oscillators in relative coordinates and one center of mass oscillator. If one applies a strict energy cutoff to the A-body states formed from single particle states and then transforms to relative coordinate harmonic oscillator states, the same total energy cutoff will be preserved.

After the transform one of the resulting harmonic oscillators will be written in terms of a CM (center of mass) coordinate. Now imagine that the spectrum of the resulting system is determined. Some A-body states will be in the CM ground state, some will be in a CM excited state. A system with translation invariance should depend only on relative coordinates, so the contamination of the spectrum by CM excited states should be eliminated. If ω_{CM} is increased then the energy step to the first excited state can be made arbitrarily large, moving the contamination out of the energy range of interest. This technique is known as the Gloeckner-Lawson projection method [31].

The important conclusion is that consistent with separability of the center of mass that the A-body model space may be cut off in total energy quanta, and restricted in total angular momentum and parity. Other than the lattice basis, which recovers translation invariance in the continuum limit, the harmonic oscillator basis is the only finite basis with this property. Any other omission of states will lead to mixing of the center of mass states with the relative states and the resulting contamination of the spectrum. To calculate accurately in a portion of the complete Hilbert space requires an effective theory treatment and provides a strong motivation for this dissertation.

Chapter 5

Constructing the Spherical H_{eff}

The process of constructing H_{eff} consists of constructing the various pieces of the reorganized Bloch-Horowitz equation from Eq.(2.1.2). The initial step is to make the substitution

$$V + V\frac{1}{E - QH}QV \rightarrow V_{IR} + V_{\delta}. \tag{5.0.1}$$

This substitution makes the transition from directly deriving the effective theory from a UV potential to specifying an effective theory expansion, V_{δ}, that will be fit to observables.

V_{IR} should be thought of as a guess at a potential that is accurate at mid and especially long range. The effective theory encoded in V_{δ} will be an expansion around that guess. The coming discussion of power counting in Section 5.5 will establish a more formal connection between LEC order and range. One can also represent V_{IR} in the expansion form that will be used for V_{δ}. The important LECs in that representation of V_{IR} are the ones beyond the order to which the effective theory will be fit. Errors in V_{IR} captured in in lower order LECS will be automatically corrected when fitting V_{δ} to observables. Errors captured in higher order LECS beyond the fitting order will persist.

Short range parts of V_{IR} are an artifact to be corrected by the real short range physics. It is therefore appropriate to subtract the contributions made to the LECs by V_{IR} up to the order of the fit of V_{δ}, leaving only contributions beyond that order. The subtraction will have no effect on the matrix elements of the effective theory, it simply removes the need to have compensating contributions to the matrix elements of V_{δ}. Procedurally, the step can be factored out and performed at the end of the process with the only result being a shift in the LEC values and the exposure of a more natural progression of their values. The procedure for performing the subtraction is detailed in Section 5.6.

For the nuclear interaction a one pion exchange potential will be our guess of choice. V_{δ}, the remainder, is short range if V is short range, and is certainly true for the nuclear interaction. The effective theory expansion will focus on V_{δ} exclusively as everything else is directly calculable. The restated H_{eff} is

$$H_{eff}(E) = PG_{TQ}\left[T - T\frac{Q}{E}T + V_{IR} + V_{\delta}\right]G_{QT}P. \tag{5.0.2}$$

Energy dependence in H_{eff} appears in the Green's function G_{QT}, its conjugate G_{TQ} and in the matrix elements of T. This is no surprise as the kinetic energy operator dominates the long range part of the interaction. V_δ will have only residual energy dependence as described in the argument following Eq.(2.1.2). The operators used in the effective theory expansion are sensitive to the momentum of the wave function and these operators can absorb much of the residual energy dependence instead of having energy dependence in the LECs (Low Energy Constants) of the expansion. Being able to treat the LECs as truly constant across the energy range of observables greatly simplifies the fit to observables taken at a range of energies.

The following sections proceed through the pieces of H_{eff}: the Green's functions, kinetic energy matrix elements, V_{IR} matrix elements, and finally the effective theory expansion of V_δ.

5.1 Green's Function for $E/(E-QT)$

In this section our objective is to understand the application of G_{QT} to basis states. The operator T, the kinetic energy operator, is a hopping operator, connecting states with the same angular momentum, but differing by 1 in nodal quantum number, see Appendix A.4. Edge states are defined to be states in P that T connects to Q. If G_{QT} is expanded in a series, it is immediately seen that it is the identity when acting on states in P that are not edge states.

$$G_{QT}\left|i\right\rangle = \frac{E}{E-QT}\left|i\right\rangle = \frac{1}{1-QT/E}\left|i\right\rangle = \left(1+\frac{1}{E}QT+\frac{1}{E^2}QTQT+\ldots\right)\left|i\right\rangle \tag{5.1.1}$$

For such states T only generates overlap with P which is then immediately removed by the adjacent Q operator. Further, $G_{QT}\left|e\right\rangle$, where e designates an edge state, overlaps states in Q with the same angular momentum as the original state $\left|e\right\rangle$. There is no generated overlap with other states in P. $G_{QT}P$ can therefore be regarded as an invertible basis transform. The edge states therefore have two representations, the first a P space state $\left|e\right\rangle$ and the second an infinite superposition of states in Q plus the original state $\left|e\right\rangle$. Both $\left|e\right\rangle$ and $G_{QT}\left|e\right\rangle$ are representations of the same state and will be referred to as edge states. The representation should be obvious from context.

The first step in implementing $G_{QT}P = E/\left(E-QT\right)P$ is to disentangle Q and T. This was solved in Luu's thesis [32], yielding $G_{QT}P = G_T\left\{P\,G_T\,P\right\}^{-1}P$ where the part in braces is a P space matrix. The inverse matrix will have numerous uses in constructing the effective Hamiltonian, so it is given a special name.

$$b_{ij} = \left\langle i\left|\frac{E}{E-T}\right|j\right\rangle^{-1}, \quad i,j\in P \tag{5.1.2}$$

For the somewhat messy details of constructing b analytically see Appendix B.5. The matrix b is block-diagonal in ℓ, m and tri-diagonal in each block because T is a hopping operator in

nodal number as is shown in Eq.(A.4.1). The symbol b may be referred to in the form $b^{\ell}_{n',n}$ or $b^{\ell,m}_{n',n}$, making the block structure explicit and indexing with the nodal quantum number. The matrix b is used to decompose G_{QT}.

$$\frac{E}{E-QT}\left|i\right\rangle = \frac{E}{E-T} b_{ij}\left|j\right\rangle \tag{5.1.3}$$

For efficiency it is advantageous to first apply $E/(E-T)$ to all states $|j\rangle$ and save them, then $G_{QT}\,|i\rangle$ may be formed by a simple sum over index j with the constant matrix b.

A next task is to form a Green's function for the resolvent G_{QT}. A key ingredient for this is the determination of boundary conditions. The boundary conditions for G_{QH} are already known.

$$(P+Q)\,H\psi_i = E_i\psi_i \quad \Rightarrow \quad (E_i - QH)\,\psi_i = E_i P\psi_i \quad \Rightarrow \quad \psi_i = \frac{E_i}{E_i - QH} P\psi_i \tag{5.1.4}$$

This tells us that a Green's function for G_{QH} with suitable boundary constraint must reconstruct the original wave function. It also reproduces the phase shift and the position of zeros in the wave function. G_{QH} can be expanded using G_{QT}.

$$\frac{E}{E-QH} = \frac{E}{E-QT-QV} = \frac{E}{E-QT}\left(1 + QV\frac{E}{E-QH}\right) \tag{5.1.5}$$

In order to reproduce the zeros outside the range of the harmonic oscillator basis, a Green's function for G_{QT} must also reproduce those zeros. In other words, it must also match the phase shift as a boundary condition. This is not a surprise because $(E-QH) \to (E-QT)$ outside the range of the potential. Care must be taken when applying this intuitive reasoning to the Green's functions for $E/\left(E-QH\right)$ and $E/\left(E-QT\right)$ because they are integral transforms sensitive to the interaction between V and the state they are applied to near the origin. The long range form of the resulting wave function is as expected, but the amplitude typically differs by 10 or 20% from the full wave function.

Consider a continuum state at positive energy E. It is expected that the long range wave function will have the form $-\cot\delta_\ell\left(E\right) j_\ell\left(kr\right) + \eta_\ell\left(kr\right)$. This specifies the location of zeros of $\langle r\left|G_{QT}\right|i\rangle$. Examining Eq.(5.1.3) shows that matching zeros must come from the Green's function for $E/\left(E-T\right)$. An analytic form for $\langle r\left|E/\left(E-T\right)\right|j\rangle$ with a specified phase shift is derived in appendix B.4.

Conceptually, the role of an edge state $G_{QT}\left|e\right\rangle$, where e is a state that is scattered to Q by T, is to restore the long range behavior of the wave function. Then the operators in H_{eff} are evaluated in that context. Lepage [33] specifies incorporating the correct long-range behavior as the first of three requirements for construction of an effective theory. The other two are a UV cutoff and local correction terms which correspond to the effective theory expansion here.

Taking the continuum example on an edge S-channel state one can visually compare in Figure (5.1) the harmonic oscillator wave function $\langle r|\,e\rangle$ to the transformed state wave

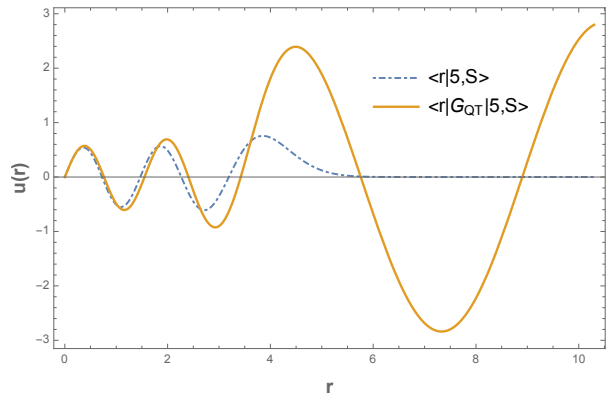

Figure 5.1: Transform of the 5th and highest S-channel state in P with the dimensionless $E = +1/2$. The transformed state has been scaled to initially match the amplitude of the original wave function.

function $\langle r\,|G_{QT}|\,e\rangle$. Initially the edge state follows the form of the harmonic oscillator state and as r passes the range of the state the result is a standard S-channel free stationary wave with the chosen phase shift.

The experiment is repeated for a negative energy state in Figure (5.2). The result is similar near the origin, but outside the range of the potential the edge state falls off exponentially as opposed to the Gaussian fall off of the harmonic oscillator state. In both bound and continuum cases the edge state recovers the long range form of the full wave function, which is essential to complete summation of the kinetic energy matrix elements.

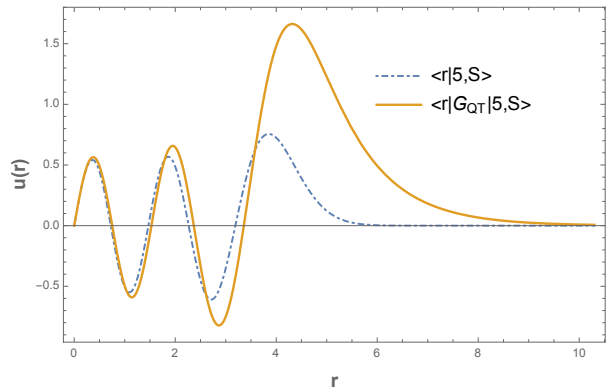

Figure 5.2: Transform of the 5th and highest S-channel state in P with $E = -1/2$. The transformed state has been scaled to initially match the amplitude of the original wave function. The expected exponential decay of a bound state is recovered from the HO state Gaussian fall off.

An important property is that $G_{QT}\,|i\rangle = |i\rangle$ unless state i is scattered into Q by T. Given

that T is a hopping operator in a harmonic oscillator basis, see Eq.(A.4.1), connecting states with the same angular momentum quantum numbers and differing by 1 in nodal quantum number, G_{QT} is the identity for most states. This both speeds up computations and serves as a useful test of correctness for b_{ij} and $\langle r\,|G_T|\,j\rangle$ implementations.

5.2 Kinetic Energy Matrix Elements

In this section the matrix elements

$$\langle n',\ell\,|T_{eff}|\,n,\ell\rangle = \left\langle n',\ell\left|\frac{E}{E-TQ}\left(T-T\frac{Q}{E}T\right)\frac{E}{E-QT}\right|n,\ell\right\rangle \tag{5.2.1}$$

are evaluated. An intermediate result is useful.

$$\frac{E}{E-TQ}\left(T-T\frac{Q}{E}T\right)=\frac{1}{E}\frac{E}{E-TQ}\left(E-TQ\right)T=T \tag{5.2.2}$$

With this result the matrix elements take on a simpler form.

$$\langle n',\ell\,|T_{eff}|\,n,\ell\rangle = \left\langle n',\ell\left|T\frac{E}{E-QT}\right|n,\ell\right\rangle \tag{5.2.3}$$

For non-edge states where $E/(E-QT)$ is the identity, one may use equation Eq.(A.4.1) to compute matrix elements directly. The direct calculation is useful for testing the result derived here. In a second test which applies to edge states a simple numeric integral can be used to take matrix elements using the analytic form of $\langle r\,|G_{QT}|\,n,\ell,m\rangle$. Here the matrix elements are computed in terms of already known elements.

$$\begin{aligned}
\left\langle n'\ell'm'\left|T\frac{E}{E-QT}\right|n\ell m\right\rangle &= \delta_{\ell',\ell}\delta_{m',m}\left\langle n',\ell'\left|T\frac{E}{E-QT}\right|n',\ell'\right\rangle \\
&= \delta_{\ell',\ell}\delta_{m',m}\left\langle n',\ell'\left|T\frac{E}{E-T}\right|n'',\ell'\right\rangle b^{\ell'}_{n'',n} \\
&= \delta_{\ell',\ell}\delta_{m',m}E\left\langle n',\ell'\left|\left(1-1+\frac{T}{E}\right)\frac{1}{1-T/E}\right|n'',\ell'\right\rangle b^{\ell'}_{n'',n} \\
&= \delta_{\ell',\ell}\delta_{m',m}E\left\langle n',\ell'\left|\frac{E}{E-T}-1\right|n'',\ell'\right\rangle b^{\ell'}_{n'',n} \\
&= \delta_{\ell',\ell}\delta_{m',m}E\left(\delta_{n',n}-b^{\ell'}_{n',n}\right)
\end{aligned} \tag{5.2.4}$$

This is a beautiful and simple result for T_{eff}.

5.3 V_{IR} Matrix Elements

The candidate of choice for V_{IR} is a OPEP (One Pion Exchange Potential), which is easily seen to be accurate at long range Figure (5.3). This can also be expected to be true for LQCD results with heavier pions as the pion remains the lightest exchange meson. For immediate purposes a single value will be used for the mass of the $\pi^{+/-}$ and π^0. A more complete treatment with independent masses can be found in [25]. Using ρ as the radial

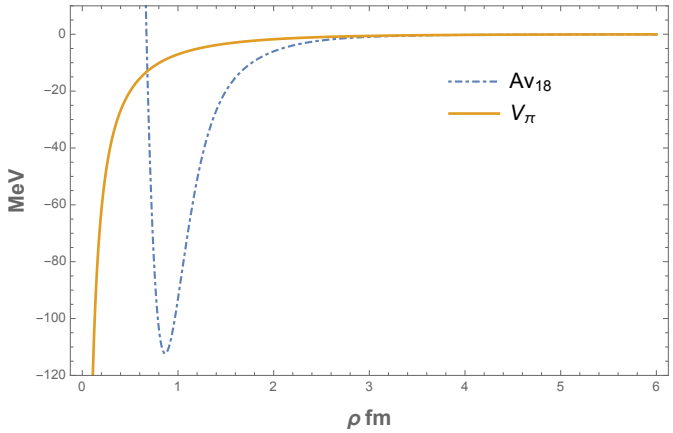

Figure 5.3: Comparision of Argonne v_{18} v.s. an OPEP in the $^1S_0$ channel. Note the divergence to negative infinity of the OPEP.

separation the OPEP can be expressed as

$$\begin{aligned} v_\pi(r) &= \frac{f_{\pi NN}^2}{4\pi}\frac{m_\pi}{3}\tau_1\cdot\tau_2\left[T_\pi(\rho)S_{12}+\left[Y_\pi(\rho)-\frac{4\pi}{m_\pi^3}\delta(\rho)\right]\sigma_1\cdot\sigma_2\right] \\ Y_\pi(\rho) &= \frac{e^{-m_\pi\rho}}{m_\pi r}, \qquad T_\pi(\rho) = \left(1+\frac{3}{m_\pi\rho}+\frac{3}{m_\pi^2\rho^2}\right)Y_\pi(\rho) \\ S_{12} &= 3\sigma_1\cdot\hat{\rho}\sigma_2\cdot\hat{\rho}-\sigma_1\cdot\sigma_2 \end{aligned} \tag{5.3.1}$$

The usual delta function part of v_π is dropped as its function is replicated in the lowest order term of V_δ and the constants are absorbed into a parameter $\tilde{f}_\pi^2$, which is more commonly written as

$$\tilde{f}_\pi^2 \approx \frac{m_\pi^2}{12\pi}\left(\frac{g_A}{\sqrt{2}f_\pi}\right)^2 \tag{5.3.2}$$

Energy is expressed in a dimensionless form as a multiple of $\hbar\omega$ and $\alpha = \sqrt{2}m_\pi b/\hbar$.

$$V_\pi(r) = \tilde{f}_\pi^2\frac{m_\pi}{\hbar\omega}\tau_1\cdot\tau_2\frac{e^{-\alpha r}}{\alpha r}\left[\left(1+\frac{3}{\alpha r}+\frac{3}{\alpha^2 r^2}\right)S_{12}+\sigma_1\cdot\sigma_2\right] \tag{5.3.3}$$

Matrix elements of S_{12} can be computed following related calculations by Mihaila [34].

$$\begin{aligned}\langle (S'\ell')\, J'm'\, |S_{12}|\, (S\ell)\, Jm\rangle = \delta_{J',J}\delta_{m',m}\delta_{S',S}\delta_{S,1}\delta_{\ell',\ell\pm 2,0}\, 2\sqrt{30}(-1)^{\ell'+j+1} \\ (2\ell+1)\sqrt{2\ell'+1}\,\langle \ell 020|\,\ell' 0\rangle \begin{Bmatrix} J & S & \ell' \\ 2 & \ell & S \end{Bmatrix} \begin{Bmatrix} \ell' & \ell' & 0 \\ \ell & \ell & 2 \end{Bmatrix}\end{aligned} \tag{5.3.4}$$

And the last piece is the scalar product of spins.

$$\langle S\,|\sigma_1\cdot\sigma_2|\,S\rangle = 4S-3 \tag{5.3.5}$$

The OPEP is accurate at longer range with $\rho > 4$ fm, which is generally outside the range of the non-edge matrix elements for reasonable length scales of the harmonic oscillator basis. One can think of V_{IR} as contributing an infinite set of LECs about which one expects that V_δ will be a convergent expansion. In the upcoming section on HOBET power counting Section 5.5 a connection between LECs and Talmi integrals is established that shows that higher order LECs are associated with longer range moments of the potential. The short range divergence of V_π will be automatically regulated by the included harmonic oscillator basis and corrected by V_δ.

The value of $\tilde{f}_\pi^2$ can be encoded as an extra "LEC" that will contribute linearly to H_{eff} matrix elements just as the real LECs do. The fitting process, described in the next chapter, configures the LECs to produce energy self-consistency of the effective Hamiltonian constructed at a set of energies. Fitting of $\tilde{f}_\pi^2$ will be most accurate at modest energies in a higher angular momentum channel such as F where the angular momentum barrier hides the short range part of the potential, leaving only the OPEP to influence scattering.

5.4 Constructing V_δ with a Contact Operator Expansion

In a momentum basis a contact gradient expansion is often used for an expansion around 0 momentum. In earlier HOBET work a modified contact gradient expansion was used to expand about the $\approx 1/b$ momentum scale of the lowest harmonic oscillator state. This expansion is briefly reviewed to motivate the approach used here.

5.4.1 Contact Gradient Expansion

In Haxton and Luu's earlier work on HOBET the expansion used for V_δ was a variant of a contact gradient expansion in powers of the Laplacian. LO and NLO operators in the S-channel had the form

$$\begin{aligned}\text{LO}: &\quad \exp\left(+r^2/2\right)\delta(r)\ \exp\left(+r^2/2\right) \\ \text{NLO}: &\quad \exp\left(+r^2/2\right)\overleftarrow{\nabla}^2\delta(r) + \delta(r)\overrightarrow{\nabla}^2\exp\left(+r^2/2\right)\end{aligned}$$

The added exponential factors, which are not used in momentum basis expansions, have the effect of canceling the Gaussian part of the harmonic oscillator basis functions on the left and right. The arrow over the Laplacian symbol in the middle of the sequence indicates the direction that it should be applied. The Laplacian is then applied to the polynomial part of the basis function, resulting in a decrease in the order of the polynomial. At the origin, $e^{-r^2/2} \to 1$ so the net result for the NLO operator is that that the maximum nodal number in the wave function being acted on is reduced, yielding a superposition of lower states in the same angular momentum channel.

A consequence of the lowering behavior is that a matrix element like $\langle 1S\,|V_\delta|\,1S\rangle$ is affected solely by the LO operator because high order operators will annihilate the states. With a potential V in hand one can directly calculate the matrix elements of $V\left(1/\left(E-QH\right)\right)QV$ using a large harmonic oscillator basis for intermediate values and a matrix inversion of $1/\left(E-QH\right)$. The resulting matrix elements can then be compared to the V_δ matrix expansion. The comparison immediately determines the LEC for the LO operator. Having determined it, the value can be substituted in the expressions for higher matrix elements. The result is that the next higher order matrix elements will now depend on a single LEC and their values can in turn be determined. This process can be repeated to determine all the LEC values. Because the lower order LECs are determined independently from the higher order ones and fixed, the procedure for determining the LEC values is a scheme independent one. The procedure used in this dissertation to fit to observables is also executed order by order, but lower order LECs are adjusted when higher order fits are done. A limitation in the scheme independent method is that the fixing procedure breaks down when the LECs at the order being determined appear only in edge state matrix elements. For $\Lambda = 8$ the limit was N3LO, and with that limit results for the bound state of the deuteron were within 0.01% of the exact results determined from Av_{18}.

5.4.2 General Contact Operator Expansion

In the previous section the gradient operators were modified by exponential factors. There is in fact quite a bit of flexibility in the definition of the operator. This freedom should be explored before choosing an expansion. In this section the dimensionality of r will not be explicitly stated, so integrals and delta functions may represent multi-dimensional cases. Wave functions and operators will be real. The first step is to write an expansion of a wave function in terms of abstract operators $O_r^{(n)}$ and complementary functions $f_n(r)$.

$$u(r) = \sum_n \left[\delta(r')O_{r'}^n u(r')\right] f_n(r) \tag{5.4.1}$$

A specific example of this construction has $O_r^{(n)} = \partial_r^n$ and $f_n(r) = r^n/n!$, which is also known as a Taylor's series expansion.

The eventual ET expansion will be

$$V_\delta = \sum_{n,m} LEC_{n,m} \overleftarrow{O}^{(m)} \delta(r) \overrightarrow{O}^{(n)}. \tag{5.4.2}$$

The arrows over the operators indicate the direction in which they are to be applied. Symmetries and hermiticity will create constraints between LECs. It is expected that the matrix elements of the ET expansion will match matrix element by matrix element with the matrix elements of

$$V_{renorm} = V - V_{IR} + V\frac{1}{E - QH}QV \tag{5.4.3}$$

An important detail is that even if V starts out as a local potential, the renormalization step will introduce non local contributions. In the case of a nuclear potential the finite size of the nucleons means that the interaction is fundamentally non-local anyway.

The matrix elements of V_{renorm} against a set of basis functions are

$$\begin{aligned}\langle u_a \left| V_{renorm} \right| u_b \rangle = \sum_{i,j} \Big[\delta(r) \left(O^{(i)} u_a \right) \left(O^{(j)} u_b \right) \\ \left(\int dr' dr'' f_i(r'') f_j(r') V_{renorm}(r'', r') \right) \Big]\end{aligned} \tag{5.4.4}$$

The integral in parenthesis can therefore be identified with the corresponding LEC_{ij}. If LECS are being fit without V in hand, then it won't be necessary to perform the integral or even explicitly know the form of $f_i(r)$, but the completeness of the wave function expansion Eq.(5.4.1) and the formal existence of the correspondence between the LEC and an integral tells us that the expansion works.

For HOBET the next step is to choose the set of operators.

5.4.3 Lowering Operator Expansion for Non-Edge States

Since the working basis is a harmonic oscillator basis, a natural set of operators are the nodal and angular momentum lowering operators. $\hat{a}$ is used as the nodal lowering operator and $\hat{c}$ as the lowering operator for ℓ. Details of these operators may be found in Appendix A.

The order of an operator is simply the number of nodal lowering operators acting to either side plus half the sum of the orbital angular momentum of the states being coupled. A standard naming convention is followed, using the prefixes a_{LO}, a_{NLO}, a_{NNLO}, a_{N3LO}, and continuing with digits to indicate the order of the operator. If the operator has more than one option for the splitting of the lowering operators to the left and right, then twice the counts is included as digits in the name. The factor of two exists to maintain naming compatibility with prior work where the count represented the number of derivatives applied by the operator. a^{20}_{NLO} indicates that $\hat{a}$ is applied to the left in one term and to the right in a second term to maintain hermiticity. Last, the angular momentum channel is included in the LEC name.

$$a^{20,S}_{NLO} \left(\hat{a}^\dagger \delta(r) + \delta(r) \hat{a} \right) \tag{5.4.5}$$

In the operator descriptions below the use of the delta function is replaced with it's matrix elements $d_{i,j}$, which are calculated in Section 5.4.4.

A useful fact is that the nuclear interaction conserves total angular momentum and parity. The nodal lowering operators naturally conserve angular momentum and parity so no additional constraints for single channel operators are required. Within a single channel with angular momentum ℓ the operator set included in V_δ is

$$\begin{aligned} \hat{v}^{\delta,S}_{q',q',\ell,\ell} &= LEC_{q',q',\ell,\ell} \qquad \sum_{i,j} d_{i,j} \left(\hat{c}^{\dagger \ell} \hat{a}^{\dagger\, q'} \left| i,0 \right\rangle \left\langle j,0 \right| \hat{a}^{q'} \hat{c}^{\ell} \right) \\ \hat{v}^{\delta,S}_{q',q<q',\ell,\ell} &= LEC_{q',q\,\ell,\ell} \quad \sum_{i,j} d_{i,j} \left(\hat{c}^{\dagger \ell} \hat{a}^{\dagger q'} \left| i,0 \right\rangle \left\langle j,0 \right| \hat{a}^{q} \hat{c}^{\ell} + \hat{c}^{\ell} \hat{a}^{\dagger q} \left| j,0 \right\rangle \left\langle i,0 \right| \hat{a}^{q'} \hat{c}^{\ell} \right) \end{aligned} \tag{5.4.6}$$

The nodal lowering operators can be turned around to act as raising operators on the delta function expansion, generating constants $K_{q',i,q,j}$, with $K = 0$ for $i, j < 1$, from the application of Eq.(A.3.12).

$$K_{q',i,q,j} = (-2)^{q'+q} \sqrt{\frac{\Gamma\left(q'+i\right)\Gamma\left(q'+i+1/2\right)\Gamma\left(q+j\right)\Gamma\left(q+j+5/2\right)}{\Gamma\left(i\right)\Gamma\left(i+1/2\right)\Gamma\left(j\right)\Gamma\left(j+5/2\right)}} \tag{5.4.7}$$

Examining the form of $d_{i,j}$ in Eq.(5.4.20) shows that K can be combined nicely with it.

$$d_{i,j} K_{q',i,q,i} = \frac{(-2)^{q'+q}\,\Gamma\left(q'+i\right)\Gamma\left(q+j\right)}{\Gamma\left(i\right)\Gamma\left(j\right)} d_{q'+i,q+j} \tag{5.4.8}$$

These operators are to be evaluated between states with the same ℓ. The generated constants are absorbed into $d^{\ell,\ell}_{n',n}$. A non-zero result occurs only for $n' = q' + i$ and $n = q + j$.

$$\left\langle n',\ell \left| \hat{v}^{\delta,S}_{q',q,\ell,\ell} \right| n,\ell \right\rangle = LEC_{q',q,\ell,\ell}\; d^{\ell,\ell}_{n',n}\; \frac{(-2)^{q'+q}\,\Gamma\left(n'\right)\Gamma\left(n\right)}{\Gamma\left(n'-q'\right)\Gamma\left(n-q\right)} \tag{5.4.9}$$

The nuclear interaction also includes a tensor interaction, coupling states of total spin $S = 1$ with ℓ differing by 2. Total angular momentum is conserved, but the distribution of angular momentum between the nucleon spins and orbital angular momentum can vary. The natural form of such an operator is the scalar product of the rank 2 spin tensor $\left[\sigma_1 \otimes \sigma_2\right]^{(2)}$ with a rank two tensor operator coupling states that differ by 2 in orbital angular momentum. The latter tensor operator is described as a combination of lowering operators and the expansion of the delta function. This operator is combined under the same LEC with its conjugate to maintain Hermiticity.

$$\hat{v}^{\delta,T}_{q',q,\ell,\ell+2} = LEC_{q',q,\ell,\ell+2} \sum_{i,j} d_{i,j} \left[\hat{c}^{\dagger \ell} \hat{a}^{\dagger q'} \left| i,0 \right\rangle \otimes \left\langle j,0 \right| \hat{a}^{q} \hat{c}^{\ell+2} \right]^{(2)} \odot \left[\sigma_1 \otimes \sigma_2\right]^{(2)} + h.c. \tag{5.4.10}$$

This operator is evaluated between states with $S = 1$ and $J = \ell + 1$.

$$\left\langle n',\left(\ell,S\right),\ell{+}1,0 \left| \hat{v}^{\delta,T}_{q',q,\ell,\ell+2} \right| n,\left(\ell{+}2,S\right),\ell{+}1,0 \right\rangle \tag{5.4.11}$$

Combining the matrix elements of the matrix function with the action of the nodal operators as in Eq.(5.4.8), the operator takes the form

$$LEC_{q',q,\ell,\ell+2}\sum_{i,j}\frac{(-2)^{q'+q}\Gamma(q'+i)\Gamma(q+j)}{\Gamma(i)\Gamma(j)}d_{q'+i,q+j}\left[\hat{c}^{\dagger\ell}\left|q'+i,0\right\rangle\otimes\left\langle q+j,0\right|\hat{c}^{\ell+2}\right]^{(2)}\odot\left[\sigma_1\otimes\sigma_2\right]^{(2)} \tag{5.4.12}$$

For matrix elements be non-zero it is required that $i=n'-q'>0$ and $j=n-q>0$.

$$\begin{aligned}\left\langle n',(\ell,S),\ell{+}1,0\left|\hat{v}^{\delta,T}_{q',q,\ell,\ell+2}\right|n,(\ell{+}2,S),\ell{+}1,0\right\rangle &= LEC_{q',q,\ell,\ell+2}\,\frac{(-2)^{q'+q}\Gamma(n')\Gamma(n)}{\Gamma(n'-q')\Gamma(n-q)}d_{n',n}\\ \times\left\langle n',(\ell,S),\ell{+}1,0\left|\left[\hat{c}^{\dagger\ell}\left|n',0\right\rangle\otimes\left\langle n,0\right|\hat{c}^{\ell+2}\right]^{(2)}\odot\left[\sigma_1\otimes\sigma_2\right]^{(2)}\right|n,(\ell{+}2,S),\ell{+}1,0\right\rangle&\end{aligned} \tag{5.4.13}$$

The tensor product $\left[\hat{c}^{\dagger\ell}\left|n',0\right\rangle\otimes\left\langle n,0\right|\hat{c}^{\ell+2}\right]^{(2)}\odot\left[\sigma_1\otimes\sigma_2\right]^{(2)}$ can be reduced using Edmonds (7.1.6). To begin, the reduced matrix elements of the two rank 2 tensors are needed. The reduced matrix element of the spin tensor is a simple constant.

$$\left\langle S=1\left\|\left[\sigma_1\otimes\sigma_2\right]^{(2)}\right\|S=1\right\rangle=2\sqrt{5} \tag{5.4.14}$$

Next the reduced matrix element for the operator connecting ℓ to $\ell+2$ is required. An easy to evaluate matrix element is chosen and the explicit tensor product expanded, generating a single non-zero contribution. The evaluation is done by applying the action of $\hat{c}$, Eq.(A.3.12), to the $\ell=0$ states in the delta function expansion.

$$\begin{aligned}d_{n',n}\left\langle n',\ell,0\left|\left[\hat{c}^{\dagger\ell}\left|n',0\right\rangle\otimes\left\langle n,0\right|\hat{c}^{\ell+2}\right]^{(2)}_{0}\right|n,\ell+2,0\right\rangle&\\ =\left\langle\ell,0,\ell{+}2,0\right|2,0\rangle\,d^{\ell,\ell+2}_{n',n}&\end{aligned} \tag{5.4.15}$$

Combining this result with a Clebsch-Gordan coefficient results in the second reduced matrix element.

$$\begin{aligned}d_{n',n}\left\langle n',\ell\left\|\left[\hat{c}^{\dagger\ell}\left|n',0\right\rangle\otimes\left\langle n,0\right|\hat{c}^{\ell+1}\right]^{(2)}\right\|n,\ell+2\right\rangle&=(-1)^{\ell}\,\frac{\sqrt{5}}{\left\langle\ell,0,\ell+2,0\right|2,0\rangle}\\ \times d^{\ell,\ell+2}_{n',n}\left\langle\ell,0,\ell{+}2,0\right|2,0\rangle&\\ =(-1)^{\ell}\,d^{\ell,\ell+2}_{n',n}\sqrt{5}&\end{aligned} \tag{5.4.16}$$

Edmonds (7.1.6) is applied to to Eq.(5.4.10).

$$\begin{aligned}&\left\langle n',(\ell,S),\ell{+}1,0\left|d_{n',n}\left[\hat{c}^{\dagger\ell}\left|n',\ell=0\right\rangle\otimes\left\langle n,\ell=0\right|\hat{c}^{\ell+2}\right]^{(2)}\odot\left[\sigma_1\otimes\sigma_2\right]^{(2)}\right|n,(\ell{+}2,S),\ell{+}1,0\right\rangle\\ &=\left\{\begin{array}{ccc}\ell{+}1 & 1 & \ell\\ 2 & \ell+2 & 1\end{array}\right\}\left((-1)^{\ell}\,d^{\ell,\ell+2}_{n',n}\sqrt{5}\right)\left(2\sqrt{5}\right)\\ &=(-1)^{\ell}\,d^{\ell,\ell+2}_{n',n}\frac{2\sqrt{5}}{\sqrt{2\ell+3}}\end{aligned} \tag{5.4.17}$$

Substituting into Eq.(5.4.13) produces the desired tensor and scalar matrix elements of V_δ.

$$\boxed{\begin{aligned}&\left\langle n', (\ell, S=1), \ell{+}1, 0 \left| \hat{v}^{\delta,T}_{q',q,\ell,\ell+2} \right| n, (\ell{+}2, S=1), \ell{+}1, 0 \right\rangle \\ &\qquad = LEC_{q',q,\ell,\ell+2}\ (-1)^\ell\, d^{\ell,\ell+2}_{n',n} \frac{2\sqrt{5}}{\sqrt{2\ell+3}} \frac{(-2)^{q'+q}\Gamma(n')\Gamma(n)}{\Gamma(n'-q')\Gamma(n-q)} \\ &\left\langle n', \ell \left| \hat{v}^{\delta,S}_{q',q,\ell,\ell} \right| n, \ell \right\rangle \\ &\qquad = LEC_{q',q,\ell,\ell}\, d^{\ell,\ell}_{n',n} \frac{(-2)^{q'+q}\,\Gamma(n')\,\Gamma(n)}{\Gamma(n'-q')\,\Gamma(n-q)}\end{aligned}} \tag{5.4.18}$$

5.4.4 Matrix Elements of the Delta Function

The matrix elements of a 3D delta function in a spherical harmonic oscillator basis are needed to implement the effective theory expansion. Only the $\ell = 0$ wave functions are non-zero at the origin.

$$d_{i,j} = \int d^3r\, \langle i,0|\vec{r}\rangle\, \delta^{(3)}(\vec{r})\, \langle \vec{r}|j,0\rangle = \int d\Omega dr\, r^2\, \langle i,0|r\rangle\, \frac{\delta(r)}{4\pi r^2}\, \langle \vec{r}|j,0\rangle$$

Simplifying

$$d_{i,j} = \int d\Omega dr\ H_{i,0}(r)\, Y_{00} \frac{\delta(r)}{4\pi} H_{j,0}(r)\, Y_{00} = \frac{2}{\pi^2} \sqrt{\frac{\Gamma(i+1/2)\,\Gamma(j+1/2)}{\Gamma(i)\,\Gamma(j)}} \tag{5.4.19}$$

For the picky, a definition of the 1D delta function is used such that

$$\int_0^\infty \delta(r) = 1$$

This is sometimes defined as 1/2 when the delta function spike is at the boundary of the integral.

For convenience in expressing matrix elements of the effective theory expansion the raising to ℓ' and ℓ is included in ket and bra of the operator using Eq.(A.3.12).

$$d^{\ell'\ell}_{i,j} = \frac{2^{(\ell'+\ell+2)/2}}{\pi^2} \sqrt{\frac{\ell'!\ \ell!}{(2\ell'+1)!!\ \ (2\ell+1)!!}} \sqrt{\frac{\Gamma(i+\ell'+1/2)\,\Gamma(j+\ell+1/2)}{\Gamma(i)\,\Gamma(j)}} \tag{5.4.20}$$

These matrix elements will be included in an overall factor that is constant for the angular momentum states coupled by the operator.

5.4.5 Evaluation of $\hat{c}^\ell H_{n,\ell}(r)$ at $r = 0$

A final part of the evaluation of effective theory operators is symbolically lowering left and right states to $\ell = 0$ and taking the value at $r = 0$ as part of a delta function. This is an easy operation for non-edge states, but computationally expensive for edge states which have analytic forms but many terms. The edge state wave function is an infinite superposition of radial states $\langle r|\, n, \ell, m\rangle$, so one can study the action of the lowering operator from that perspective. The analytic form is also challenging to evaluate at 0 because the expression contains terms diverging to both positive and negative infinity, canceling to leave a small remainder.

The solution to this problem has two parts. The first is to show that for a state of good total angular momentum ℓ that

$$\hat{c}^\ell H_{n,\ell}(r)\big|_{r=0} = \mathrm{K}(\ell)\, \partial_r^\ell H_{n,\ell}(r)\big|_{r=0}, \tag{5.4.21}$$

for a function $K(\ell)$ that does not depend on n. This is important because it means that this rule can be applied to superpositions of harmonic oscillator states.

The derivation of this result uses the fact the expansion of $H_{n,\ell}(r)$ contains a Gaussian factor, r^ℓ, and a Laguerre polynomial $L_{n-1}^{\ell+1/2}(r^2)$. When the differential operator is applied in $\hat{c}$, $(\partial_r + (\ell+1)/r + r)$, to $H_{n,\ell}(r)$, only the first two terms can reduce the power of r by one. The last term increases the power of r, meaning that it will make no contribution when evaluated at $r = 0$. One can also ignore the action of the derivative on the Gaussian because that will also increase the power of r. This leaves only $r^\ell L_{n-1}^{\ell+1/2}(r^2)$. Using the rule of throwing away terms that can't lead to non-zero contributions results in

$$\begin{aligned} &\partial_r r^\ell L_{n-1}^{(\ell+1/2)}\left(r^2\right) \to \ell r^{\ell-1} L_{n-1}^{(\ell+1/2)}\left(r^2\right) - \cancel{2r^{\ell+1} L_{n-1}^{(\ell+3/2)}\left(r^2\right)}, \\ &\left((\ell+1)/r\right) r^\ell L_{n-1}^{(\ell+1/2)}\left(r^2\right) \to (\ell+1)\, r^{\ell-1} L_{n-1}^{(\ell+1/2)}\left(r^2\right). \end{aligned} \tag{5.4.22}$$

This shows that the only difference, with respect to the eventual evaluation at $r = 0$, between the application of ∂_r (the first row) and $\hat{c}$ (the sum of both rows) is an ℓ dependent constant. $K(\ell)$ can be easily determined as the ratio

$$K(\ell) = \left.\frac{\hat{c}^\ell H_{1,\ell}(r)}{\partial_r^\ell H_{1,\ell}(r)}\right|_{r=0} = \sqrt{\frac{(2\ell+1)!!}{\ell!\, 2^\ell}} \tag{5.4.23}$$

The optional second part of the problem is to skip symbolic differentiation and the difficult evaluation at $r = 0$. Instead one can numerically compute the desired derivative from k evenly spaced samples starting away from 0. Taking $k > \ell$ samples with a step size s of the complicated function $f(r) = \langle r\,|\hat{a}^n|\, edge\rangle$ the ℓth derivative can be determined as

$$\begin{aligned} &\boldsymbol{f} = (f(s), f(2s), \ldots, f(ks)) \\ &\boldsymbol{M}_{ij} = \frac{i^{j-1}}{(j-1)!}, \quad i,j = 1\ldots k \\ &\boldsymbol{d} = \boldsymbol{M}^{-1}\boldsymbol{f} \\ &\partial_r^\ell f(r)\big|_{r=0} \approx \boldsymbol{d}_{\ell+1} s^{-\ell} \end{aligned} \tag{5.4.24}$$

These steps solve a set of linear equations formed by sampling a Taylor's series about $r = 0$ of degree $k-1$ at k points to produce the derivatives. It is a good idea to make k substantially larger than ℓ because the function will have higher order contributions. This procedure is fast and accurate.

5.4.6 Evaluation of Edge States Lowered to $\ell = 0$ at the Origin

Part of computing V_δ matrix elements for edge states will be lowering their ℓ content to 0 and evaluating the wave function at the origin. Edge state wave functions will be indicated by

$$\tilde{e}_\ell(r) = \langle r \left| G_{QT} \right| e, \ell, 0 \rangle = \sum_{j \in P_\ell} b^\ell_{e,j} G_T H_{j,\ell}(r) \tag{5.4.25}$$

The desired result is

$$\left\langle 0 \left| \hat{c}^\ell G_{QT} \right| e, \ell, 0 \right\rangle = \hat{c}^\ell \tilde{e}_\ell(r)\big|_{r=0} \tag{5.4.26}$$

In the equation below the summation is over all $j \in P$, but only states j with angular momentum $\ell = \ell_i$ will have non zero entries in b^ℓ_{ij}, so ℓ is used throughout.

$$\begin{aligned} \hat{c}^\ell \tilde{e}_\ell(r) &= \hat{c}^\ell \left\langle r \left| \frac{E}{E - QT} \right| n\ell 0 \right\rangle \\ &= \hat{c}^\ell \sum_{j \in P} b^\ell_{ij} \int_0^\infty dr' r'^2 G_T(r, r') H_{n_j \ell}(r) \end{aligned}$$

The Green's function Eq.(B.3.3) has two parts corresponding to $r < r'$ and $r > r'$. Only the first part is needed as r will remain infinitesimally close to 0.

$$\hat{c}^\ell \tilde{e}_\ell(r)\big|_{r=0} = k^3 \left(\hat{c}^\ell \, j_\ell(kr)\right)\big|_{r=0} \sum_{j \in P} b^\ell_{ij} \int_0^\infty dr' r'^2 \left(-\cot\delta_\ell j_\ell(kr') + \eta_\ell(kr')\right) H_{n_j \ell}(r')$$

The fact that all contributions have the same ℓ enables factoring $j_\ell(kr)$ out of the sum where $\hat{c}$ acts directly on it. Eq.(5.4.21) can be used to replace the lowering operator with a simple derivative.

$$\begin{aligned} \left(\hat{c}^\ell \, j_\ell(kr)\right)\big|_{r=0} &= K(\ell) \lim_{r \to 0} \partial^\ell_r j_\ell(kr) \\ &= K(\ell) k^\ell \lim_{u \to 0} \partial^\ell_u j_\ell(u) \\ &= K(\ell) k^\ell \ell! \lim_{u \to 0} u^{-\ell} j_\ell(u) \\ &= \frac{K(\ell)\ell!}{(2\ell+1)!!} k^\ell \end{aligned} \tag{5.4.27}$$

In the last step Abramowitz and Stegun [35] equation 10.1.4 was used to evaluate the limit. The other part of the result is had by expanding $H_{n\ell}(r)$ with Eq.(A.3.2) and integrating the pieces.

$$\int_0^\infty dr' r'^2 \left(-\cot\delta_\ell j_\ell\left(kr'\right)+\eta_\ell\left(kr'\right)\right) H_{n_j\ell}\left(r'\right) = \sqrt{\frac{2\Gamma(n)}{\Gamma(n+\ell+1/2)}}\Gamma(n+\ell+1/2)$$
$$\times \sum_{p=0}^{n_j-1} \frac{(-1)^p}{(n-p-1)!\,\Gamma(p+\ell+3/2)\,p!} \int_0^\infty dr' \left(-\cot\delta_\ell j_\ell\left(kr'\right)+\eta_\ell\left(kr'\right)\right) e^{-r'^2/2} r'^{2p+\ell+2}$$

The two definite integrals are standard results.

$$\int_0^\infty dr r^2 j_\ell\left(kr\right) e^{-r^2/2} r^m = \frac{k^\ell\sqrt{\pi}\Gamma\left(\left(\ell+m+3\right)/2\right)}{\sqrt{2^{\ell-m+1}}\Gamma\left(\ell+3/2\right)}\ {}_1F_1\left(\frac{\ell+m+3}{2},\ \ell+\frac{3}{2},\ -\frac{k^2}{2}\right)$$
$$\int_0^\infty dr r^2 \eta_\ell\left(kr\right) e^{-r^2/2} r^m = \frac{\sqrt{2^{\ell+m}\pi}\Gamma\left(\left(-\ell+m+2\right)/2\right)}{(-k)^{\ell+1}\Gamma\left(1/2-\ell\right)}\ {}_1F_1\left(\frac{-\ell+m+2}{2}, -\ell+\frac{1}{2}, -\frac{k^2}{2}\right)$$

Letting $X(\ell,m,k)$ be the first integral and $Y(\ell,m,k)$ be the second, the complete result can be stated as follows.

$$\hat{c}^\ell \tilde{e}_\ell\left(r\right)\big|_{r=0} = \frac{K\left(\ell\right)\ell!}{(2\ell+1)!!} k^{\ell+3} \sum_{j\in P} b_{ij}^\ell \sqrt{2\Gamma(n_j)\Gamma(n_j+\ell+1/2)} \tag{5.4.28}$$
$$\times \sum_{p=0}^{n_j-1} \frac{(-1)^p}{(n_j-p-1)!\,\Gamma(p+\ell+3/2)\,p!} \left(-\cot\delta_\ell\ X\left(\ell,2p+\ell,k\right)+Y\left(\ell,2p+\ell,k\right)\right)$$

This expression also gives the result for a derivative repeated ℓ times, for which one should omit the factor $K(\ell)$.

5.4.7 Lowering Operator Expansion for Edge States

In Eq.(5.4.18) one can see that the scalar matrix elements of $v^{\delta,S}_{q',q,\ell,\ell}$ come from the delta function and the action of the nodal and angular momentum lowering operators. The tensor matrix elements are almost the same, gaining a simple ℓ dependent constant $2\sqrt{5}/\sqrt{2\ell+3}$. This gives us the recipe to evaluate matrix elements of edge states, $G_{QT}\left|e,\ell\right\rangle$, where $\left|e+1,\ell\right\rangle$ is in Q. The technique described here can be applied to non edge states and the results can be compared to Eq.(5.4.18) as an important check of the implementation.

The effect of $\hat{a}$ on the edge states can be directly calculated. To start, the edge state expansion and a useful associated function $S_{m,n}(r)$ are defined.

$$\begin{aligned}
\tilde{e}(r) &= \langle r \left| G_{QT} \right| e, \ell \rangle = \sum_{j \in P_\ell} b_{e,j} \frac{E}{E-T} H_{j,\ell}(r) \\
S_{0,0}(r) &= (E-T)\, \tilde{e}(r) = E \sum_{j \in P_\ell} b_{e,j} H_{j,\ell}(r) \\
S_{m,n}(r) &= \hat{c}^m \hat{a}^n S_0 = E \sum_{j \in P_\ell} b_{e,j}\, \hat{c}^m \hat{a}^n H_{j,\ell}(r)
\end{aligned} \tag{5.4.29}$$

Looking ahead, the differential operator form of $\hat{a}$ from Eq.(A.5.3) can also be written in a useful form for acting on $\tilde{e}$ in terms of the kinetic energy operator.

$$\begin{aligned}
\hat{a} &= (1/2)(\partial_r^2 + (2/r)\partial_r - \ell(\ell+1)/r^2) + \frac{3}{2} + \frac{1}{2} r^2 + r\partial_r \\
\hat{a} &= (E-T) + \frac{3}{2} - E + \frac{1}{2} r^2 + r\partial_r
\end{aligned}$$

Some commutators will also be useful in the derivation.

$$\begin{aligned}
\left[T, r^2\right] &= -2r\partial_r - 3 \\
\left[T, r^n\right] &= -n r^{n-1} \partial_r - (n(n+1)/2) r^{n-2} \\
\left[T, r\partial_r\right] &= 2T
\end{aligned}$$

Applying the second form of lowering operator to the edge state causes $(E-T)$ to demote $\tilde{e}(r)$ to $S_{0,0}(r)$ and results in

$$\hat{a}\tilde{e}(r) = \left(\frac{3}{2} - E + \frac{1}{2} r^2 + r\partial_r \right) \tilde{e}(r) + S_{0,0}(r) \tag{5.4.30}$$

For $\ell = 0$ terms with remaining powers of r will vanish at the origin. The $\ell > 0$ cases still need the application of b^ℓ to lower the angular momentum to 0 before evaluation. The $\ell = 0$ case evaluated at $r = 0$ as is needed for the V_δ matrix elements yields a simple expression.

$$\hat{a}\tilde{e}(r)|_{r=0} = \left(\frac{3}{2} - E \right) \tilde{e}(0) + S_{0,0}(0) \tag{5.4.31}$$

The next step is to generalize the procedure. Further application of $\hat{a}$ will act directly on $S_{0,k}$, sending it to $S_{0,k+1}$. This suggests that the result of applying $\hat{a}$ m times can be written as a sum of coefficient operators times $S_{0,i}(r)$ and $\tilde{e}(r)$. In the base case of the expression below $m = 0$, $\beta^{(0)} = 1$ and there are no $\alpha_k^{(0)}$.

$$\hat{a}^m \tilde{e}\,(r) = \beta^{(m)} \tilde{e}\,(r) + \sum_{k=0}^{m-1} \alpha_k^{(m)} S_{0,k}\,(r) \tag{5.4.32}$$

Applying $\hat{a}$ generates the next result.

$$\begin{aligned}\hat{a}^{m+1}\tilde{e}\left(r\right) &= \hat{a}\left[\beta^{(m)}\tilde{e}\left(r\right)+\sum_{k=0}^{m-1}\alpha_k^{(m)}S_{0,k}\left(r\right)\right]\\ &= \left(\left[\hat{a},\beta^{(m)}\right]+\beta^{(m)}\left(\frac{3}{2}-E+\frac{1}{2}r^2+r\partial_r\right)\right)\tilde{e}\left(r\right)+\beta^{(m)}S_{0,0}\left(r\right)\\ &\quad+\sum_{k=0}^{m-1}\left(\left[\hat{a},\alpha_k^{(m)}\right]S_{0,k}\left(r\right)+\alpha_k^{(m)}S_{0,k+1}\left(r\right)\right)\end{aligned} \tag{5.4.33}$$

The expression above can now be reorganized to put it back in the original form, yielding a recursive procedure for constructing the next result.

$$\begin{aligned}\alpha_{-1}^{(m)} &= \beta^{(m)}-\gamma,\quad \alpha_m^{(m)}=0\\ \alpha_k^{(m+1)} &= \left[\hat{a},\alpha_k^{(m)}\right]+\alpha_{k-1}^{(m)}\\ \beta^{(m+1)} &= \left(\left[\hat{a},\beta^{(m)}\right]+\beta^{(m)}\left(\frac{3}{2}-E+\frac{1}{2}r^2+r\partial_r\right)\right)+\gamma(E-T)\\ \hat{a}^{m+1}\tilde{e}\left(r\right) &= \beta^{(m+1)}\tilde{e}\left(r\right)+\sum_{k=0}^{m}\alpha_k^{(m+1)}S_{0,k}\left(r\right)\end{aligned}$$

The newly introduced γ factor is used to transfer a term of the form $-\gamma(E-T)$ generated by the commutator $\left[\hat{a},\beta^{(m)}\right]$ from $\beta^{(m+1)}$ to the $\alpha_0^{(m+1)}$ via $\alpha_{-1}^{(m)}$. The above expressions give the rules for producing $\beta^{(m)}$ and $\alpha_k^{(m)}$ from the $m-1$ expressions. Applying them to produce the pieces of $\beta^{(2)}$ yields the following.

$$\begin{aligned}\left[\hat{a},\beta^{(1)}\right] &= -\left[T,\ \frac{1}{2}r^2+r\partial_r\right]=-2T+\frac{3}{2}+r\partial_r\\ \left(\beta^{(1)}\right)^2 &= r^2\partial_r^2+\left(r^3+4r-2rE\right)\partial_r+\left(E^2-3E+\frac{9}{4}+\left(\frac{5}{2}-E\right)r^2+\frac{1}{4}r^4\right)\end{aligned} \tag{5.4.34}$$

To form $\beta^{(2)}$ the T is removed by setting $\gamma=-2$, which also makes a compensating contribution to $\alpha_{-1}^{(1)}$ and subtracts $2E$ from $\beta^{(m+1)}$.

$$\beta^{(2)}=r^2\partial_r^2+\left(r^3+5r-2rE\right)\partial_r+\left(E^2-5E+\frac{15}{4}+\left(\frac{5}{2}-E\right)r^2+\frac{1}{4}r^4\right) \tag{5.4.35}$$

The $\alpha^{(2)}$ coefficients are needed too.

$$\begin{aligned}\alpha_0^{(2)} &= [\hat{a},1]+\beta^{(1)}-\gamma=\left(\frac{7}{2}-E+\frac{1}{2}r^2+r\partial_r\right)\\ \alpha_1^{(2)} &= 1\end{aligned}$$

The result for $\ell = 0$ is

$$\hat{a}^2\tilde{e}(r)\big|_{r=0} = \left(E^2 - 5E + \frac{15}{4}\right)\tilde{e}(0) + \left(\frac{7}{2} - E\right)S_{0,0}(r) + S_{0,1}(r) \tag{5.4.36}$$

The calculation of $\hat{a}^3\tilde{e}(r)|_{r=0}$ raises a new issue. It is possible to have terms like ∂_r^2 or $r^{-1}\partial_r$ that are not protected by a power of r. Since the evaluation is near 0 one can treat the multiplication of a function that goes to 0 at $r = 0$ by r^{-1} as a derivative operation. This means that $r^{-1}\partial_r \to \partial_r^2$ and $r^{-2} \to (1/2)\partial_r^2$, which can in turn be converted to a T operator. Skipping some of the details, a preliminary $\beta^{(3)}$ is calculated with $\gamma = -4\,(1 + E)$.

$$\begin{aligned}
\beta^{(3)} = &\left(r^3 + 2r\right)\partial_r^3 + \left(8 + \left(\frac{23}{2} - 3E\right)r^2 + \frac{3}{2}r^4\right)\partial_r^2 \\
&+ \left(4\left(-\ell^2 - \ell + 1\right)r^{-1} + \left(\frac{113}{4} - 17E + 3E^2\right)r + \left(\frac{21}{2} - 3E\right)r^3 + \frac{3}{4}r^5\right)\partial_r \\
&+ \frac{1}{8}r^6 + \left(-\frac{3}{4}E + \frac{21}{8}\right)r^4 + \left(\frac{3}{2}E^2 - \frac{17}{2}E + \frac{105}{8}\right)r^2 \\
&+ \left(-E^3 + \frac{21}{2}E^2 - \frac{73}{4}E + \frac{105}{8} - 2\ell\,(\ell + 1)\right)
\end{aligned}$$

$$\begin{aligned}
\alpha_0^{(3)} = &\left[\hat{a}, \left(\frac{7}{2} - E + \frac{1}{2}r^2 + r\partial_r\right)\right] + \beta^{(2)}(r) - \gamma \\
&= -2T + r^2\partial_r^2 + \left(r^3 - 2rE + 6r\right)\partial_r + \left(E^2 - 9E + \frac{37}{4} + \frac{5}{2}r^2 + \frac{1}{4}r^4 - Er^2\right) \\
\alpha_1^{(3)} = &\frac{7}{2} - E + \frac{1}{2}r^2 + r\partial_r \\
\alpha_2^{(3)} = &1
\end{aligned}$$

In the expression for $\alpha_0^{(3)}$ the operator T appears on the right hand side. T can be expressed in terms of $\hat{a}$ as $T = -\hat{a} + 3/2 + r^2/2 + r\partial_r$. The resulting $\hat{a}$ can then be applied to $S_{0,0}(r)$, promoting it to $S_{0,1}(r)$.

In the expression for $\beta^{(3)}$ expression there are terms that can be converted to references to T very near $r = 0$. They are first collected into a single term with coefficient A.

$$8\partial_r^2 + 4\left(-\ell^2 - \ell + 1\right)r^{-1}\partial_r \to -4\left(\ell^2 + \ell - 3\right)\partial_r^2 = A\partial_r^2 \tag{5.4.37}$$

Then the coefficient of ∂_r^2 is converted to a coefficient for T very near $r = 0$.

$$\begin{aligned}
A\partial_r^2 &= B(-1/2)\left(\partial_r^2 + 2\partial_r^2 - \ell\,(\ell + 1)\,\frac{1}{2}\partial_r^2\right) = BT \\
B &= \frac{4A}{\ell^2 + \ell - 6} = -16\frac{\ell^2 + \ell - 3}{\ell^2 + \ell - 6}
\end{aligned}$$

To compensate for the additional BT term in $\beta^{(3)}$, γ is adjusted to include B.

$$\gamma^{(3)} = -4(1+E) + B = -4(1+E) - 16\frac{\ell^2+\ell-3}{\ell^2+\ell-6} \tag{5.4.38}$$

These change flows through to $\beta^{(3)}$, $\alpha_0^{(3)}$ and $\alpha_1^{(3)}$.

$$\begin{aligned}
\beta^{(3)} =& \left(r^3+2r\right)\partial_r^3 + \left(\left(\frac{23}{2}-3E\right)r^2+\frac{3}{2}r^4\right)\partial_r^2 \\
&+\left(\left(\frac{113}{4}-17E+3E^2\right)r+\left(\frac{21}{2}-3E\right)r^3+\frac{3}{4}r^5\right)\partial_r \\
&+\frac{1}{8}r^6+\left(-\frac{3}{4}E+\frac{21}{8}\right)r^4+\left(\frac{3}{2}E^2-\frac{17}{2}E+\frac{105}{8}\right)r^2 \\
&+\left(-E^3+\frac{21}{2}E^2+\left(-\frac{73}{4}-16\frac{\ell^2+\ell-3}{\ell^2+\ell-6}\right)E+\frac{105}{8}-2\ell\left(\ell+1\right)\right) \\
\alpha_0^{(3)} =& \left[\hat{a},\left(\frac{7}{2}-E+\frac{1}{2}r^2+r\partial_r\right)\right]-\gamma = \\
=& r^2\partial_r^2+\left(r^3-2rE+6r\right)\partial_r+\left(E^2-9E+\frac{25}{4}+16\frac{\ell^2+\ell-3}{\ell^2+\ell-6}+\frac{5}{2}r^2+\frac{1}{4}r^4-Er^2\right) \\
\alpha_1^{(3)} =& \frac{11}{2}-E+\frac{1}{2}r^2+r\partial_r \\
\alpha_2^{(3)} =& 1
\end{aligned}$$

For $\ell = 0$ the result is

$$\begin{aligned}
\hat{a}^3\tilde{e}(r)\big|_{r=0} =& \left(-E^3+\frac{21}{2}E^2-\frac{105}{4}E+\frac{105}{8}\right)\tilde{e}(0) \\
&+\left(E^2-9E+\frac{57}{4}\right)S_{0,0}(0)+\left(-E+\frac{11}{2}\right)S_{0,1}(0)+S_{0,2}(0)
\end{aligned}$$

For $\ell > 0$ the resulting expressions for $\hat{a}^m\tilde{e}(r)$ have a list of terms with a simple form.

$$c\, r^n\partial_r^m f(r)$$

The symbol c is a constant, and $f(r)$ is either $\tilde{e}(r)$ or $S_{0,k}(r)$. To finish the contribution to a matrix element the angular momentum also needs to be lowered to 0. If $\ell < n$, the power of r in the term, then the result will have a remaining power of r and will yield 0. Assuming instead that $\ell >= n$, the lowering of ℓ can be determined using results from Section 5.4.5 as follows.

$$\begin{aligned}
\hat{c}^\ell\left(c\, r^n\partial_r^m f(r)\right)\big|_{r=0} &= c\, K(\ell)\partial_r^\ell r^n\partial_r^m f(r)\big|_{r=0} \\
&= c\, K(\ell)\frac{\ell!}{(\ell-n)!}\left(\partial_r^{\ell+m-n}f(r)\big|_{r=0}\right)
\end{aligned}$$

The final application of the derivative to $f(r)$ may be done numerically as described in Section 5.4.5 which is simple and accurate but will require extended precision for $\tilde{e}(r)$ if the extrapolation points are taken very close to 0. An alternative analytic solution for lowering $\tilde{e}(r)$ to $\ell = 0$ and evaluating at 0 is given in Section 5.4.6. As usual, the numeric technique is simple to implement and provides a crosscheck for the analytic solution. For $S_{0,i}(r)$ is it straightforward to apply $\hat{c}^m$ to the defining sum over harmonic oscillator basis functions to produce $S_{m,i}(r)$.

5.4.8 Edge State V_δ Summary

V_δ matrix elements are formed from operator pairs $\hat{c}^\ell \hat{a}^n$ acting to the left and right that can be independently evaluated at the origin. The tables below give results for the action of one of the operators, left or right, acting on a state with angular momentum ℓ and evaluated at 0. All such states, including edge states, have a minimum power of r^ℓ in their wave function, so the operators must have $\hat{c}^\ell$ in them or evaluating the result at $r = 0$ will yield 0. To simplify the notation in the table, W_ℓ will represent $\hat{c}^\ell \tilde{e}(r)\big|_{r=0}$ for an edge state with angular momentum ℓ and can be evaluated using Eq.(5.4.28). The definition of $S_{m,n}(r)$ may be found in Eq.(5.4.29). The following formulas, which are sufficient up to N3LO. These formula are also correct for non edge states, which is useful in testing correctness.

Results for S($\ell = 0$) are

n	Result
0	W_0
1	$(-E + 3/2)\, W_0 + S_{0,0}(0)$
2	$(E^2 - 5E + 15/4)\, W_0 + (-E + 7/2)\, S_{0,0}(0) + S_{0,1}(0)$
3	$(-E^3 + (21/2)E^2 - (105/4)E + 105/8)\, W_0 + (E^2 - 9E + 57/4)\, S_{0,0}(0)$ $+ (-E + 11/2)\, S_{0,1}(0) + S_{0,2}(0)$

Results for P($\ell = 1$) are

n	Result
0	W_1
1	$(-E + 5/2)\, W_1 + S_{1,0}\,(0)$
2	$(E^2 - 7E + 35/4)\, W_1 + (-E + 9/2)\, S_{1,0}\,(0) + S_{1,1}\,(0)$

Results for D($\ell = 2$) are

n	Result
0	W_2
1	$(-E + 7/2)\, W_2 + S_{2,0}\,(0)$
2	$(E^2 - 9E + 63/4)\, W_2 + (-E + 11/2)\, S_{2,0}\,(0) + S_{2,1}\,(0)$

Results for F($\ell = 3$) are

n	Result
0	W_3
1	$(-E + 9/2)\, W_3 + S_{3,0}\,(0)$
2	$(E^2 - 11E + 123/4)\, W_3 + (-E + 13/2)\, S_{3,0}\,(0) + S_{3,1}\,(0)$

Results for G($\ell = 4$) are

n	Result
0	W_4
1	$(-E + 11/2)\, W_4 + S_{4,0}\,(0)$
2	$(E^2 - 13E + 239/4)\, W_4 + (-E + 15/2)\, S_{4,0}\,(0) + S_{4,1}\,(0)$

5.5 Power Counting in HOBET

HOBET's intended use is to fit the LECs to observables without knowledge of short-range physics. Without an explicit representation of the short-range physics there is no explicit power counting, e.g., a series expansion in a small scaling parameter like a ratio of pion mass to a cutoff mass.

In testing of HOBET, the order by order values of observables and wave functions can be compared to known results to gain confidence in HOBET's convergence, but it is good to give some theoretical justification for the convergence. With a explicit model for V_{renorm}, defined in Eq.(5.4.3), the LECs can be explicitly calculated.

$$V_{renorm}(\rho) = V_{core} e^{-(\rho/R_0)^2} = V_{core} e^{-2(b/R_0)^2 r^2} \tag{5.5.1}$$

This potential represents a hard core that might be omitted from a $V_{IR}(r)$ function. It is expected that the range of of the short range part of V that is omitted from from $V_{IR}(r)$ is substantially less than the harmonic oscillator length scale b. It is also a local correction, which simplifies the analysis below, but doesn't change the conclusion.

Because of a relationship between the gradient operator and the harmonic oscillator lowering operator the LECs can be determined from Talmi integrals of the potential. The Talmi integral of $V(r)$ is a moment of $V(r)$ and is defined in Moshinsky section 1.2 [36] as

$$I_p \equiv \frac{2}{\Gamma(p + 3/2)} \int_0^\infty dr r^2\, V(r) e^{-r^2} r^{2p} \tag{5.5.2}$$

The generalization to non local potentials involves separation of the power $2p$ into a left and right power and integration over two sets of spatial coordinates. Applying this simpler definition to $V_{renorm}(r)$ yields the following.

$$I_p = V_{core} \left(1 + \frac{2b^2}{R_0^2}\right)^{-p-3/2} \tag{5.5.3}$$

The connection between Talmi integrals and matrix elements in a harmonic oscillator basis is apparent when one expands the Laguerre polynomial of the radial function.

$$h_{n,\ell}(r) = e^{-r^2/2} r^\ell \sum_{k=0}^{2(n-1)} a_{n,\ell,k} r^{2k}, \qquad a_{n,\ell,k} = \frac{(-1)^k \sqrt{2\Gamma(n)\Gamma(n+\ell+1/2)}}{(n-k-1)!\Gamma(k+\ell+3/2)k!} \tag{5.5.4}$$

Harmonic oscillator matrix elements may be expanded in terms of Talmi integrals.

$$\langle n'\ell m \,|V(r)|\, n\ell m\rangle = \sum_{p=\ell}^{\ell+n'+n-2} B(n',\ell,n,\ell,p) I_p$$
$$B(n',\ell',n,\ell,p) = \frac{1}{2}\Gamma\left(p+\frac{3}{2}\right) \sum_{k+k'=p-(\ell'+\ell)/2} a_{n',\ell',k'} a_{n,\ell,k}$$

The above relationship between harmonic oscillator matrix elements and Talmi integrals can be easily inverted because each increase in n' or n introduces just one new Talmi integral.

$$I_{\ell+0} = \frac{1}{B(1,\ell,1,\ell,\ell)} \langle 1,\ell,m \,|V(r)|\, 1,\ell,m\rangle$$
$$I_{\ell+1} = \frac{1}{B(2,\ell,1,\ell,\ell+1)} \left(\langle 2,\ell,m \,|V(r)|\, 1,\ell,m\rangle - B(2,\ell,1,\ell,\ell) I_\ell\right)$$
$$I_{\ell+j} = \frac{1}{B(j+1,\ell,1,\ell,\ell+j)} \left(\langle j+1,\ell,m \,|V(r)|\, 1,\ell,m\rangle - \sum_{m=0}^{j-1} B(j+1,\ell,1,\ell,\ell+m) I_{\ell+m}\right)$$

Focusing on $\ell = 0$, on the left side Eq.(5.5.3) can be inserted for I_p and on the right the scalar V_δ expansion from Eq.(5.4.18) can be inserted, establishing the relationship between Talmi integrals and LECs. After some simplification one obtains the following expressions for the LECs.

$$a_{LO} = \pi^{3/2} I_0 = V_{core} \pi^{3/2} \left(1+\frac{2b^2}{R_0^2}\right)^{-3/2}$$
$$a_{NLO} = \frac{\pi^{3/2}}{2} I_1 = V_{core} \frac{\pi^{3/2}}{2} \left(1+\frac{2b^2}{R_0^2}\right)^{-5/2}$$
$$a_{NNLO} = \frac{\pi^{3/2}}{8} I_2 = V_{core} \frac{\pi^{3/2}}{8} \left(1+\frac{2b^2}{R_0^2}\right)^{-5/2}$$
$$a_{N3LO} = \frac{\pi^{3/2}}{48} I_3 = V_{core} \frac{\pi^{3/2}}{48} \left(1+\frac{2b^2}{R_0^2}\right)^{-7/2}$$
$$a_{NxLO} = \frac{\pi^{3/2}}{2^{x-1}(x-1)!} I_x = V_{core} \frac{\pi^{3/2}}{2^{x-1}(x-1)!} \left(1+\frac{2b^2}{R_0^2}\right)^{-(2x+1)/2}$$

The LECs of the expansion are controlled by the power-law dependence on $(1 + 2b^2/R_0) > 1$ as well as factorial and geometric factors.

The decline in LEC values reflects the declining importance of higher order Talmi integrals which progressively weigh longer distances as can be seen in Figure (5.4). Equally important is that higher order Talmi basis functions become insensitive to short range parts of $V(r)$. For a realisitic potential the hard core is mostly inside of 0.5 fm, and with $b = 1.7$ fm the corresponding value of r is 0.2, so only the lower p value Talmi integrals shown in the figure are directly sensitive to the hard core. The other part of $V_{renorm}(r)$ is $V(1/(E - QH))QV$, which will smear out beyond the hard core but remains limited by the range of V which is presumed to be a short range nuclear potential, so the principle still applies. Higher order LECs correspond to higher order Talmi integrals that in turn are suppressed by the short range potential. Even if the length scale of the harmonic oscillator is made small enough that $(1 + 2b^2/R_0) \approx 1$, the LECs will still converge because of the factorial and geometric factor in the denominator, but convergence will be delayed.

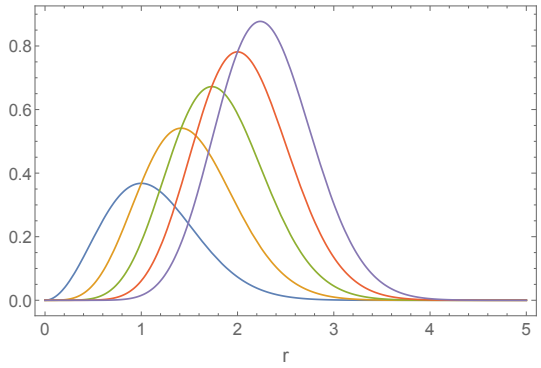

Figure 5.4: Talmi basis functions $e^{-r^2} r^{2p+2}$ with p ranging from 0 to 4 and scaled with $1/p!$ for viewing. The peak of each curve is located at $\sqrt{p+1}$.

5.6 Removing Correctable Parts of V_{IR}

Short range parts of V_{IR} do not represent real physics because unknown short range physics corrects it. It make sense then to remove from V_{IR} contributions that can be corrected by LECs introduced in non-edge states. As seen in the previous section LECs are associated with Talmi integrals and that association can be exploited to calculate them. However, given that harmonic oscillator matrix elements of V_{IR} must be taken for other purposes, it is easier to directly equate the matrix elements in P^- with the expansion Eq.(5.4.18). The lowest order LECs in each channel are immediately determined. Substituting the determined LECs into the remaining equations determines the next order and so on.

A related issue is that V_{IR} may diverge at $r = 0$. The Harmonic oscillator basis is a basis for $L^2(\mathbb{R})$ which does not include functions diverging as fast or faster than $r^{-1/2}$. A

strongly divergent V_{IR} such as occurs with a one pion exchange potential in a tensor channel is therefore not representable in the basis, so a representation in terms of an infinite set of LECs is only a partial representation. V_{UV} must contain a matching counter contribution that cancels the divergence because $V = V_{UV} + V_{IR}$ lacks such a divergence, so nothing is actually lost. The lack of representation of strong divergence can be regarded as an automatic subtraction of the non-physical divergent behavior of V_{IR}.

5.7 Green's Functions in the Coupled Channel Case

In 5.1 the boundary conditions were set by the phase shift of the asymptotic wave function. The concept needs generalization for for coupled channels. The observable used to construct asymptotic boundary conditions is the S-matrix. For most channels of the nuclear interaction the S-matrix is diagonal and one can simply use the phase shift δ_ℓ in the channel to implement the asymptotic boundary condition for the Green's function for $E/(E-T)$ by setting the coefficient for the homogeneous term to $-\cot\delta_\ell$. However, the nuclear interaction also includes a tensor interaction which couples triplet states differing in ℓ by 2. The result is a set of 2×2 subblocks of $S(E)$ that mix these pairs of channels. One cannot simply read off a phase shift from $S(E)$ to implement the asymptotic constraint. In what follows one such sub-block will be selected and referred to as the S-matrix. The coupled channesl will be referred to as S and D channels, meaning ${}^3S_1$ and ${}^3D_1$ and it should be understood that the following discussion applies to all such pairs of coupled channels.

A common parameterization of $S(E)$ is the "nuclear-bar" parameterization and many tables specifying experimental parameter values at a range of energies are available. As can be seen below the S-matrix is a complex symmetric matrix.

$$S = \begin{pmatrix} e^{2i\bar{\delta}_0}\cos 2\bar{\Sigma} & e^{i\left(\bar{\delta}_0+\bar{\delta}_2\right)} i\sin 2\bar{\Sigma} \\ e^{i\left(\bar{\delta}_0+\bar{\delta}_2\right)} i\sin 2\bar{\Sigma} & e^{2i\bar{\delta}_2}\cos 2\bar{\Sigma} \end{pmatrix} \tag{5.7.1}$$

The problem here is to extract the asymptotic boundary conditions from the S-matrix. The desired asymptotic boundary condition is a consistent pair of phase shifts to apply to S and D channels. The key requirement for our implementation on the asymptotic wave function is that it be real. Suppose the input state is described as a pair of coefficients $C_{in,S}$ and $C_{in,D}$ for S and D channel input states. Then $C_{out} = SC_{in}$. To obtain a real total wave function it is required that $|C_{out,S}| = |C_{in,S}|$ and $|C_{out,D}| = |C_{in,D}|$. An easy way to obtain such input states is to diagonalize the above S-matrix, putting it in a form known as the Blatt-Biedenharn or eigen phase parameterization [37]. Note that this is the same S matrix, only the parameterization has changed. The columns of O below are simply the normalized eigenvectors of S, which must be orthogonal and real, parameterized by angle Σ.

$$S{=}O^{-1}\begin{pmatrix} e^{2i\delta_0} & 0 \\ 0 & e^{2i\delta_2} \end{pmatrix} O, \text{ with } O{=}\begin{pmatrix} \cos\Sigma & -\sin\Sigma \\ \sin\Sigma & \cos\Sigma \end{pmatrix} \tag{5.7.2}$$

The rows of O then specify two orthogonal input states that the S matrix maps to output states with coefficients of the same magnitude in each channel. The multi channel state corresponding to the first row picks up a phase shift of δ_0 for both channels and the state corresponding to the second row picks up a phase shift of δ_2. If the potential couples 4 channels, then one would obtain 4 input states and 4 phase shifts. Each such state generates an independent boundary condition for the involved channels. In each case the sum of the incoming wave function and resulting outgoing wave function can be made real with an appropriate phase factor and any asymptotic solution can be written as a superposition of the base states. In the two channel case the asymptotic basis can be written as follows.

$$|x\rangle = \cos(\Sigma)\,|S\rangle - \sin(\Sigma)\,|D\rangle$$
$$|y\rangle = \sin(\Sigma)\,|S\rangle + \cos(\Sigma)\,|D\rangle$$

If $|x\rangle$ is used as the asymptotic boundary condition, then both S and D components will have δ_0 as the phase shift. Likewise, if $|y\rangle$ is used, then both S and D components will have δ_2 as the phase shift.

For concreteness, with an Argonne v_{18} based S-matrix at 5 MeV the parameters are $\delta_0 = -1.35087$, $\delta_2 = -0.011847$, and $\Sigma = -0.0205005$. Because Σ is quite small, $\cos\Sigma$ is near 1 and $\sin\Sigma$ is quite small. Consequentially, $|x\rangle$ is mostly S-channel and $|y\rangle$ is mostly D-channel.

It is important to note that the phase shifts are used in building the Green's function, but the relative amplitudes of the S and D channel wave functions specified by the S-matrix are ignored in the process. The relative amplitude is controlled by the mixing angle, which is an essential part of the S-matrix.

Another way of looking at this is that since $|x\rangle$ is mostly S-channel the eigenvalues of H_{eff} built with $|x\rangle$ as a boundary condition will be sensitive to the S to S matrix elements of V_δ. Likewise, H_{eff} built with $|y\rangle$ as a boundary condition will be sensitive to the D to D matrix elements of V_δ. What is needed to make the fit sensitive to the S to D matrix elements is a boundary state with both S and D content.

Due to mixing a real coefficient linear combination of $|x\rangle$ and $|y\rangle$ will result in complex wave functions. Instead, a complex weight is required for an appropriate linear combination of $|S^-\rangle$ and $|D^-\rangle$ states where the minus sign indicate that the states are the incoming parts only.

$$|\psi_-(\alpha)\rangle = cos(\alpha)e^{i\beta}\left|S^-\right\rangle - sin(\alpha)\left|D^-\right\rangle \tag{5.7.3}$$

When $\alpha = \Sigma$ the state is the incoming part of $|x\rangle$ and therefore it is expected that $\beta = 0$. Likewise, when $\alpha = \Sigma - \pi/2$, the state is the incoming part of $|y\rangle$ and it is also expected that $\beta = 0$. for values of α in between these two values β will be non-zero. Applying the S

matrix to $|\psi_-(\alpha)\rangle$, the outgoing state is

$$\begin{aligned}\left|\psi^+(\alpha)\right\rangle = &\begin{bmatrix}\left(e^{2i\delta_0}-e^{2i\delta_2}\right)\sin(\alpha)\sin(\Sigma)\cos(\Sigma)\\ +e^{i\beta}\cos(\alpha)\left(e^{2i\delta_0}\cos^2(\Sigma)+e^{2i\delta_2}\sin^2(\Sigma)\right)\end{bmatrix}\left|S^+\right\rangle\\ &+\begin{bmatrix}e^{2i\delta_2}\cos(\Sigma)\left(-\sin(\alpha)\cos(\Sigma)+e^{i\beta}\cos(\alpha)\sin(\Sigma)\right)\\ -e^{2i\delta_0}\sin(\Sigma)\left(\sin(\alpha)\sin(\Sigma)+e^{i\beta}\cos(\alpha)\cos(\Sigma)\right)\end{bmatrix}\left|D^+\right\rangle\end{aligned} \tag{5.7.4}$$

For a real wave function the magnitude of the incoming wave and outgoing wave for each channel must match. Focusing on the S-channel and letting $\delta_{02}=\delta_0-\delta_2$ this requirement yields a messy equation.

$$\begin{aligned}\cos^2(\alpha) = &\frac{1}{4}\cos^2(\alpha)\left(\cos(4\Sigma)+3\right)\\ &+\frac{1}{4}\sin^2(2\Sigma)\left(1+\cos(2\alpha)\left(2\cos(2\delta_{02})-1\right)\right)\\ &+\sin(2\Sigma)\sin(\delta_{02})\sin(2\alpha)\left(\cos^2(\Sigma)\sin(\beta+\delta_{02})+\sin^2(\Sigma)\sin(\beta-\delta_{02})\right)\end{aligned} \tag{5.7.5}$$

If this equation is satisfied, then by unitarity of the S-matrix, the incoming and outgoing D-channel magnitudes will also match. This equation is a constraint between α and β. α controls the S and D amplitudes, so β, the relative incoming shift between $|S^-\rangle$ and $|D^-\rangle$ will be expressed in terms of α. A first step is to partially isolate β.

$$\begin{aligned}X &= \frac{\cos^2(\alpha)\left(1-\cos(4\Sigma)\right)-\sin^2(2\Sigma)\left(1+\cos(2\alpha)\left(2\cos(2\delta_{02})-1\right)\right)}{4\sin(2\Sigma)\sin(\delta_{02})\sin(2\alpha)\sin^2(\Sigma)}\\ Y &= \cot^2(\Sigma)\\ X &= \left(Y\sin(\beta+\delta_{02})+\sin(\beta-\delta_{02})\right)\end{aligned} \tag{5.7.6}$$

Solving the last equation above for β yields

$$\beta = \pm\cos^{-1}\left(\frac{X\sin(2\delta_{02}) \;\pm\; |Y+\cos(2\delta_{02})|\sqrt{Y^2+2Y\cos(2\delta_{02})-X^2+1}}{Y^2+2Y\cos(2\delta_{02})+1}\right)-\delta_{02} \tag{5.7.7}$$

The $\pm$ symbols are independent, giving 4 solutions. At a given energy, with $\alpha=\Sigma$, one of the 4 solutions corresponding to the two sign choices will yield $\beta=0$. That solution is used with other values of α to maintain continuity. With α and β in hand, the phase shifts needed for Green's functions can be computed from Eq.(5.7.4).

$$\begin{aligned}\delta_0(\alpha) &= \left(\arg(\left\langle S^+\right|\left.\psi^+(\alpha)\right\rangle/\cos(\alpha))-\beta\right)/2\\ \delta_2(\alpha) &= \left(\arg(\left\langle D^+\right|\left.\psi^+(\alpha)\right\rangle/(-\sin(\alpha)))\right)/2\end{aligned}$$

The division by $\cos(\alpha)$ and $-\sin(\alpha)$ handle the sign of the initial state components.

One advantage of working with these states is that at low energy $\delta_2(E)$ can become very close to 0. When that happens $\cot(\delta_2)$ becomes extremely large making numerics difficult. α can be controlled to limit the value of $\cot(\delta_2)$. Another important advantage is that using these states essentially reduces the problem of constructing and eventually fitting coupled channel effective Hamiltonians to the procedure used for the single channel case.

5.8 Divergences in $b^{\ell}_{n'n}$

An interesting issue is that at some combinations of P space, dimensionless E_d, and $cot\delta_\ell$, the matrix elements of $\langle n', \ell \,|E/(E-T)|\, n, \ell\rangle$ are not invertible. In this section the cause and specific conditions under which this occurs are determined.

The matrix $b^{\ell}_{n'n}$ diverges when a row of matrix elements of $E/(E-T)$ goes to 0 as E_d is approached.

$$\langle n', \ell \,|E/(E-T)|\, e, \ell\rangle \to 0 \tag{5.8.1}$$

e, ℓ is an edge state and n', ℓ is a state in P. The divergence happens because the condition indicates that a row of the matrix is 0 and therefore the inverse does not exist. The conditions for the divergence condition can be explicitly derived. The action of $E/(E-T)$ on an edge state can be expanded over harmonic oscillator basis components with the same angular momentum.

$$\frac{E}{E-T}\,|e,\ell\rangle = \sum_n a_n\,|n,\ell\rangle \tag{5.8.2}$$

Applying $(E-T)$ to both sides yields an expansion using Eq.(A.4.1).

$$\begin{aligned} E\,|e,\ell\rangle &= \sum_n a_n (E-T)\,|n,\ell\rangle \\ &= \frac{1}{2}\sum_n a_n \begin{bmatrix} (2E-(2n+\ell-1/2))\,|n,\ell\rangle \\ -\sqrt{n\,(n+\ell+1/2)}\,|n+1,\ell\rangle - \sqrt{(n-1)\,(n+\ell-1/2)}\,|n-1,\ell\rangle \end{bmatrix} \end{aligned}$$

The expansion can be reorganized as a simple sum over the basis.

$$E\,|e,\ell\rangle = \frac{1}{2}\sum_n \begin{bmatrix} a_n\,(2E-2n-\ell+1/2) \\ -a_{n-1}\sqrt{(n-1)\,(n+\ell-1/2)} - a_{n+1}\sqrt{n\,(n+\ell+1/2)} \end{bmatrix} |n,\ell\rangle$$

This equation is actually an infinite set of independent equations, one per basis element. The constraint expressed by Eq.(5.8.1) is that expansion Eq.(5.8.2) can't overlap P, immediately giving the values of the first few a_n.

$$a_n = 0, \quad n \le e \tag{5.8.3}$$

There is a special case for $n = e$ giving a_{e+1}.

$$E = -\frac{1}{2}a_{e+1}\sqrt{e\,(e+\ell+1/2)} \quad \Rightarrow \quad a_{e+1} = -\frac{2E}{\sqrt{e\,(e+\ell+1/2)}} \tag{5.8.4}$$

For higher n a recurrence relation is obtained.

$$a_{n+1} = \left((2E-2n-\ell+1/2)\,a_n - \sqrt{(n-1)\,(n+\ell-1/2)}\,a_{n-1}\right)/\sqrt{n\,(n+\ell+1/2)} \tag{5.8.5}$$

Outside the range of the P space, the a_n do in fact encode the expansion of a free wave radial function of angular momentum ℓ and a specific value of $cot\delta_\ell$. The solution depends on E through the base value a_{e+1} and the recurrence relation. It should be clear that at a given E there is exactly one solution with its associated $cot\delta_\ell$ satisfying Eq.(5.8.1).

To make the solution concrete the case of an S-channel only P space with $\Lambda = 10$ is analyzed. Setting the dimensionless E to 1 and expanding for 300 states yields Figure (5.5). The solid line with fine wiggles is the expansion of Eq.(5.8.2) and has no overlap with P. The wiggles are a consequence of the cutoff of the harmonic oscillator basis. The dashed line is a matching $\ell = 0$ phase shifted free wave with its amplitude set to match the expansion.

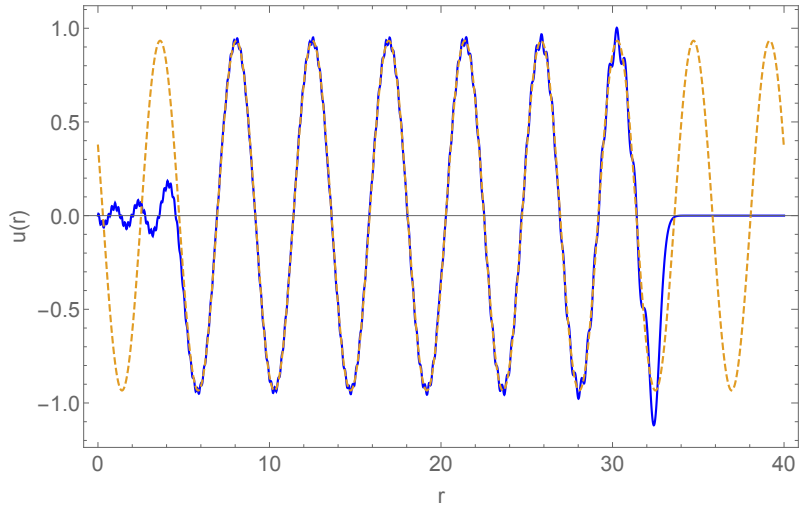

Figure 5.5: The dashed line is a phase shifted free wave with $E = 1$ and $\cot\delta = -2.29$ that matches the harmonic oscillator expansion corresponding to a divergence of b_{ij}.

Using the expansion, the divergent phase shift at any energy can be computed. For the specific case of an S-channel P space with $\Lambda = 10$ the relationship is shown in Figure (5.6). The figure includes a line indicating $\cot\delta_0$ for an example potential to be used later. The crossings will be important points for fitting to phase shifts and energy consistency.

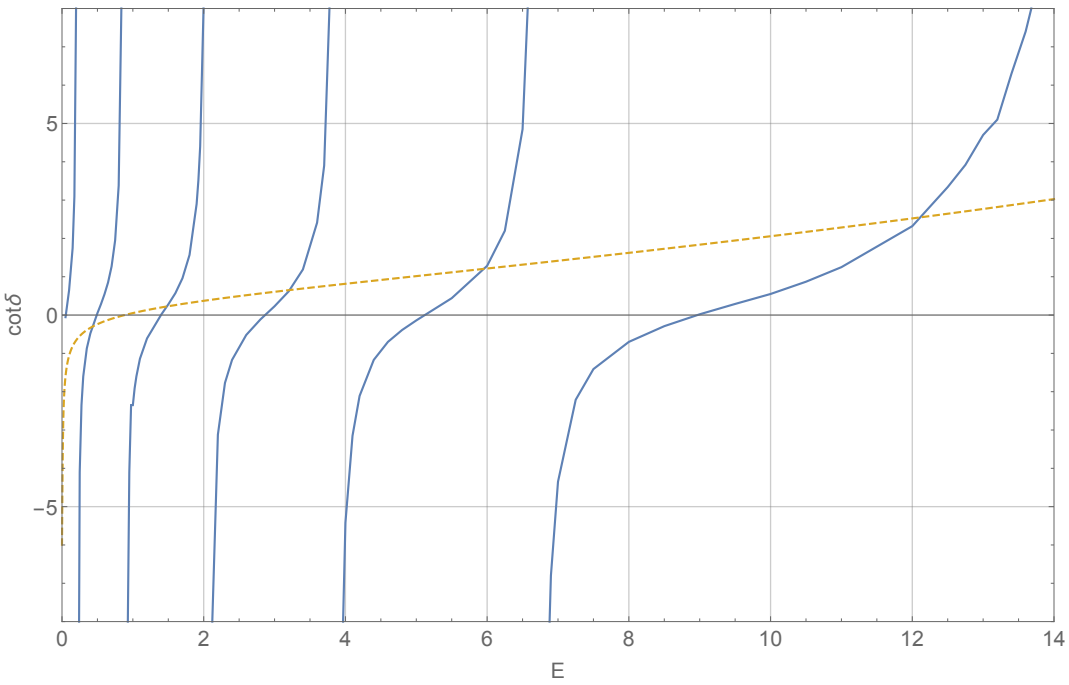

Figure 5.6: The solid blue lines indicate the $\cot\delta_0$ values as a function of dimensionless E at which $b_{n'n}$ will diverge. The dashed golden line shows the $cot\delta_0$ for a potential to be used later. The points where the lines cross are the divergence points for that potential and this P space.

Chapter 6

Fitting LECs

The fitting process begins with a set of sample pairs of energy eigenvalue and boundary condition. Each such sample can be used to construct a corresponding effective Hamiltonian with matrix elements expressed as a constant plus a linear combination of LECs. A cutoff for the operator order is chosen, resulting in a bounded set of LECs that must be fit to reproduce the sample eigenvalues as closely as possible. Because the energy dependence of the LECs is expected to be weak and the operators are themselves sensitive to energy the LECs will be assumed to be constant for the fitting process.

In the prior work by Haxton [38] the LECs were determined from a known potential. In the case of a known potential one can exploit the correspondence

$$\left\langle P \left| \frac{E}{E-TQ} V_\delta \frac{E}{E-TQ} \right| P \right\rangle = \left\langle P \left| \frac{E}{E-TQ} V \frac{1}{E-QH} QV \frac{E}{E-TQ} \right| P \right\rangle \tag{6.0.1}$$

Using the fact that $E/(E-QH)$ acting on non edge states is the identity and letting P^- be a projection operator to non edge states in P, the V_δ expansion Eq.(5.4.18) can be related to the large basis results.

$$\left\langle P^- \left| V_\delta \right| P^- \right\rangle = \left\langle P^- \left| V \frac{1}{E-QH} QV \right| P^- \right\rangle \tag{6.0.2}$$

The expression on the right can be computed directly with intermediate results in a large HO basis, capturing almost all of the effect of scattering through Q. Each matrix element of V_δ is a linear combination of LECs, giving a set of independent linear equations which may be solved for the LEC values. The solution can be simplified even further by starting with matrix elements defined in terms of a single LEC. This allows order LO LECs to be immediately determined. Then the contribution of these LECs are subtracted from matrices on both sides, producing a new set of matrix elements defined in terms of a single NLO LEC and so on. Because the LECs of each order can be determined without consideration of higher order LECs, this is a scheme independent fitting process.

In this work, the UV potential is not known. V_{IR} may be defined, but this is insufficient to use the prior technique. Instead, the process is to minimize the energy consistency error

for the effective Hamiltonians. The exact effective Hamiltonian, acting on a projection of an eigenstate is self consistent.

$$H_{eff}(E_i)P\left|\psi_i\right\rangle = E_i\left|\psi_i\right\rangle \tag{6.0.3}$$

Self consistency says that an effective Hamiltonian built at energy E_i in the spectrum of H will have E_i as an eigenvalue. When the operator expansion is cut off at finite order there is a mismatch.

$$H_{eff}(E_i)P\left|\psi_i\right\rangle = \varepsilon_i\left|\psi_i\right\rangle \tag{6.0.4}$$

ε_i is near, but usually not equal to E_i. $Err_i = E_i - \varepsilon$ is called the self consistency error. The goal is to pick a set of LECs that minimizes the self consistency error across all the effective Hamiltonians. An overall cost function for minimization has the form

$$\sum_i W(i)\ C(Err_i, E_i) \tag{6.0.5}$$

$C(Err_i, E_i)$ reflects the cost to be associated with the error. One very simple choice for C that doesn't use E_i is

$$C(Err_i, E_i) = |Err_i| \tag{6.0.6}$$

A more sophisticated choice will be examined later. An issue is that the importance of LECs above the order of the current fit is not known. Their unknown values mean that the energy E_i is not quite the right target. If more weight could be given to samples where the excluded LECs have the least effect, and where ε_i is more sensitive to the LEC(s) being fit, then the target would more faithfully represent the desired fit. This bias can be taken into account in $W(i)$.

$W(i)$ reflects the importance of sample i to the LECs being fit. Once source of importance comes from the distribution of sample energies. Each sample can be assigned an energy or momentum range and then the density of states can be integrated across that range to produce a weight.

6.1 Normalization of Continuum States of a Compact Potential

Part of assigning discrete weights to energy and phase shift pairs is deciding how much of the spectrum is represented by each pair. Proper normalization and the formulation of a resolution of identity can inform the construction of the weights.

Box normalization is used in a large spherical box of radius R. Wave functions are normed to one in this volume, implying the amplitude of the asymptotic wave function. V is compact and therefore its effect on the asymptotic wave function is simply to determine the phase shift. The wave function outside the potential can be written as

$$\begin{aligned} R\left(r\right)Y_{\ell m}\left(\hat{r}\right) &= A_\ell\left\langle\vec{r}\right|k,l,m\rangle = A_\ell\left[k\left(\sin\delta_\ell\ \eta_\ell\left(kr\right) - \cos\delta_\ell j_\ell\left(kr\right)\right)\right]Y_{\ell m}\left(\hat{r}\right) \\ &\rightarrow A_\ell\frac{1}{r}sin\left(kr + \delta_\ell - \ell\pi/2\right)Y_{\ell m}\left(\hat{r}\right) \end{aligned} \tag{6.1.1}$$

where a convenient factor of k has been included that will simplify future equations. As the $Y_{\ell m}$ is already properly normalized it is also convenient to work with $u(r) = rR(r)$ because the resulting asymptotic radial wave function is a simple constant amplitude sine wave. A reference normalization of continuum wave functions is chosen as follows.

$$u(r) = r\langle r|\, k, \ell, m\rangle = kr\left(\sin\delta_\ell\ \eta_\ell(kr) - \cos\delta_\ell j_\ell(kr)\right) \tag{6.1.2}$$

The phase shift and behavior of the wave function near the origin can be ignored if R is large, swamping edge effects. Then

$$1 = A_\ell^2 \int_0^R dr\ \sin^2(kr) = A_\ell^2 \frac{R}{2} \quad \Rightarrow \quad A_\ell = \sqrt{2/R}$$

From this point the development takes place in a specific $|\ell, m\rangle$ channel and $|k\rangle$ represents the radial state in that channel. For a resolution of the identity the sum is over all normalized states including both bound and continuum states. The allowed momenta k in the box form a discrete set defined by $kR + \delta(k) = n\pi$.

$$1 = \sum_{i\in bound} |i\rangle\langle i| + \sum_{n\in continuum} A_\ell^2\ |n\rangle\langle n|$$

The sum over n is now turned into an integral over k.

$$\sum_n \to \int dn = \int dk \frac{dn}{dk} = \frac{1}{\pi}\int dk\left(R + \frac{d\delta(k)}{dk}\right) \approx \frac{R}{\pi}\int dk$$

With this conversion the final form of the resolution of identity is

$$1 = \sum_{i\in bound} |i\rangle\langle i| + \left(\frac{2}{\pi}\right)\int_0^\infty dk\ \ |k\rangle\langle k| \tag{6.1.3}$$

An important use of this equation is to provide weights for individual samples pairs of energy and phase shift. Continuum samples will be assigned ownership of a range of momentum values and the totaling of the objective function should be thought of as a sum across the momentum basis as specified in Eq.(6.1.3).

6.2 Fitting with Uncertainty

Experimental data and Monte-Carlo data from LQCD comes with uncertainty. We focus on energy uncertainty because it is easier to handle in fitting. For small changes in phase shift, the energy will shift linearly, so one can replace phase shift uncertainty with energy uncertainty.

Another source of uncertainty when fitting at a given order is the effect of LECs beyond that order. The effect can be estimated by assuming naturalness, meaning that the next order LECS are only a fraction of of the size of the current order. This natural size can be combined with the derivative of ε_i with respect to the LECs. The variations are added in quadrature to estimate the combined effect of the next order LECs. Applying this strategy to a_{LO} automatically finds a low energy range where ε_i is not affected much by higher order LECs.

Regardless of the source of uncertainty, for each sample, (E_i, Boundary Condition), E_i is replaced with a mean value and variance, ($\bar{E}_i$, σ_i^2, Boundary Condition). This suggests that the fitting cost function should correspond to maximizing the probability of the set of ε_i values. The goal is to maximize

$$\prod_{i\in states}\left[\frac{1}{\sqrt{2\sigma^2\pi}}\exp\left(-\frac{(\varepsilon_i-E_i)^2}{2\sigma_i^2}\right)\right]^{W(i)} \tag{6.2.1}$$

$W(i)$ is interpreted as a probability which indicates the number of times sample i is included in Eq.(6.2.1). Instead of maximizing this product the negative of it's log can be minimized instead, throwing away constants that don't affect the position of the minimum.

$$C\left(LECs\right)=\sum_{i\in samples}W(i)\frac{(\varepsilon_i-E_i)^2}{\sigma_i^2} \tag{6.2.2}$$

Monte-Carlo results from LQCD will have correlations in the energy eigenvalues measurements taken from the same configuration. The data can be organized into rows which give observations for all the eigenvalues across all the lattice volumes. All measurements from the same configuration will be in the same sample and will be correlated, but eigenvalues from different volumes will not be correlated. A correlation matrix between the different energy eigenvalue measurements can be constructed as

$$C_{i,j}=\frac{1}{N-1}\sum_{r\in rows}\delta_{vol_i,vol_j}\left(\varepsilon_{r,i}-\mu_i\right)\left(\varepsilon_{r,j}-\mu_j\right) \tag{6.2.3}$$

The delta function enforces the lack of correlation between measurements in different volumes. The diagonal elements of the correlation matrix are the variance values from Eq.(6.2.2). We could diagonalize $C_{i,j}$ and apply the same transform to the vectors ε_i and E_i, alowing the use of Eq.(6.2.2). However, it is simpler and equivalent to use the inverse of $C_{i,j}$.

$$C\left(LECs\right)=\sum_{i\in samples}W(i)\left(\varepsilon_i-E_i\right)C^{-1}_{i,j}\left(\varepsilon_j-E_j\right) \tag{6.2.4}$$

6.3 Minimizing the Fit Function

Each effective Hamiltonian is a matrix over the P space with matrix elements that are linear combinations of LECs. Associated with each effective Hamiltonian is an target eigenvalue E_i

and our goal is to configure the LECs so that the matrices have eigenvalues closely matching the associated E_i. In addition there are weights for each matrix from statistical and other sources. This problem falls into the general class of problems known as IEP or inverse eigenvalue problems. A survey of IEP problems and techniques by Chu and Golub can be found in [39]. Given the extensive literature on the problem it is clear that the techniques described here can be improved.

In the fit cost function there is an innocent symbol ε_i which is the nearest eigenvalue to E_i of $H_{eff}(E_i)$. In the current implementation the nearest eigenvalue is found by simply finding all eigenvalues and then selecting the nearest. This is appropriate for the initial LO fit because the difference $(E_i - \varepsilon_i)$ may not be that small. At higher order however, we expect the difference to shrink. In this case a different algorithm, the inverse iteration method [40], should be used to find the nearest eigenvalue. It is also possible to take advantage of the knowledge of an approximate eigenvector associated with E_i from previous iterations of the fitter. Let b_0 be the previous fitter iteration eigenvector for sample i. Then

$$b_{k+1} = \frac{\left(H_{eff}(E_i) - E_i\right)^{-1} b_k}{\left|\left(H_{eff}(E_i) - E_i\right)^{-1} b_k\right|} \tag{6.3.1}$$

The inverse matrix only needs to be computed once, with the expectation that taking the inverse is significantly cheaper than finding the eigenvalues. Convergence is determined by comparing the component ratios of b_{k+1} and b_k. When the ratio stabilizes across all components, it is $(\varepsilon_i - E_i)$, the difference between the nearest eigenvalue and the target eigenvalue E_i.

Even with the above optimization of the evaluation of the cost function, it will be an expensive operation. Further, at higher orders the number of LECs will grow substantially; at N3LO in a coupled channel problem there are 13 LECs to be adjusted. Initial experiments with a simple gradient following algorithm were discouraging as only very short steps could be taken before the improvement direction changed. Instead, many random points are generated about the current best point according to an adaptive distribution function and the cost function is evaluated at those points to select a new best point. The distribution function is parameterized with a range for each LEC which is adjusted up or down based on the change in that LEC from the previous iteration. An advantage of the random point method is that it is trivially parallelized and spread across a large number of processors. A typical number of points at N3LO is 500k, increasing with order.

After each iteration there is a new best point and the derivatives of the cost function with respect to the LECs change. The estimated variance due to higher order LECs is updated to adapt to the change.

It was also found that adding a quadratic solve step to the iterations speeds up the solution. The local cost function is modeled as a quadratic equation in terms of a displacement d_i from the current point with the Hessian, A, and the gradient, B evaluated numerically.

$$f = A_{i,j} d_i d_j + B_i d_i + C \tag{6.3.2}$$

The minimum for f is found by setting all derivatives with respect to d_i to 0.

$$d_i = -\frac{1}{2} A^{-1}_{i,j} B_j \tag{6.3.3}$$

Points are generated in the vicinity of the line from the current best point to the quadratic minimum and the best cost point found is selected.

An additional important consideration is that the cost function has points where the cost spikes, often quite close to the minimum. If the fitting process simply moved downhill, then iterations would move the current best point farther from the minimum. An advantage of the random point method is that the distribution can be tuned to generate some points at a substantial distance from the starting point, allowing the fitting process to jump past the discontinuities. In practice, the fitting proceeds order by order with the best LEC values at one order taken as the initial point for the next order. This process improves the odds of starting on the right side of discontinuities at the next order.

If one picks a single H_{eff} and plots the nearest eigenvalue to the target energy with respect to a_{LO}, then the graph will look have the form seen in Figure (6.1).

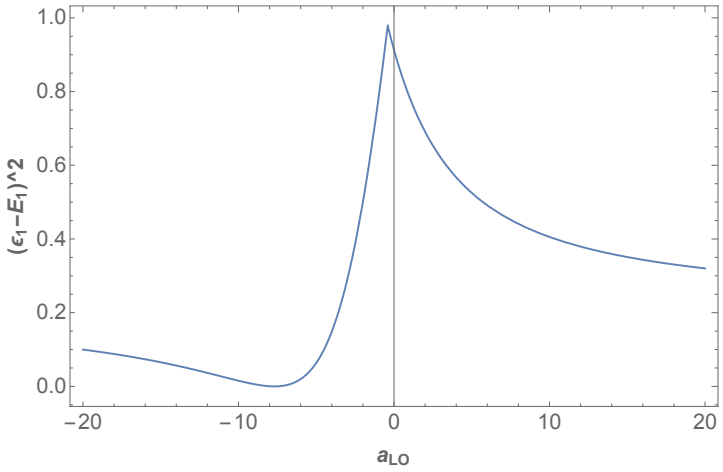

Figure 6.1: A specific H_{eff} for energy 0.5 is evaluated for a range of a_{LO} values and the squared difference between the eigenvalue and 0.5 is plotted. The sharp point just to the left of $a_{LO} = 0$ is the result of jumping from one eigenvalue that is moving away to one that is moving nearer. A simple algorithm that starts at or to the right of 0 will drift right to larger and larger a_{LO} values, missing the minimum near $a_{LO} = -8$.

Chapter 7

Tests of H_{eff} from Scattering Data

The first test is is a demonstration that the energy dependence of the LECs of one order can be absorbed in the action of the next order of operators, which as harmonic oscillator lowering operators are naturally energy dependent. Next is a demonstration of the construction of H_{eff} from phase shifts in a realistic S-channel only case. Last is a more realistic case based on coupled channel S-matrix data from a realistic potential.

The general procedure in these tests is to pick a potential V from which one can derive both scattering data and wave functions at continuum energies and possible bound states. The direct solutions of $H\psi = E\psi$ are useful as checks of the effective theory, which fundamentally should depend only on the scattering data.

The effective theory is constructed from the scattering data with a few choices of V_{IR}. One choice is simply $V_{IR} = 0$, another might be a match of the potential at long range and a third the actual potential. This allows us to see the effect of the accuracy of V_{IR} on convergence.

7.1 A Test of LEC Energy Independence

One of the goals in HOBET is to able to fit the effective theory to continuum data and then to use the LECs produced in the fit to predict bound states. If the LECs vary with energy, then one wouldn't know their values in the vicinity of the bound states. So the question is, can one produce a good fit with constant LECs.

To explore this question the numerical experiment begins with phase shifts derived from a realistic S-wave potential, a square well plus a square hard core, from which exact phase shifts were calculated at 10 energies from 1 to 10 MeV. A P space defined by $b = 1.7$ fm and $\Lambda = 8$ was selected for the test. A best fit a_{LO} was found separately for each energy, resulting in a slow drift of the LEC. The result can be seen in the upper sequence of blue dots of Figure (7.1), slowly rising with energy. Subsequently a second fit was done using only the two sample energies 10 MeV and 1 MeV. This time the fit was done at NLO and determined a_{NLO} in addition to a_{LO}. Finally, holding the new value of a_{NLO} fixed the first measurements

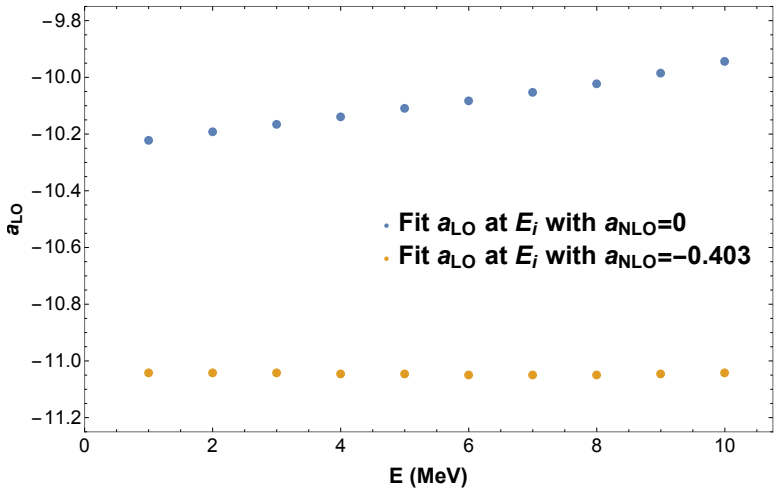

Figure 7.1: Energy dependence of a_{LO} at LO (upper dots) fit separately at each energy and residual energy dependence of a_{LO} at NLO (lower dots) fit separately at each energy after a_{NLO} is fixed by fitting both a_{LO} and a_{NLO} at 1 MeV and 10 MeV. On this range a_{NLO} absorbs the energy dependence.

are repeated, finding the best fit a_{LO} at each of the 10 energy values. This time the lower sequence of dots was obtained, running along in a nearly flat sequence. The conclusion is that the residual energy dependence of a_{LO} in an LO fit has now been absorbed into into the action of the NLO operator, itself with a constant LEC. Of course, if the range of the fit were increased, then energy dependence in the lower sequence of dots would manifest and the cure would be to fix NNLO LECs, again yielding a constant set of LECs over the fitting range.

7.2 An S-Channel Only Interaction

This demonstration is based on a potential with both a hard core and a relatively shallow well. The hard core presents the usual mixed scale problem of a weakly bound state and a potential reaching GeV energies without introducing the additional complication of coupled channels. To begin the length scale for the harmonic oscillator basis is set to $b = 2.0$fm, which will be seen to be to large enough to delay but not stop convergence.

$$E_{core} = 2181.24 \text{ MeV}, \qquad R_{core} = 0.25 \text{ fm}$$
$$E_{well} = 65.4823 \text{ MeV}, \qquad R_{well} = 1.70 \text{ fm}$$
$$V_S(r) = E_{core} e^{-(\rho/R_{core})^4} - E_{well} e^{(\rho/R_{well})^4}$$

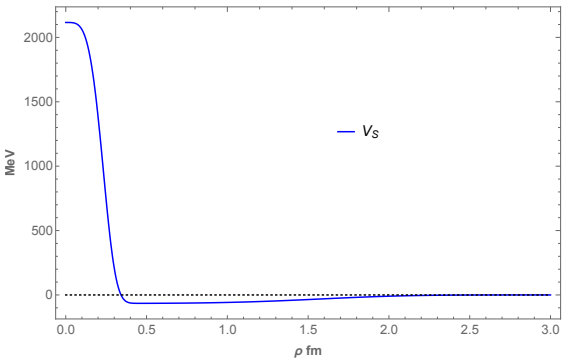

Figure 7.2: S-channel potential.

The potential shown in Figure (7.2) is tuned to reproduce a deuteron binding energy of -2.2245 MeV.

The remaining parameter defining the P space is the number of quanta, which is set to $\Lambda = 10$. As a first step in understanding the effective theory the LECs are determined by taking matrix elements of H in a large harmonic oscillator basis with $\Lambda = 800$, with a resulting lowest resulting eigenstate having an energy of -2.22446 MeV. This tells us that the large basis captures almost all of scattering through Q from the P space for the ground state. The resulting large basis matrix elements of T and V can then be used to compute $V\left(1/\left(E - QH\right)\right)QV$. The matrix elements in P^-, the P space minus the edge, must directly match those of V_δ^-.

$$\langle iS \left| V_\delta \right| jS \rangle = \begin{pmatrix} \text{-0.649726} & \text{-0.764885} & \text{-0.820725} & \text{-0.849773} & \text{-0.863267} \\ \text{-0.764885} & \text{-0.905108} & \text{-0.975789} & \text{-1.014714} & \text{-1.034921} \\ \text{-0.820725} & \text{-0.975789} & \text{-1.056586} & \text{-1.103164} & \text{-1.129314} \\ \text{-0.849773} & \text{-1.014715} & \text{-1.103164} & \text{-1.156115} & \text{-1.187654} \\ \text{-0.863267} & \text{-1.034921} & \text{-1.129314} & \text{-1.187654} & \text{-1.224066} \end{pmatrix} \tag{7.2.1}$$

This correspondence allows a direct determination of the LECs, shown in Table (7.1), starting with a_{LO} from the relationship $\langle 1S \left| V_\delta \right| 1S \rangle = \pi^{-3/2}\, a_{LO}$.

LEC	Value
a_{LO}	-3.61789
a_{NLO}	-7.01617E-2
a_{NNLO}^{22}	-5.67915E-3
a_{NNLO}^{40}	-3.28989E-5
a_{N3LO}^{42}	-1.68371E-4
a_{N3LO}^{60}	3.29957E-5

Table 7.1: LECs determined directly from V_S at $E = -2.2245$ MeV.

Based on the LECs determined at the bound state energy, the energy consistency of effective Hamiltonians at continuum energies can be explored. Energy consistency is shown for an N3LO set of LECs in Figure (7.3). There are a few features of note. The energy consistency is generally good at around 0.05%, but not as good as the prediction of the bound state. One can also see that the energy consistency stops improving at NNLO. This is a real effect caused by the direct calculation of LECs at a specific energy directly from a known potential. LECs calculated in this way run with energy.

Another feature shown in Figure (7.3) are the points at which the energy consistency diverges. In Section 5.8 this issue is studied, identifying the cause of the divergence and the specific energies at which it occurs. In Figure (5.6) the phase shifts are from the potential used here. If the indicated crossing point energies in the figure are multiplied by $\hbar\omega$ the divergence points of Figure (7.3) are reproduced. The divergences are an artifact associated with the choice of harmonic oscillator length scale b. At certain energies a row of $b_{ie}^{-1} = \langle i \left| E/\left(E-T\right)\right| e\rangle$ goes to 0 where e indicates a state on the edge of P. b_{ee} then diverges, causing the kinetic energy part of H_{eff} to diverge. At infinite order, this divergence will be canceled by V_δ, but as one realistically works at finite order there will be a narrow region around these special energies where the eigenvalue of H_{eff} will not be self consistent. In a single channel P space with N basis states this failure of $1/(E-T)P$ to overlap the P space state will occur $N-1$ times. With each increase in the order of the fit, the width in energy of the divergence is narrowed, but it is not removed. With an increase in the order of the

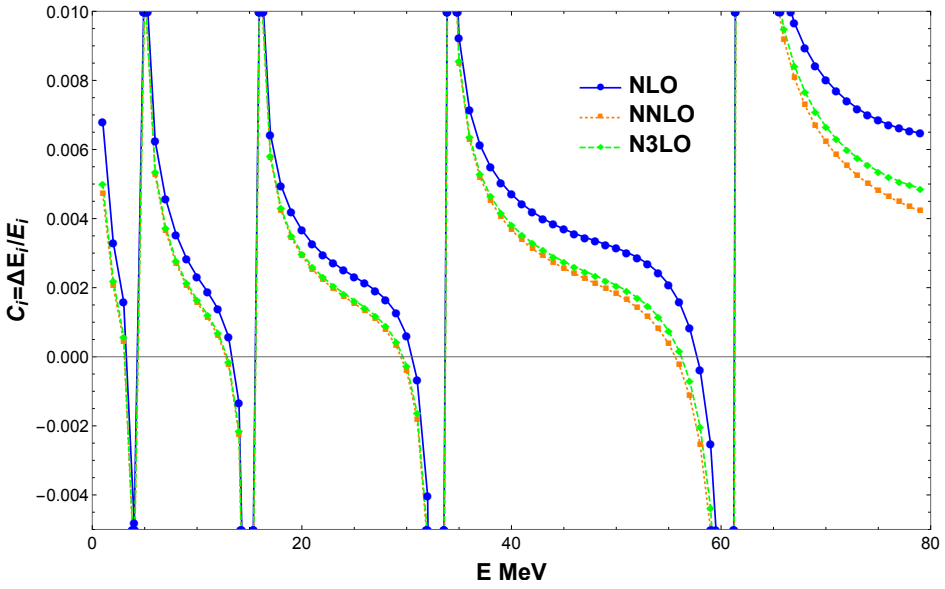

Figure 7.3: Continuum energy consistency at NLO to N3LO based on LECs directly calculated from V_S.

LECs to NNLO the energy consistency error reduces, but beyond that the improvement is small. This is caused by the running of the LECs with energy. The running can be examined

by performing the large basis calculation at continuum energies. At the selected energy E H_{eff} will have an eigenvalue $\varepsilon = E$, but at other continuum energies the general shape of the curve between the divergence points will remain the same.

The running of LECs can also be seen by calculating LEC values directly from the UV potential at a sequence of continuum energies. Figure (7.4) shows a_{LO} as calculated every 0.5 MeV between 1 and 40 MeV. The strategy for dealing with this residual energy dependence is to take advantage of the inherent energy sensitivity of the effective theory operators to find a constant set of LECs that give a much tighter energy consistency across a broad range of energies. For this fitting experiment phase shifts were generated at 80

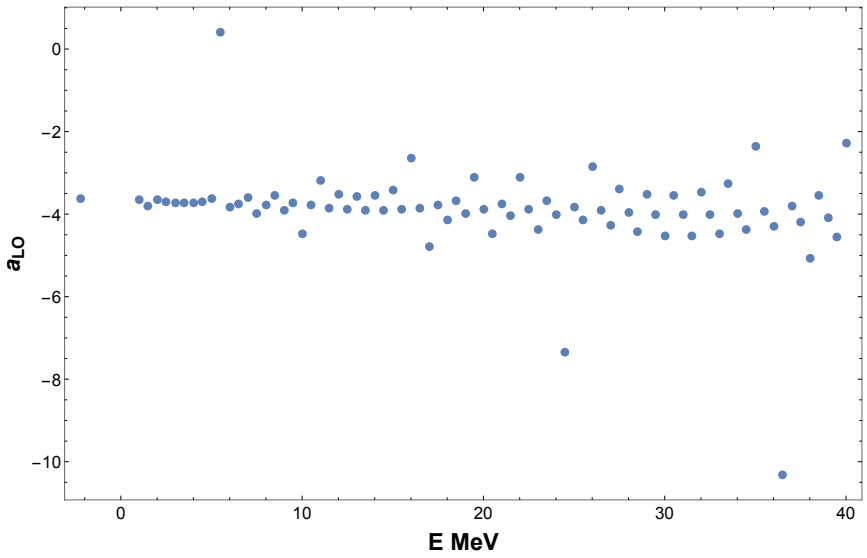

Figure 7.4: Running of a_{LO} with energy. The leftmost dot is the a_{LO} calculation at the bound state energy.

energies from 1 to 80 MeV. The minimization cost function used can be found in Eq.(6.2.1). The variance used in the cost function was estimated by assuming naturalness of the LECs and calculating the derivative of ε_i with respect to higher order LECs. With the estimated variance there is no need to manually select an energy range for fitting. Figure (7.5) shows the relative weights generated for the LO fit. Of note is that the variance becomes large near the previously described divergence points, automatically suppressing their influence in the fitting. In addition, a constraint was added requiring that $\Delta E_{i+1} - \Delta E_i <= 0$ between divergence points. This addition was motivated by the shape of the energy consistency curve shown in Figure (7.3). The additional constraint had a very minor effect on the overall cost but improved the low and high energy results. With this cost function the fitter produced fits at several orders and the energy consistency is shown in Figure (7.6). As can be clearly seen in Figure (7.6) the resulting value of $\Delta E/E$ converges rapidly across the entire range, showing that a single set of LECs of sufficient order produces a very accurate energy fit across the entire range, with the exception of the divergence points. With higher order, the

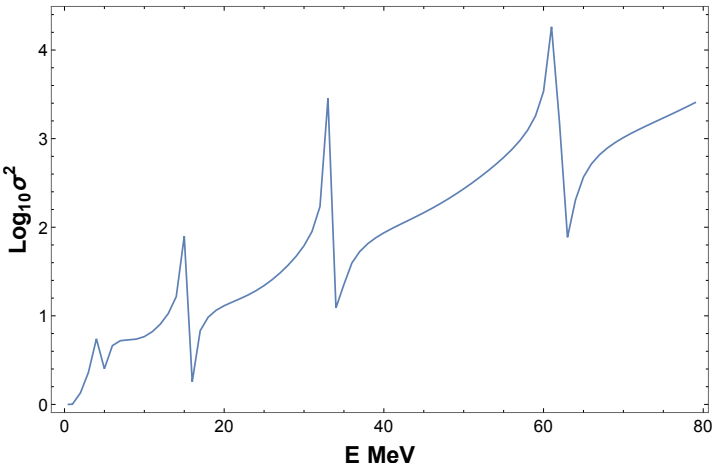

Figure 7.5: The log_{10} of the variance generated for LECs beyond NLO. The low points in the curve generate the highest weight in the fitting process at points where higher order LECs have less influence on the $H_{eff}(E)$ eigenvalue.

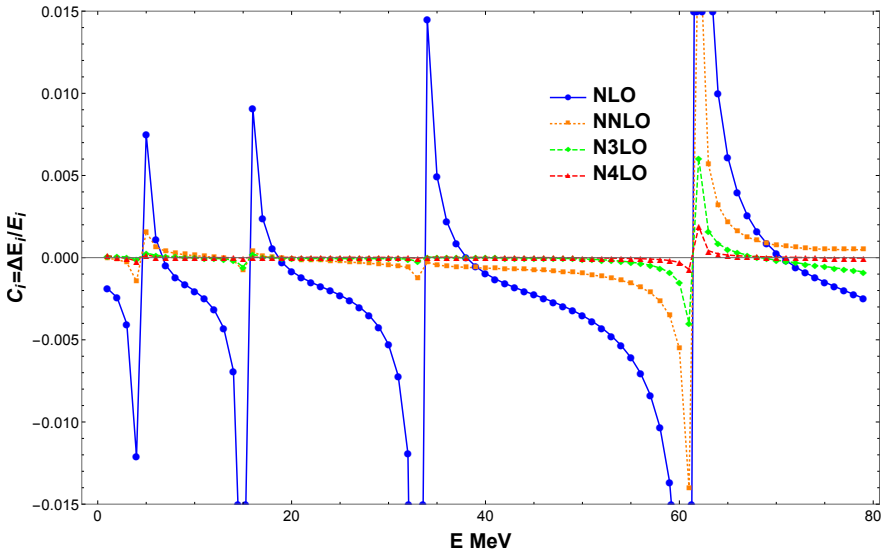

Figure 7.6: ΔE over the fitting range at orders from NLO to N4LO. Energy consistency improves significantly with each order.

region around the divergence points with substantial error become quite narrow. It should be emphasized that these divergence points are simply artifacts of the choice of harmonic oscillator length scale and have no dependence on the potential. When using the resulting effective theory to compute observables that are expected to evolve smoothly with energy a good strategy is to compute the observables at nearby points and interpolate. If there is an understanding of how the observable evolves with energy, e.g., one would expect phase shifts

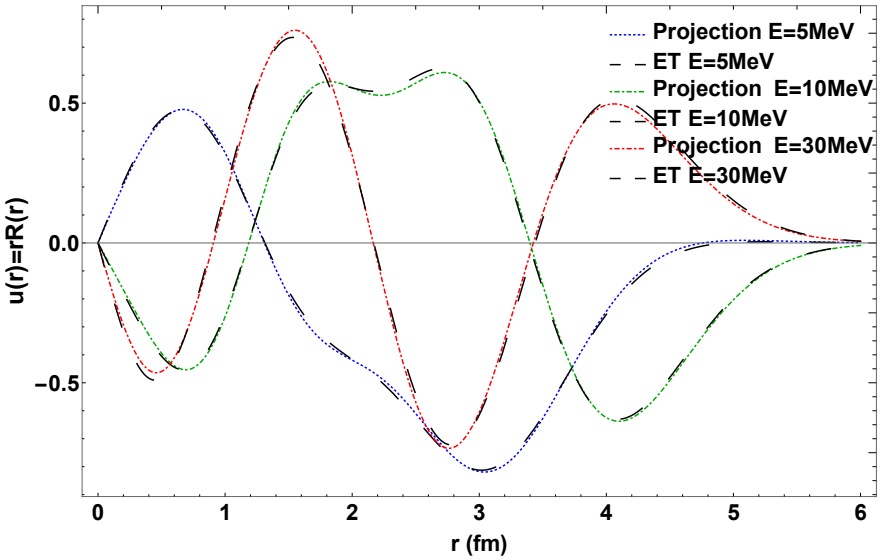

Figure 7.7: The projection of the numerical solution of the Schrödinger equation is compared with the with the $b = 2.0$fm, $\Lambda = 10$ N4LO effective theory wave function at three continuum energies. The H_{eff} solutions closely follow the projections of the full wave functions.

to evolve according to the effective range expansion, then that knowledge can be used for a more accurate interpolation. In it's eventual use in A-body calculations, the divergence points and regions can be pre-calculated and a simple linear interpolation is expected to suffice.

The effective Hamiltonian is represented as a matrix over the basis states. The matrix has N eigenvectors, one (or more) of which matches the continuum energy at which it was built. Continuity tells us that as the energy is smoothly varied that the eigenvector will also smoothly evolve unless there is an eigenvalue crossing or the energy crosses one of the divergence points. In all the examples that were tried the crossing of a divergence point comes with a jump from eigenvector i to eigenvector $i+1$. In the full effective Hamiltonian, the left limit of eigenvalue i and the right limit of eigenvalue $i+1$ will match, producing the eigenvalue crossing. At finite order, the lack of the higher order terms yields the observed jump.

An important property of the Bloch-Horowitz equation is that the eigenstates are the projections of the full wave functions. The fit can be tested by comparing the projections of a numerical solution at a set of energies with the eigenstates of the effective theory. Results are shown for a set of continuum energies in Figure (7.7) and for the bound state in Figure (7.8). The bound state energy and wave function should be regarded as a prediction because the LEC fit was restricted to the continuum energy phase shifts. For the bound state with harmonic oscillator length scale $b = 2.0$ fm the wave functions visually converges with order. A general observation is that the binding energy converges first and then the wave functions

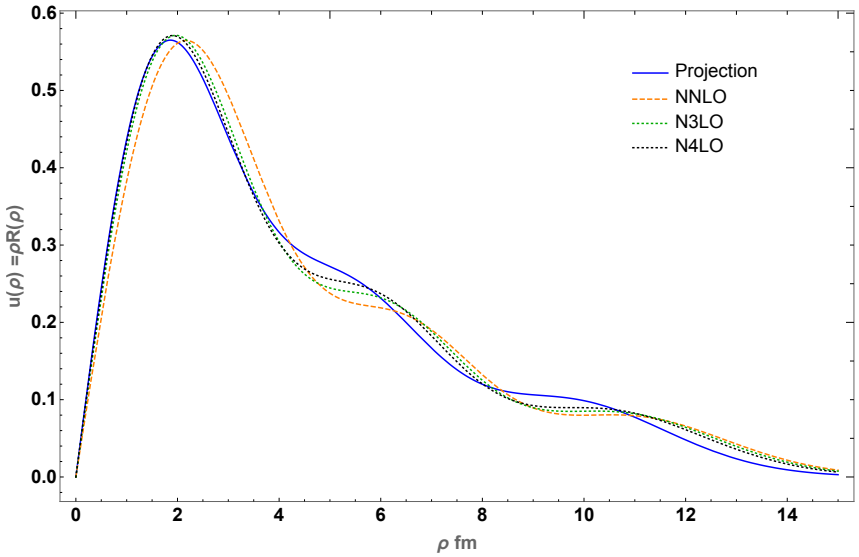

Figure 7.8: The projection of the numerical S-channel solution at $E = -2.2245$MeV is compared with with $b = 2.0$fm, $\Lambda = 10$ H_{eff} wave functions at orders NNLO through N4LO. As the order is increased the fidelity of the H_{eff} wave function improves.

follow. This means that once the eigenvalues have converged that the remaining changes are unitary in nature. The effect of dropping the hard core from V_{IR} is examined in Figure (7.9). The change in V_{IR} has very little effect on convergence as V_δ at N4LO is able to absorb most of the change in V_{IR}. This is an important point as a pion exchange model for V_{IR} will be used later when fitting to LQCD nucleon scattering eigenstates.

On the other hand, changes in b, the length scale for the harmonic oscillator basis, have a substantial effect on convergence as can be seen in Figure (7.10). Energy convergence is already good at NLO. While the eventual results do not depend on the choice of b, choosing an appropriate b for a problem can accelerate convergence.

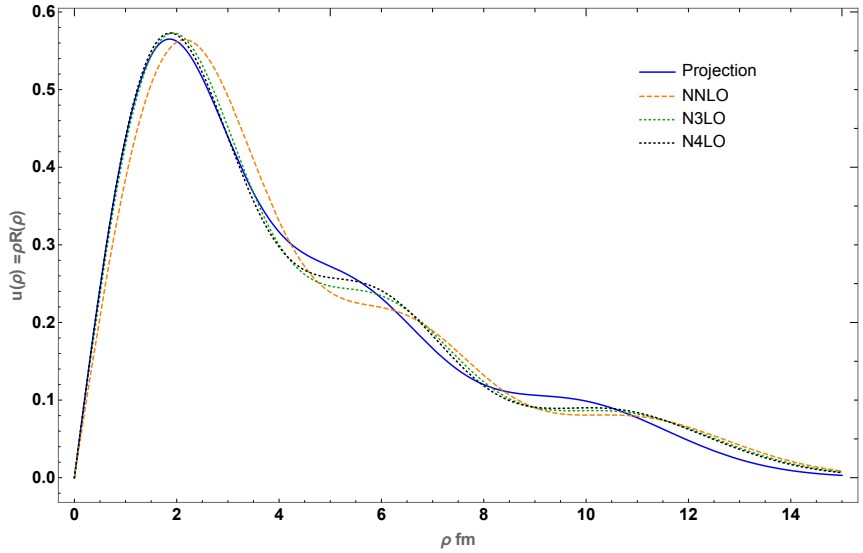

Figure 7.9: The projection of the numerical solution at $E = -2.2245$MeV is again compared with $b = 2.0$fm, $\Lambda = 10$ H_{eff} wave functions at orders NNLO through N4LO, but with $V_{IR} = -E_{well} \exp(\rho^4/R_{well}^4)$, which is the long range part of V. The wave function convergence is essentially unchanged. Almost all of the matrix elements of the hard core have been absorbed into V_δ via the fit to phase shifts.

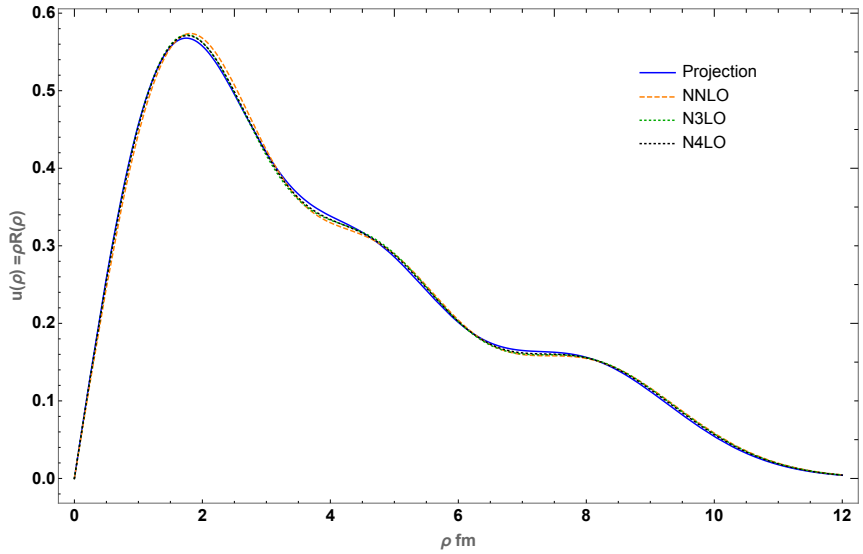

Figure 7.10: A change to $b = 1.5$ fm for the harmonic oscillator length scale dramatically improves the convergence of the wave function over the $b = 2.0$ fm choice made earlier.

7.3 A P-Channel Example with V_{IR} =Long Range Part of v_{18}

Single channels above S are the easiest to fit accurately as the angular momentum barrier reduces the contribution of the hard core. For this demonstration the Argonne v_{18} is used outside of 3 fm and an 8th degree polynomial is used to extrapolate in to the origin, throwing away the short range detail in the potential. Phase shifts were generated from the full potential at 40 sample energies from 1 to 40 MeV. The effective Hamiltonians were built with $\Lambda = 8$, giving four harmonic oscillator basis states, and length scale $b = 1.7$ fm. Fitting of the LECs was done at NLO through N4LO with the variance estimate based on sensitivity to higher order LECs. There is no LO fit because the lowest operator in the channel is $a^{1P1}_{NLO}\ \hat{c}^\dagger\delta(r)\hat{c}$. Each angular momentum lowering operator contributes one to the order.

In Figure (7.11) the resulting energy consistency is shown for uncorrected effective Hamiltonians (all LECs set to 0), and NLO through N3LO. Even the uncorrected effective Hamiltonian results in only a 1% error, telling us that the corrections from V_δ are small. The introduction of each order of operators with their LECs results in a substantial decrease in energy consistency error. The divergence points of $b_{n'n}$ occur at 9.077 and 28.80 MeV, both

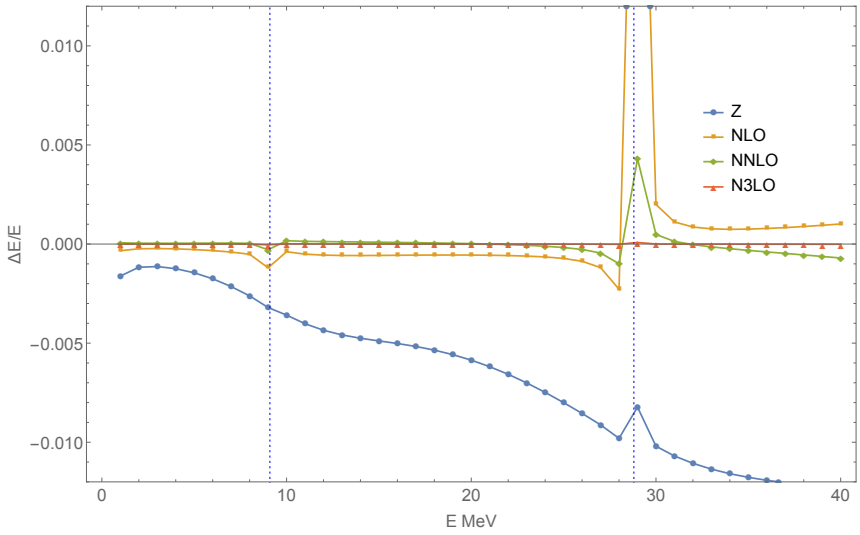

Figure 7.11: Energy consistency for Z(no correction), NLO, NNLO, N3LO for energy samples from 1 to 40 MeV. The vertical dotted lines indicate the energies at which $b_{i,j}$ diverges.

near sample points. The locations of these divergence points depends only on the phase shifts, Λ and harmonic oscillator length scale and can be calculated independently of the choice of V_{IR}. The sample point at 9 MeV is to the left of the divergence point resulting in the effective Hamiltonian energy for that state being low while the sample point at 29 MeV is to the right of the divergence point resulting in effective Hamiltonian energy for that state

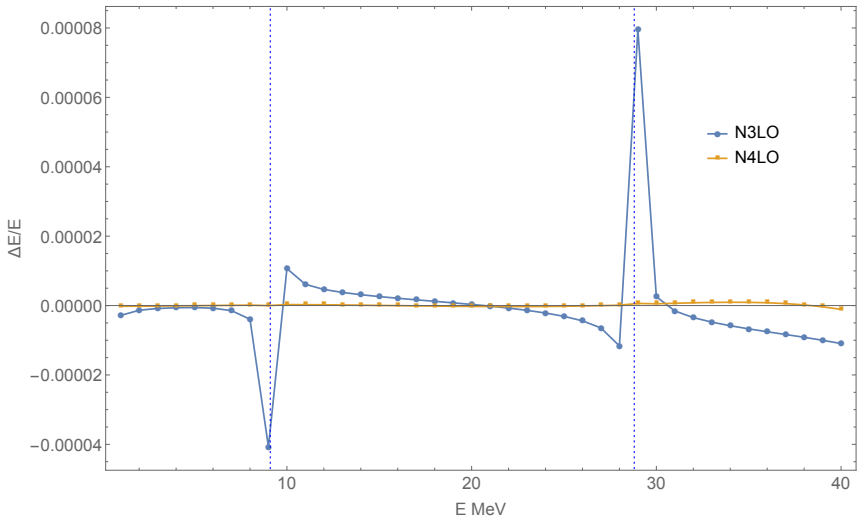

Figure 7.12: Energy consistency at N3LO and N4LO for energy samples from 1 to 40 MeV.

being high. At low order the weight for these points is automatically suppressed due to the variance calculation while at high order the fitting process focuses on reducing the errors. Figure (7.12) zooms in on the higher order N3LO and N4LO fits, showing that the errors near the divergence points continues to reduce.

A further test of the effective Hamiltonians is that the wave functions are the projections of the full theory wave functions. Reference wave functions were computed directly from the v_{18} potential and compared to ET wave functions for three energies in Figure (7.13).

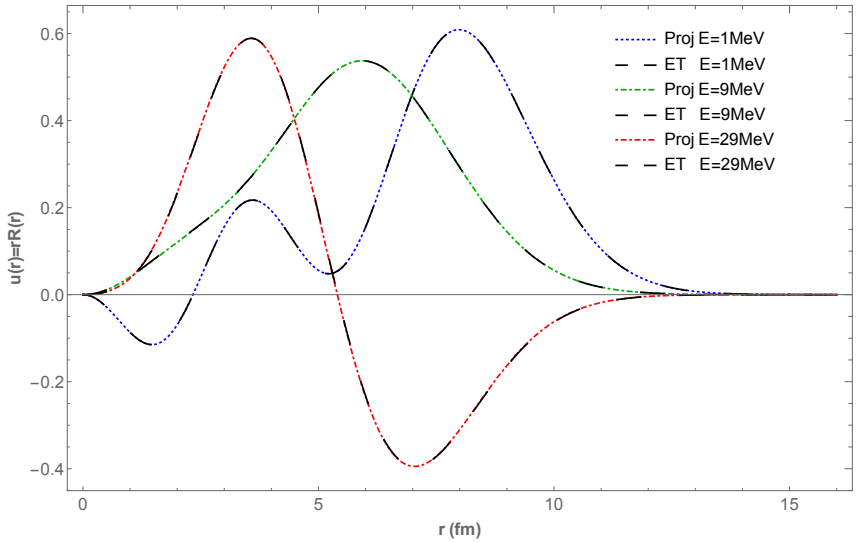

Figure 7.13: Projections and NNLO ET wave functions at 1, 9, and 29 MeV .

The effective theory wave functions are a close visual match to the projections, confirming their Bloch-Horowitz behavior. Energies 9 and 29 MeV were specifically chosen because they were near the divergence points, which should be the most difficult to match.

P-channel and higher single channels converge easily, yielding both energy and wave form matches. This can be partially attributed to the angular momentum barrier, hiding the hard core at modest scattering energies.

7.4 A Difficult Coupled Channel Interaction, the Deuteron in the S and D-channel

The most challenging coupled channel to fit is the S and D-channel of the Deuteron. The D-channel projection of the wave function in particular is very sensitive to the details of the interaction. Those details are subject to the residual energy dependence of the LECs which has been ignored in fitting so far. This remaining energy dependence is small as seen in Section 7.1.

An initial example will set $V_{IR} = Av_{18}$ and use phase shifts derived from the potential. Fits over different continuum energy ranges will be seen to produce very similar results. Effective theory wave functions will be compared to projections of numerical solutions. A second example will set V_{IR} to the long range part of Av_{18}, essentially the one pion exchange part of Av_{18}. The same phase shifts will be used as before. A heuristic workaround for the residual energy dependence in the SD-channel is also examined.

The S-matrix, $S(E)$, in all these examples are derived from Av_{18}. The "variable phase" method as described by Calogero [41] was used to generate the S-matrix. The essential idea is to parameterize the disclosure of the matrix potential $U(r)$ with R specifying the range of a cutoff, $U(r,R) = \Theta(R-r)U(r)$. One then writes a differential equation for S as a function of R. Integrating out from $R = 0$, where the initial condition for $S(R = 0)$ is the identity, to beyond the range of the potential yields the usual S-matrix. In the equation below u_{in} and u_{out} are diagonal matrices of unperturbed incoming and outgoing spherical waves in each channel.

$$S'(R) = \frac{1}{2ik}\left[S(R)u^{(out)}(R) - u^{(in)}(R)\right] U(R) \left[u^{(in)}(R) - u^{(out)}(R)S(R)\right] \tag{7.4.1}$$

$$u^{(in)}_{m,n}(r) = \delta_{m,n} kr(-i)h^{(2)}_{\ell_n}(kr), \quad u^{(out)}_{m,n}(r) = \delta_{m,n} kri h^{(1)}_{\ell_n}(kr)$$

$$u(r) = u^{(in)}(r) - u^{(out)}(r)S$$

The resulting S-matrix at each sample energy is parameterized as in Eq.(5.7.2).

Because this is a coupled channel situation, three pairs of S and D phase shifts were generated based on a choice of α in Eq.(5.7.3). When $\alpha = \Sigma$, the resulting asymptotic wave

function is mostly S-channel. In a second choice, α is chosen to make the asymptotic wave function mostly D-channel, but to limit $\cot\delta_D$ to about 20 to avoid numerical difficulty when the inner and outer solutions used in the Green's function construction are too much alike. A third mixed choice was included by taking 3/8 of the difference in α between the first two choices. Labels of S, D, and X are used for the three choices of phase shift pairs reflecting the predominant content of the asymptotic wave function. These specific choices are not very important. What is important is that the three choices emphasize different matrix elements in H_{eff}, making the fitting cost function sensitive to their values.

Divergences in $b_{i,j}(E)$ depend on the harmonic oscillator length scale, P, and on the phase shifts. Length scale $b = 1.7$ fm and $\Lambda = 8$ result in divergence points in the three asymptotic states as follows.

$$\begin{aligned} \text{S}: &\quad 5.35, 8.56, 25.88, 28.55 \text{ MeV} \\ \text{D}: &\quad 8.71, 12.91, 28.49 \text{ MeV} \\ \text{X}: &\quad 8.60, 12.19, 28.52 \text{ MeV} \end{aligned}$$

These divergence points were found by evaluating $b_{i,j}^{-1}$ every 0.1 MeV and then interpolating the crossing of 0 by rows associated with edge states. The location of these points are useful to know because sample energies too close to them require high order corrections to fit. Changes to α can be used in some cases to create a separation from an energy, S-matrix sample, but this doesn't always work. An example can be found in the list above where all three asymptotic choices have divergences near 8.6 MeV. Samples can be dropped, or alternatively the length scale b or Λ can be adjusted to move the points.

In these examples, the phase shifts or S-matrix values, are available at all energies, so the sample energies can be chosen to avoid direct hits on the divergence points. In a small improvement, samples were positioned at roughly equal spacing on both sides of divergence points. The specific energies used with each asymptotic state are given in Table (7.2). Again, the specific energies selected are not too important except near divergence points when fitting at low order. Each sample is assigned a portion of the energy spectrum and gets a weight from the corresponding momentum range according to summation over the resolution of the identity found in Eq.(6.1.3); therefore the introduction of extra samples will not substantially change the fit cost function.

Table 7.2: Sample energies for asymptotic states.

S	D	X
0.2	0.2	0.2
0.4	0.486	0.5
0.7	0.686	0.8
1.0	1.0	0.858
1.5	1.5	1.058
2.0	2.0	1.5
4.0	4.0	2.0
5.246	8.611	4.0
5.446	8.811	8.502
8.458	10.0	8.702
8.658	12.814	10.0
11.0	13.014	12.087
15.0	15.0	12.287
20.0	20.0	15.0
25.776	25.0	20.0
25.976	28.386	25.0
30.0	28.586	28.422
		28.622

7.4.1 $V_{IR} = Av_{18}$

The most accurate prediction of the bound state will come from the lowest energy continuum data. In this case the range from 0.2 to 10.0 has sufficient data to constrain LECs up to N3LO. Energy convergence of the N3LO fit can be seen in Figure (7.14) for all three asymptotic states. Energies at which b_{ij}^{-1} diverges are indicated with vertical lines. This fit estimated the variance from the N4LO LEC sensitivity. The fit also continues to produce good energy consistency well above the fit range.

The known bound state energy for this potential is -2.224574 MeV. The ET bound state is easily found by making an initial guess such as -1 MeV and solving for a self consistent energy iteratively, resulting in a bound state energy of -2.22466 MeV. The result for a large basis, $\Lambda = 500$, calculation with the same harmonic oscillator length scale finds -2.22452 MeV and the result immediately produces the reference wave function components to test the effective theory against. The reference values are compared to NLO, NNLO, and N3LO wave functions in Figure (7.15). The S-channel portion of the wave function matches quite closely, but the D-channel portion at N3LO is significantly off.

Individual components for no correction through N3LO are given in Table (7.3). While the energy converged accurately at N3LO, the wave function components are off by a noticeable amount. Of note is the comparison between D-channel wave function components at LO and the projection of the full wave function. The single LEC a_{LO}^{S} makes the bulk of the

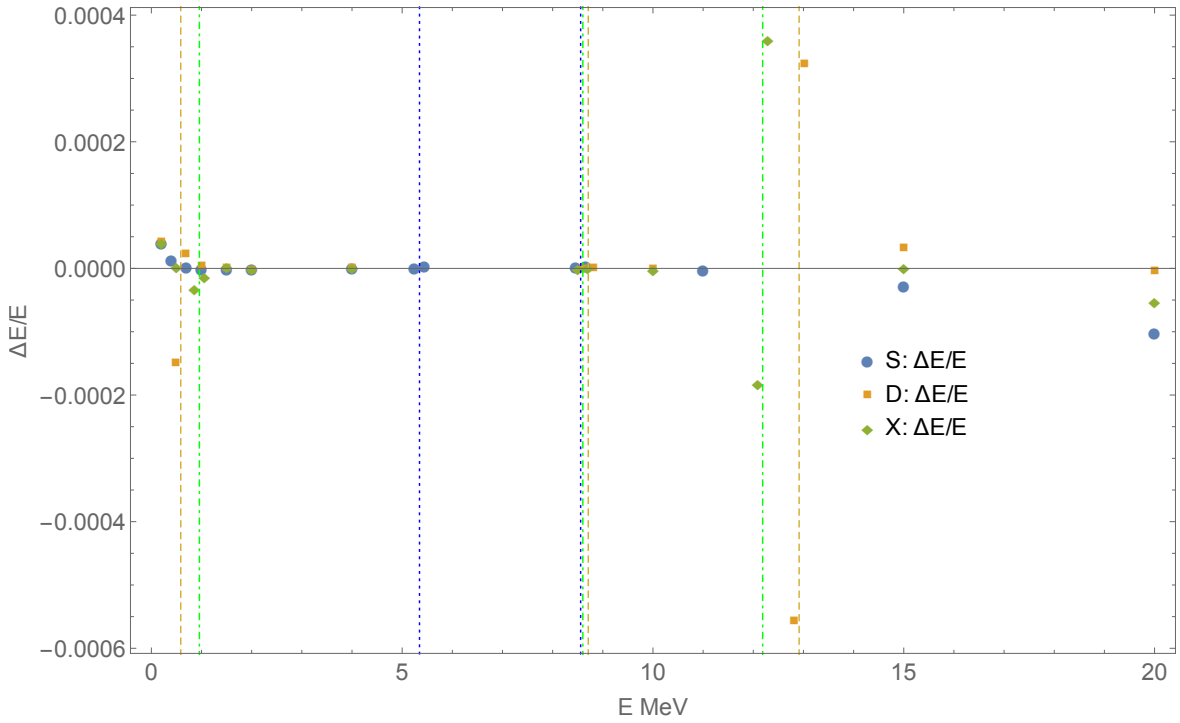

Figure 7.14: N3LO energy convergence from a 0.2 MeV to 10.0 MeV fit. Vertical lines indicate divergence points for b_{ij} with dotted corresponding to S, dashed to D, and dot-dashed to X.

corrections to S to S matrix elements, resulting in a S-channel wave function that is close to the projection. The low lying matrix elements of V are the only connection between S and D states and result in correcting the D wave function to nearly match the projected one. This observation will be used in a heuristic for correcting for the residual energy dependence of the LECs. The overlap between the N3LO wave function and the normalized projection, $\langle \psi_{N3LO} | \psi_P \rangle = 0.995$, is a good measure of the wave function match, with most of the error concentrated in the D-channel part of the wave function.

Table 7.3: Convergence of Bound State Components. SP and DP indicate state probabilities.

Order	SP	DP	1S	2S	3S	4S	5S	1D	2D	3D	4D
Z	0.991	0.009	0.589	-0.512	0.417	-0.370	0.265	0.085	0.016	0.040	0.014
LO	0.955	0.045	0.927	-0.047	0.273	-0.018	0.136	0.151	0.085	0.097	0.073
NLO	0.986	0.014	0.951	-0.087	0.249	-0.072	0.089	0.104	0.038	0.040	0.013
NNLO	0.980	0.020	0.947	-0.087	0.252	-0.080	0.078	0.128	0.045	0.040	-0.002
N3LO	0.979	0.021	0.945	-0.084	0.257	-0.075	0.079	0.130	0.048	0.041	-0.004
Proj	0.961	0.039	0.934	-0.105	0.249	-0.074	0.101	0.145	0.077	0.088	0.0634

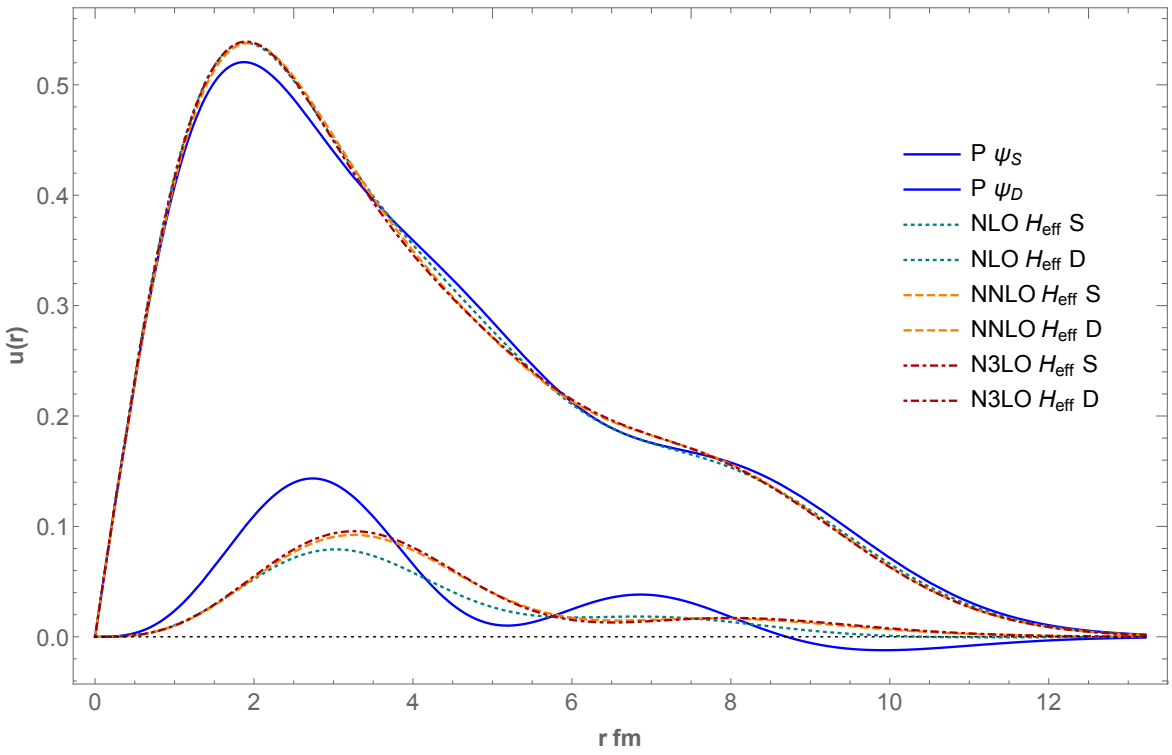

Figure 7.15: N3LO wave functions from a 0.2 MeV to 10.0 MeV fit compared to the projection of the full wave function.

To examine the effect of the fitting range the limits are now changed to 1.0 to 30.0 MeV. The energy convergence over the fitting range is shown in Figure (7.16). Energy convergence over the higher part of the energy range improves significantly, but at the expense of the fit below the low end of the range. The choice of fitting range has an effect a little like squeezing a balloon. With the new set of LECs the predicted binding energy shifts slightly to -2.2249 MeV. The wave function components shown in Table (7.4) also have small changes compatible with a small residual energy dependence of the LECs.

Table 7.4: Bound state components based on fitting range from 1 to 30 MeV. SP and DP indicate state probabilites.

Order	SP	DP	1S	2S	3S	4S	5S	1D	2D	3D	4D
N3LO	0.980	0.019	0.946	-0.083	0.258	-0.075	0.077	0.127	0.044	0.037	-0.007
Proj	0.961	0.039	0.934	-0.105	0.249	-0.074	0.101	0.145	0.077	0.088	0.063

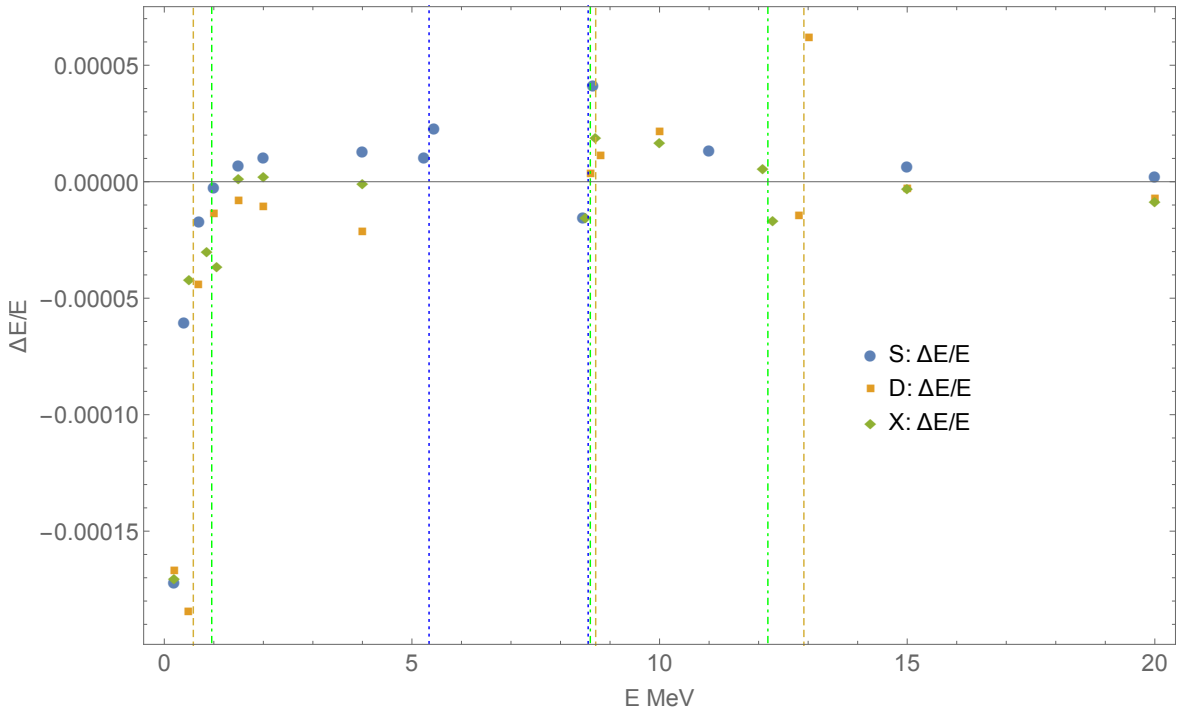

Figure 7.16: N3LO energy convergence from a 1.0 MeV to 30.0 MeV fit.

7.4.2 V_{IR} = Long Range Part of Av_{18}

The long range part of Av_{18} is essentially a one pion exchange potential, but with the coupling constant varying about 5% across SS, DD, and SD coupling. The point of this section is to show that the effective theory is independent of the short range parts of the potential and that the real dependence is on the observables. In this case the observables are S-matrix values at the sample energies. $V_{IR} = Av_{18}$ for $r > 3$ fm and a simple 8th order polynomial is used to extend it inwards to $r = 0$ with a goal of keeping the first few derivatives smooth. V_{IR} is shown graphically in Figure (7.17). As can be seen, the short range hard core is eliminated.

The fit uses the same sample points as before. A fit at NNLO yields a small energy consistency error, $\Delta E/E$, over the fitting range of 0 to 10.0 MeV which can be seen in Figure (7.18). Above that range the energy fit remains good with notable deviations at the already described divergence points of b_{ij} that can be seen near 12 and 13 MeV. They have the usual pattern of a low energy eigenvalue to the left and a high eigenvalue to the right of the divergence point.

The predicted bound state energy at NNLO is -2.22456 MeV, showing that the short range part of the potential is not important. As before, the D-channel wave function at NNLO shows a noticeable error. Also as before, the D-channel wave function at LO can be seen to have an accurate match to the reference wave function, indicating that this behavior

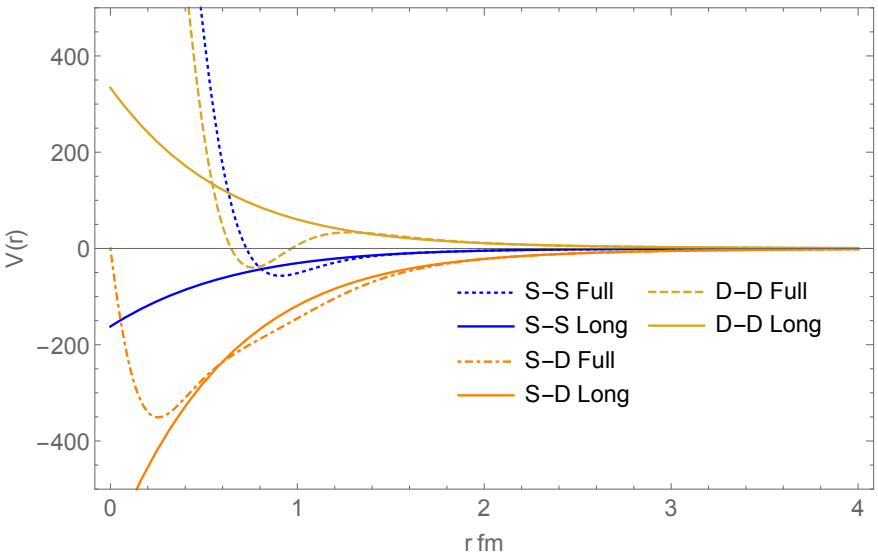

Figure 7.17: The long range potential is an interpolation from outside 3 fm, throwing away all the short range content of Av_{18} including the hard core.

is insensitive to the choice of V_{IR}. The dotted line indicating the LO H_{eff} D-channel wave function is barely visible over the projected wave function.

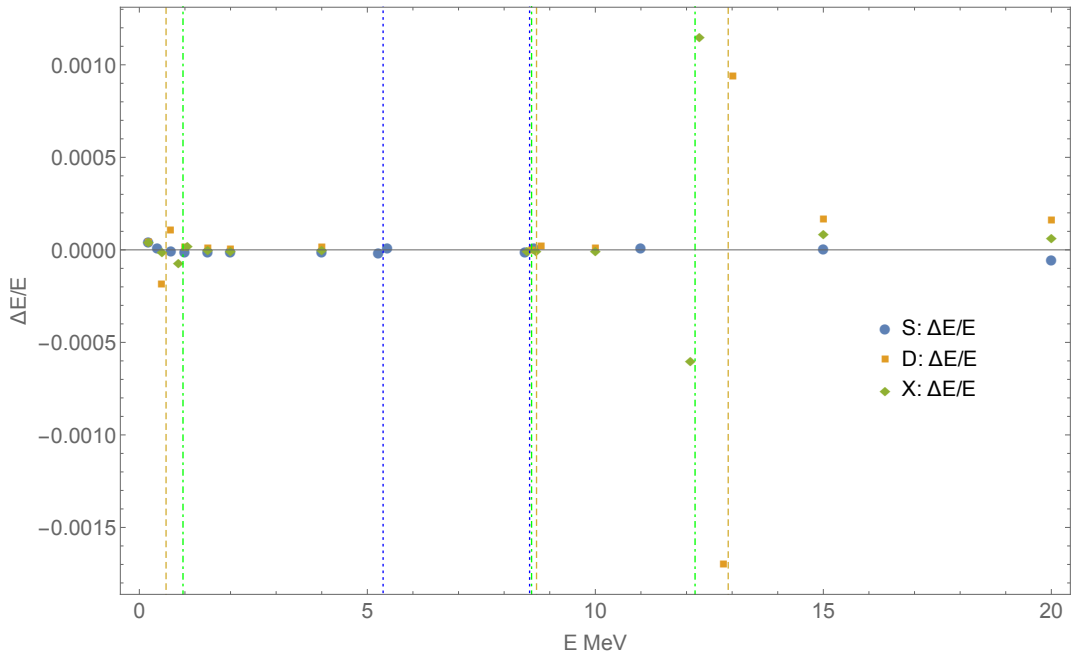

Figure 7.18: NNLO energy convergence from a 0.2 MeV to 10.0 MeV fit with V_{IR} = long range part of Av_{18}.

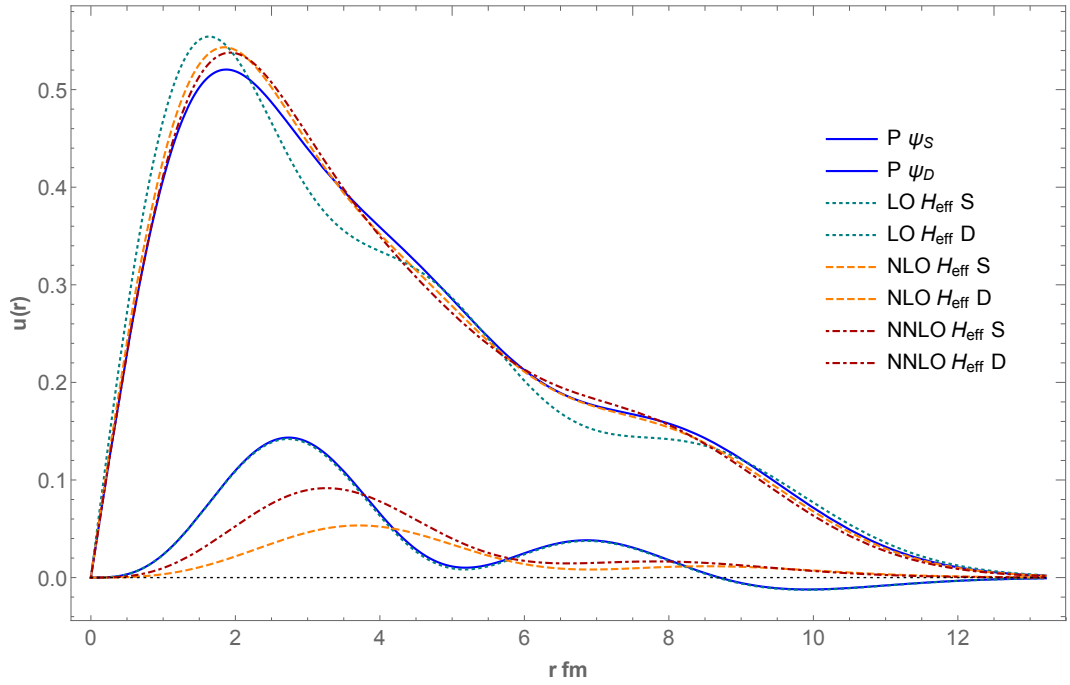

Figure 7.19: LO through NNLO wave functions compared to the known wave function components.

7.4.3 A Heuristic for Residual LEC Energy Dependence

At LO there is a single LEC in the S-S sector, which means that a single energy sample is sufficient to fit at LO. The energy of the bound state is also easily determined, so the LO fit can be performed at the bound state energy. When the fit is performed with V_{IR} = the long range part of Av_{18}, then the D-channel components of the bound state, shown in Table (7.5), are very close to the projected D-channel components. SP and DP stand for the S and D state probability. Wave functions can be seen in Figure (7.19) where the LO D-channel wave function is barely visible against the reference D-channel wave function.

Table 7.5: LO components fit at just the bound state energy.

Order	SP	DP	1S	2S	3S	4S	5S	1D	2D	3D	4D
LO	0.963	0.037	0.928	-0.065	0.278	-0.031	0.137	0.141	0.076	0.087	0.063
Proj	0.961	0.039	0.934	-0.105	0.249	-0.074	0.101	0.145	0.077	0.088	0.063

On the other hand the S-channel components at LO have some substantial differences. Now suppose that the match to the LO D-channel components is included in the fit cost function by simply adding in the square of the difference in components along with a coefficient that can be raised until a good match is found. What happens to the S-channel components? The fit is performed over a smaller energy range using data as close to the bound state eigenvalue as possible, including the bound state itself as well. The resulting wave function components are:

Table 7.6: NNLO components from fit across the -2.2245 to 4.0 MeV range. D-channel components are included in the fit cost function.

Order	SP	DP	1S	2S	3S	4S	5S	1D	2D	3D	4D
NNLO	0.963	0.037	0.938	-0.092	0.248	-0.082	0.076	0.156	0.074	0.077	0.039
Proj	0.961	0.039	0.934	-0.105	0.249	-0.074	0.101	0.145	0.077	0.088	0.063

At NNLO the new fit, shown in Figure (7.20), is greatly improved. To recapitulate, this fit has been obtained from continuum phase shifts and the reasonable assumption that the more delicate D-channel components are actually a function of the long range parts of the potential coupled with the angular momentum barrier and the largest S-channel components, which respond immediately to the LO correction.

The same process will work at continuum energies enabling LEC values to be evolved with energy to preserve the delicate balance between S and D-channel wave functions at low energy.

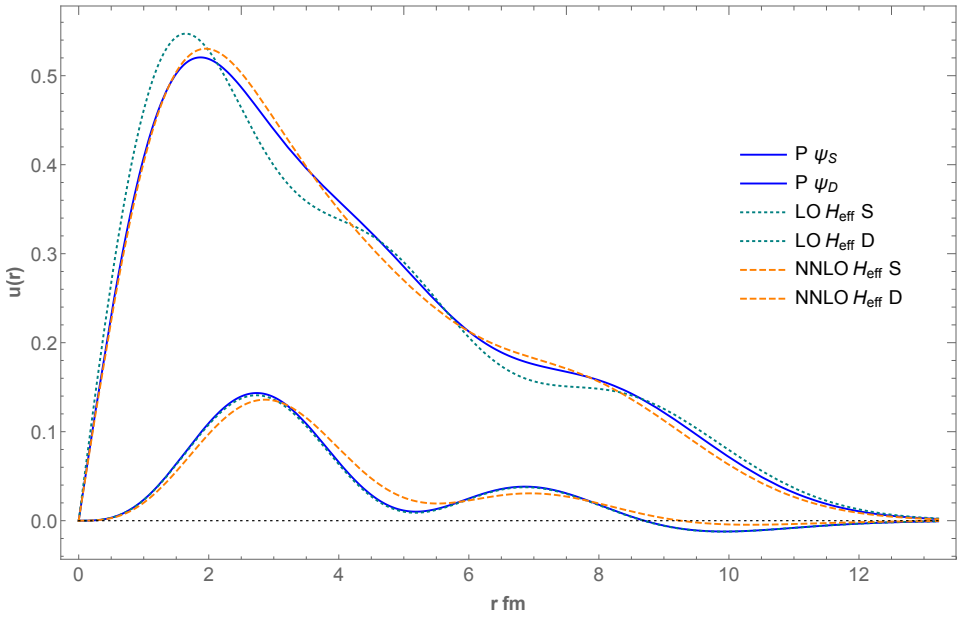

Figure 7.20: A comparison the H_{eff} wave functions at LO and then at NNLO including the D-channel cost function.

Chapter 8

Connecting LQCD to HOBET

In the previous chapters a successful path from experimental phase shifts and bound states to an effective theory was constructed and demonstrated. The natural or obvious path to connect LQCD calculations to HOBET is to follow the same route and extract phase shifts from those calculations. This is much better than the historical route taken for experimental data where thousands of phase shift measurements were used to fit realistic potentials followed by failed attempts to renormalize those potentials into appropriate sized model spaces for shell model calculations. The renormalization step is bypassed by directly configuring the effective theory in a small model space to a modest set of phase shifts that are feasibly calculated in LQCD.

Connecting the HOBET interaction to an A-body effective interaction for the configuration interaction shell model will in practice bypass the fermion sign problem and make nuclear structure calculations from QCD practical.

There are two methods in use for extracting phase shifts that are reviewed here: Lüscher's method and the HAL QCD potential method. The separate limitations of these methods motivate an alternate and more direct approach discussed and implemented in the following chapters.

8.1 Lüscher's Method

In quantum mechanics or QFT an often used trick is to work in a periodic volume. If the results can be parameterized in terms of the length of a side of the volume then results can be calculated first and the infinite volume limit taken later. Another trick used in combination with a periodic volume is to make space-time discrete. This allows conversion of the Hamiltonian or Lagrangian of the problem into a discrete form. Lattice QCD or LQCD uses this approach to compute observables from QCD in a regime where perturbative expansions fail. The grid sizes used for these calculations are coarse. $64^3 \times 96$ space-time sites would be a large lattice as of 2017. The coarseness of the grid can be compensated for with improved numerical implementation of operators, recovering accuracy and rotational

invariance. For the rest of this discussion such lattice effects will be ignored and instead the focus will be on the periodic volume effects. The goal is to be able to extract infinite volume observables from periodic volume observables.

Lüscher [42] showed that QFT and quantum mechanics have the same finite volume behavior. This is a key result in Lüscher's formalism for interpreting LQCD results and HOBET will rely on it also in later chapters. A second part of Lüscher's method is in relating two body energy eigenstates in a finite volume to infinite volume phase shifts.

A short review of Lüscher's method will be presented as it is the current preferred method of connecting finite volume LQCD calculations to infinite volume scattering. The essence of the method is to express the free wave function outside the range of the potential, but inside the period volume in two ways, as an expansion over spherical harmonics, and as an expansion over a constrained periodic momentum basis. The latter expansion is then shown to determine the phase shifts in the spherical form.

In infinite volume the wave function outside of the range of the potential is separable and may be written as a sum over products of radial functions and $Y_{\ell m}$'s.

$$\psi\left(\vec{r}\right) = \sum_{\ell m} \psi_{\ell m}\left(r\right) Y_{\ell m}\left(\hat{r}\right) = \sum_{\ell m} a_{\ell m}\left(\cot\delta_\ell \; j_\ell\left(kr\right) + \eta_\ell\left(kr\right)\right) Y_{\ell m}\left(\hat{r}\right) \tag{8.1.1}$$

There is a such a solution for each continuum(positive) energy value. There are also an infinite set of negative energy solutions with $\cot\delta_\ell$ imaginary, but only cases with $\cot\delta_\ell = i$ are normalizable. The rest diverge exponentially in infinite volume.

The strategy here is to write a Green's function for the Helmholtz operator $(\nabla^2 + k^2)$ in two ways: a spherical form with a regular part that must be configured to meet the periodic boundary conditions, and in a periodic momentum basis where the boundary conditions are met automatically. The parameters of the regular part of the spherical form are then determined by matching with the periodic form.

8.1.1 A Spherical Green's Function

A Green's function for the Helmholtz operator can be written as a linear combination of the divergent solution $\eta_0(r)$ and a regular solution indicated by the hat accent.

$$G\left(\vec{r}; k^2\right) = \frac{k}{\sqrt{4\pi}} Y_{00}\left(\hat{r}\right) \eta_0\left(kr\right) + \hat{G}\left(\vec{r}; k^2\right) \tag{8.1.2}$$

$\hat{G}$ is chosen to meet boundary conditions.

$$\hat{G}\left(r; k^2\right) = \sum_{\ell m} g_{\ell m} Y_{\ell,m}\left(\hat{r}\right) j_\ell\left(kr\right)$$

A complete basis of solutions should include the other divergent solutions at the origin. Derivative operations commute with the Helmholtz operator and can be used to generate additional solutions. A complete set of derivative operators for the purpose can be formed

using harmonic polynomials which are defined by $\mathcal{Y}_{\ell m}(\vec{r}) = r^\ell Y_{\ell m}(\hat{r})$. Derivative operators can be formed by substituting ∇ for $\vec{r}$. The key identity is the application of $\mathcal{Y}_{\ell m}(\nabla)$ to a spherical Bessel function, with f below being either j or η.

$$\mathcal{Y}_{\ell m}(\nabla) f_0(kr) = (-k)^\ell Y_{\ell m}(\hat{r}) f_\ell(kr) \tag{8.1.3}$$

The application to Eq.(8.1.2) results in a Green's function with a divergence of the form $\eta_\ell(r)Y_{\ell m}(\hat{r})$. The strategy in the next section will be to develop precisely the same Green's functions in a periodic basis, forcing the choice of boundary condition and then to extract the $\mathcal{M}_{lm,l'm'}$ below from the periodic form.

$$\begin{aligned} G_{\ell m}\left(\vec{r}; k^2\right) &= \mathcal{Y}_{\ell m}\left(\nabla\right) G\left(\vec{r}; k^2\right) \\ &= -\frac{(-k)^{\ell+1}}{4\pi}\left[Y_{\ell m}\left(\hat{r}\right)\eta_\ell\left(kr\right) + \sum_{\ell' m'} \mathcal{M}_{lm,l'm'} Y_{\ell' m'}\left(\hat{r}\right) j_{\ell'}\left(kr\right)\right] \end{aligned} \tag{8.1.4}$$

where

$$g_{\ell m} = -\frac{(-k)^{\ell+1}}{4\pi}\mathcal{M}_{00,\ell m} \tag{8.1.5}$$

Before moving on to the periodic form, can the $g_{\ell m}$ coefficients be determined from $G\left(\vec{r}; k^2\right)$? The most straightforward way is to integrate $G\left(\vec{r}; k^2\right)$ against the spherical harmonic $Y_{\ell m}(\hat{r})$, extracting $g_{\ell m} j_\ell(kr)$ and then to take the limit as $r \to 0$ after multiplying by r^ℓ to cancel the order of the 0 in $j_\ell(kr)$.

$$\lim_{r\to 0} r^{-\ell} \int d\Omega\; Y_{\ell m}(\hat{r})^* \left(G\left(r;\; k^2\right) - \frac{1}{4\pi r}\right) = \lim_{r\to 0} r^{-\ell} g_{\ell m} j_\ell\left(kr\right) = \frac{k^\ell}{(2\ell+1)!!} g_{\ell m} \tag{8.1.6}$$

The necessary limit for the spherical Bessel function can be found in [35]. The $1/(4\pi r)$ subtraction is to cancel the divergent part of G so that only the regular part contributes. Once the $g_{\ell m}$ are determined, Eq.(8.1.4) can be used to determine the rest of the $\mathcal{M}$ using an expansion of the spherical tensor gradient operator's action found in [43].

$$\mathcal{Y}_{\ell m}\left(\nabla\right) Y_{js}\left(\hat{r}\right) j_j\left(kr\right) = \frac{k^\ell}{\sqrt{4\pi}} \sum_{\ell'=|j-\ell|}^{j+\ell} \sum_{m'=-\ell'}^{\ell'} C_{\ell,m,j,s,\ell',m'} Y_{\ell' m'}\left(\hat{r}\right) j_{\ell'}\left(kr\right) \tag{8.1.7}$$

$$C_{\ell,m,j,s,\ell',m'} = (-1)^{m'}\, i^{\ell-j+\ell'} \sqrt{(2\ell+1)(2j+1)(2\ell'+1)} \begin{pmatrix} \ell & j & \ell' \\ 0 & 0 & 0 \end{pmatrix} \begin{pmatrix} \ell & j & \ell' \\ m & s & -m' \end{pmatrix} \tag{8.1.8}$$

8.1.2 The Periodic Green's Function

Now suppose periodic constraints are imposed with a box sufficiently large that the range of the potential does not reach the edge of the box. Instead of a continuous spectrum of solutions a discrete spectrum is found instead. With a positive energy solution k is real

and the wave function may be continued to infinite volume and remain a solution in the usual scattering sense. The periodic volume acts as a filter, selecting specific energies and amplitudes for the partial waves. For negative energy states k will be pure imaginary with $\cot\delta_\ell \neq i$.

If one continued a negative energy wave function with imaginary $\cot\delta$ to infinite volume it would exponentially diverge, meaning that it could not be normalized in the usual sense of scattered waves. Despite this, such states carry valuable information that will be used to constrain HOBET in later chapters.

It should also be noted that if Eq.(8.1.1) is extended to the origin that each term diverges as $-1/r^\ell$ courtesy of the $\eta_\ell(kr)$ term. This observation will guide the choice of a periodic basis for the free wave function. The essence of Lüscher's method is to insist that Eq.(8.1.1) is equal to an expansion over a periodic basis, yielding constraints on the parameters of the expansion over the spherical harmonics. A first step is to pick a set of basis elements showing the same singular behavior as $\eta_\ell(kr)$.

A Green's function has divergent behavior at the origin, making it a good candidate. A Green's function for the Helmholtz operator in a periodic volume is formed by summing over $\vec{p} \in \{(2\pi/L)\,\vec{n} | \vec{n} \in \mathbb{Z}^3\}$.

$$G\left(\vec{r};k^2\right) = L^{-3}\sum_{\vec{p},p^2\neq k^2}\frac{e^{i\vec{p}\cdot\vec{r}}}{p^2-k^2} \tag{8.1.9}$$

Strictly speaking, G is only a Green's function if k^2 is never in the set of p^2 values.

$$\left(\nabla^2+k^2\right)G\left(r;k^2\right) = -\delta\left(r\right)+\sum_{k^2=p^2}\exp\left(i\vec{p}\cdot\vec{r}\right)$$

This result can be seen by adding and subtracting the offending terms and then taking a limit as p approaches the matching value of k. The Green's function can be repaired in this case (see Lüscher [42] section 3.3 for details), but the repair has no effect on the conclusions to be drawn. It will be assumed that p^2 is not equal to any k^2.

Eq.(8.1.9) can be shown to diverge at the origin in the same way as $\eta_0(kr)$, but solutions for other values of ℓ and m are still needed.. Derivatives commute with the Helmholtz operator, so by applying them a set of additional solutions can be formed that can be shown to be independent and to cover the required set of divergences. A solid harmonic is applied to the gradient operator to form the required set of differential operators, $\mathcal{Y}_{\ell m}(\nabla)$. Some useful identities are

$$\mathcal{Y}_{\ell m}(\nabla)\,\eta_0(kr) = (-k)^\ell\eta_\ell(kr)\,Y_{\ell m}(\hat{r}) \tag{8.1.10}$$

$$\mathcal{Y}_{\ell m}(\nabla)\,e^{i\vec{p}\cdot\vec{r}} = i^\ell\mathcal{Y}_{\ell m}(\vec{p})\,e^{i\vec{p}\cdot\vec{r}} \tag{8.1.11}$$

Eq.(8.1.10) tells us that the rest of the singular part of the basis can be generated by applying the solid harmonic of the gradient to G. Eq.(8.1.11) tells us what happens to G when it is applied.

$$\mathcal{Y}_{\ell m}(\nabla)\,G = G_{\ell m}\left(\vec{r};k^2\right) = L^{-3}i^\ell\sum_{\vec{p}}\frac{\mathcal{Y}_{\ell m}(\vec{p})\,e^{i\vec{p}\cdot\vec{r}}}{p^2-k^2} \tag{8.1.12}$$

8.1.3 Connecting Spherical and Periodic Forms

A connection between the spherical form of the Green's function and the periodic form can be established using

$$e^{i\vec{p}\cdot\vec{r}} = 4\pi \sum_{\ell m} i^{\ell}\, Y_{\ell m}(\hat{p})^{*}\, Y_{\ell m}(\hat{r})\;\; j_{\ell}(pr) \tag{8.1.13}$$

This form is inserted in Eq.(8.1.9).

$$G\left(\vec{r};k^2\right) = 4\pi L^{-3} \sum_{\ell' m'} i^{\ell'} Y_{\ell' m'}(\hat{r}) \sum_{\vec{p}} \frac{Y_{\ell' m'}(\hat{p}) j_{\ell'}(pr)}{p^2-k^2} \tag{8.1.14}$$

When combined with Eq.(8.1.6) only component $\ell' = \ell, m' = m$ survives the integration.

$$\frac{k^{\ell}}{(2\ell+1)!!} g_{\ell m} = \lim_{r\to 0}\left(\frac{4\pi L^{-3} i^{\ell}}{(2\ell+1)!!} \sum_{\vec{p}} \frac{\mathcal{Y}_{\ell m}(\vec{p})}{p^2-k^2} - \delta_{\ell,0} \frac{1}{\sqrt{4\pi} r} \right) \tag{8.1.15}$$

This relation establishes the expansion coefficients $g_{\ell m}$ from which phase shifts can be determined. Evaluation of the right hand side can be written in terms of of a zeta function described by Lüscher. The zeta function is defined by the following equation, but requires analytic continuation to the case where $s = 1$. Expressions for evaluation at $s = 1$ may be found in [44].

$$\mathcal{Z}_{\ell m}(s;q^2) \equiv \sum_{\vec{n}\in\mathbb{Z}^3} \frac{\mathcal{Y}_{\ell m}(\vec{n})}{(n^2-q^2)^s} \tag{8.1.16}$$

With this definition $g_{\ell m}$ can be expressed as

$$g_{\ell m} = \frac{i^{\ell}}{\pi L q^{\ell}} \mathcal{Z}_{\ell m}(1;q^2), \quad q = kL/(2\pi) \tag{8.1.17}$$

A last step is to note that in a periodic volume that the spectrum will be discrete and that the wave function corresponding to a member of the spectrum must necessarily match the singular periodic free wave function derived above in Eq.(8.1.4). If the sum in that equation is truncated at $\ell' = 0$, then the leading order expression for the $\ell = 0$ phase shift can be extracted by comparing Eq.(8.1.1), Eq.(8.1.4), and Eq.(8.1.17).

$$k \cot \delta_0 = \frac{2}{\sqrt{\pi} L} \mathcal{Z}_{0,0}(1;q^2) \tag{8.1.18}$$

In general the sum in Eq.(8.1.4) is truncated at a higher value of ℓ' where the phase shifts should become small, resulting in a set of linear equations involving phase shifts in different channels that must be solved together.

8.1.4 Comments

Lüscher's relationship between energy eigenstates of a two particle system and scattering phase shifts is derived by requiring that the standard spherical expansion of the wave function and an expansion in a periodic momentum basis match in the free region between the range of the potential and the edge of the periodic volume. The existence of a free region is essential to the mathematical analysis and results. Complicating the analysis is that such an expansion will necessarily diverge at the origin. A HOBET implementation in a periodic volume, found in Chapter 9, will work in a related way, building in periodicity by expanding Green's functions over a restricted momentum basis. However, the free region is not required as the connection to a spherical effective theory will be made in a different way. Also important is the that result is a spherical effective theory with a variety of uses, only one of which is the production of phase shifts.

8.2 The HAL QCD Potential Method

The HAL QCD potential method is a newer method for extracting infinite volume results from the finite volume calculations of LQCD. The method begins with the Bethe-Salpeter (BS) wave function for the interacting particles, which will be assumed to be nucleons here. The propagator for a pair of nucleons, with t representing Euclidian time, can be used to produce the wave function for the pair.

$$\phi_E\left(\vec{r}\right) e^{-Et} = \sum_{\vec{x}} \left\langle 0 \left| N_a\left(\vec{x}+\vec{r},t\right) N_b\left(\vec{x},t\right) \right| N=2,E \right\rangle \tag{8.2.1}$$

Given an initial asymptotic state the matrix element expresses the amplitude for a pair of nucleons at time t to have separation $\vec{r}$, which is a wave function for the pair. The ket indicates an initial asymptotic state of two nucleons. This is approximated with a wall source operator for the two nucleons at $t = 0$. The wall source is an approximation in part because the initial state will be contaminated with excited states which may well include other particles than the two nucleons. Euclidian time propagation will eventually suppress the excited states but there is a race with the usual growing Monte-Carlo noise with larger time separation.

Once a wave function is obtained, a non-local potential is extracted, relying like Lüscher's method on the range of the potential being small enough to avoid interactions with periodic images. The potential is constructed as a local potential plus a non-local correction and once it is produced, phase shifts are extracted.

Relatively large lattices with $m_\pi L \approx 7.6$ were used in reference [45] to reduce the problem with images of the potential. However, it will be seen that even at $m_\pi L = 10$ that the contribution from images can shift results for Lüscher's method. It would seem that the HAL QCD potential method will also be perturbed by image contributions, and the magnitude of the perturbations needs quantification.

Chapter 9

HOBET in a Box

In the previous chapter two methods for connecting LQCD calculations to phase shifts were reviewed. Both methods have unquantified sources of error. A common source of error is that because of the expense of lattice QCD calculations they are performed in small volumes where the assumption that the potential goes to 0 at the boundary is violated. In the case of Lüscher's method the convergence of the expansion is also at risk because successive terms in the expression for the phase shift include zeta functions with divergences at a sequence of energies, making it hard to claim that one can truncate the expansion. In the case of the HAL QCD potential method there appear to be uncontrolled systematics associated with the presence of inelastic excited states in the approximation used for the incoming asymptotic state.

This chapter is a response to these concerns. The question is: Can the effective interaction be fit directly to the spectrum of two nucleons in a periodic box, avoiding the complexity of extracting the phase shifts and suppressing the sensitivity to assumptions about the range of interaction? An anticipated future advantage is the extension to determining the 3-body effective interactions where the spectrum continues to have a simple definition, unlike the description of 3 body scattering states.

Putting HOBET in a box means construction of the HOBET effective theory in a periodic volume instead of the infinite volume domain of the previous chapters. The objective is to fit a Cartesian effective theory to the spectrum in a box and then to relate the expansion coefficients to the LECs of an infinite volume spherical HOBET formulation, automatically taking into account the finite volume effects. The construction bypasses all need for an intermediate high-momentum potential and associated renormalization.

A remarkable property of the harmonic oscillator basis that is relied on here is the relationship between Cartesian and spherical representations of the basis. In each energy shell there is separately a unitary transform between the Cartesian and spherical states. The non-edge states in P^- in either basis cover the same part of the Hilbert space and the same can be said for the edge states which are scattered by T into Q. Much of the development of HOBET carries over into the Cartesian basis and the basis relationship will allow Cartesian and spherical results to be related.

In the infinite volume HOBET construction the Green's function for G_{QT} acts on the edge states of the included P space and reproducs the form of the known long range wave function. The phase shift specifies the boundary condition needed to construct the Green's function. In a periodic box the boundary condition for the wave function is that it must be periodic and smooth at the edge of the volume. While the box is periodic, it may have distinct lengths for the sides as will happen if the LQCD state has non-zero total momentum, which is corrected by boosting to the center of momentum frame. Boosting is important because it allows more states to be extracted from the same set of expensive lattice configurations. The natural way to meet the periodic boundary condition is to write the Green's function as an expansion over a periodic basis of sine and cosine waves. With a reasonable cutoff on the maximum spatial frequency of the waves this turns out to be computationally reasonable.

Part of the formulation of HOBET in a box is to describe the effective theory expansion in a Cartesian harmonic oscillator basis so that overlaps between harmonic oscillator states and the periodic basis can be more easily computed. Since the range of the basis and and the V_δ^- part of the interaction are both assumed to be shorter than the distance to the edge of the box, the effective theory expansion will also be independent of the periodic boundary conditions and the transformed expansion will be valid in the spherical infinite volume as well. Even in the case where the interaction is longer range, creating contributions from neighboring images of the potential, the impact on the effective theory expansion will be demonstrated to be small, with most of the impact of the images captured in matrix elements of V_{IR} and segregated from the LECs of the expansion. This is in contrast to Lüscher's method where an overly long range interaction results in substantial loss of accuracy in the determined phase shifts. For HOBET, the phase shifts required for the infinite volume Green's functions can be found by constructing $H_{eff,sph}(E)$ and then dialing the phase shift until an eigenvalue match is found. These phase shifts will be the same values as those produced by the Lüscher method. However, the result is much more powerful, yielding an effective theory from which wavefunctions for bound and scattering states can be determined and used to compute observables of the system.

The procedure for producing the effective theory then consists of the following steps which will appear in sections to follow: 1) forming the needed Green's function, 2) computing the matrix elements of T, 3) computing the matrix elements of V_{IR} which will often be a one pion exchange potential, 4) constructing the Cartesian ET and relating the expansion LECs to the original spherical LECs, 5) fitting the LECs to the available periodic box pairs, 6) determining the infinite volume phase shifts.

9.1 Green's Function of G_{QT} in a Periodic Box

G_{QT} is a key building block in the construction of H_{eff}, connecting the effective theory to the boundary conditions of the theory. In the spherical case the connection is to the phase shifted asymptotic wave function, here it is to the requirement that the wave function be periodic, a condition most easily expressed in a periodic momentum basis.

A momentum basis in a periodic box is naturally Cartesian. Fortunately the 3D harmonic oscillator basis can be easily cast in either spherical or Cartesian form. A unitary transform Eq.(A.6.1) is available to convert one into the other.

As before, the included space $P(\Lambda, b)$ is constrained by Λ. Oscillator states will be indexed by the vector $\vec{n} = (n_x, n_y, n_z)$. The states are constrained by

$$n_x + n_y + n_z \leq \Lambda \tag{9.1.1}$$

The periodic box has side lengths L_i (coordinates from -$L_i/2$ to $L_i/2$) and a lattice spacing a_i which divides L_i. The length of the sides are independent in order to support boosted states, a technique used in LQCD to extract more states at lower computation cost. States with non-zero momentum are boosted to their center of mass frame, adjusting the lengths of the sides of the volume.

The same number of lattice sites are used in each direction: $N = L_i/a_i$ with $i \in x, y, z$. A complete basis of states in the periodic box is a set of sin and cosine waves in each dimension. N will be chosen to be large enough for convergence and normalized odd and even wave functions will be used.

$$\begin{aligned}
&\phi_{i,s,m}(x) = \sqrt{\frac{2}{L_i}} \sin(\alpha_{i,m} x), && n = 1, \ldots, N/2 \\
&\phi_{i,c,0}(x) = \sqrt{\frac{2}{L_i}} (1/\sqrt{2}), && n = 0 \\
&\phi_{i,c,m}(x) = \sqrt{\frac{2}{L_i}} \cos(\alpha_{i,m} x), && n = 1, \ldots, N/2 \\
&\text{with } \alpha_{i,m_i} = 2\pi |m| / L_i
\end{aligned} \tag{9.1.2}$$

Letting m range from $-N/2$ to $N/2$, negative indices are used to indicate the sine solutions and non-negative indices to indicate the cosine solutions. This set of solutions for large enough N is an accurate periodic basis for the periodic box. The basis of 3D solutions can be written as

$$\phi_{\vec{m}}(x, y, z) = \phi_{m_x}(x)\ \phi_{m_y}(y)\ \phi_{m_z}(z) \tag{9.1.3}$$

The kinetic energy operator is a bit complicated by the varying side lengths.

$$\hat{T}\phi_{\vec{m}}(x, y, z) = 2\pi^2 \left(\sum_i \frac{m_i^2}{L_i^2} \right) \phi_{\vec{m}} = \lambda_{\vec{m}} \phi_{\vec{m}}(x, y, z) \tag{9.1.4}$$

The strategy is to use this basis set to compute

$$G_{QT} P = \frac{E}{E - T} \left\{ P \frac{E}{E - T} P \right\}^{-1} P \tag{9.1.5}$$

Using an bilinear eigenfunction expansion the Green's function can be written as

$$G_T(E;\ \mathbf{r}', \mathbf{r}) = \sum_{\vec{m}} \frac{E}{E - \lambda_{\vec{m}} + i\varepsilon} \phi_{\vec{m}}(\mathbf{r}')\, \phi_{\vec{m}}(\mathbf{r})$$

where $+i\varepsilon$ has been added to avoid the possible pole. In following equations the $i\varepsilon$ term will be understood to be present. G_{QT} will have well behaved limits as $\varepsilon \to 0^+$. The matrix elements can be written as

$$\langle \vec{n}' \left| G_T \right| \vec{n} \rangle = \sum_{\vec{m}} \frac{E}{E - \lambda_{\vec{m}}} \langle \vec{n}' \left| \phi_{\vec{m}} \left(\mathbf{r}' \right) \phi_{\vec{m}} \left(\mathbf{r} \right) \right| \vec{n} \rangle$$

The individual matrix elements in the sum decompose nicely as

$$\langle \vec{n}' \left| \phi_{\vec{m}} \left(\mathbf{r}' \right) \phi_{\vec{m}} \left(\mathbf{r} \right) \right| \vec{n} \rangle = \chi_{\vec{n}',\vec{m}}, \chi_{\vec{n},\vec{m}}$$

with χ representing the integrals

$$\chi_{n,m} = \int_{-\infty}^{\infty} dx \; H_n \left(x \right) \phi_m \left(x \right)$$

$$\chi_{\vec{n},\vec{m}} = \chi_{n_x,m_x} \chi_{n_y,m_y} \chi_{n_z,m_z}$$

To perform the integrals the Hermite polynomial is decomposed, with a parity match yielding non-zero integrals of the form

$$S_{2q+1,m} = \int_{-L/2}^{L/2} dx \; e^{-x^2/2} x^{2q+1} \sin \left(\alpha_m x \right)$$

$$C_{2q,m} = \int_{-L/2}^{L/2} dx \; e^{-x^2/2} x^{2q} \cos \left(\alpha_m x \right)$$

These integrals can be accurately evaluated by extension of the integration bounds assuming that the Gaussian factor suppresses the integrand beyond $L_{min}/2$. A numerical integration on the range $-L/2$ to $L/2$ is used to check that the length scale is small enough to confine the harmonic oscillator basis to the box.

$$\begin{aligned} S_{2q+1,m} &\approx \int_{-\infty}^{\infty} dx \; e^{-x^2/2} x^{2q+1} \sin \left(\alpha_m x \right) \\ &= \alpha_m \; 2^{q+\frac{3}{2}} \; \Gamma \left(q + \frac{3}{2} \right) \; {}_1F_1 \left(q + \frac{3}{2}, \frac{3}{2}, -\frac{\alpha_m^2}{2} \right) \\ C_{2q,m} &\approx \int_{-\infty}^{\infty} dx \; e^{-x^2/2} x^{2q} \cos \left(\alpha_m x \right) \\ &= 2^{q+1/2} \; \Gamma \left(q + \frac{1}{2} \right) \; {}_1F_1 \left(q + \frac{1}{2}, \frac{1}{2}, -\frac{\alpha_m^2}{2} \right) \end{aligned}$$

Using these results χ can be constructed as

$$\begin{aligned}\chi_{n,m} &= n! \sum_{q=0}^{\lfloor n/2 \rfloor} \frac{(-1)^q}{q!\,(n-2q)!\,2^q} \int_{-L/2}^{L/2} dx\; e^{-x^2/2} x^{n-2q} \phi_m(x) \\ &= \sqrt{\frac{2}{L}} n! \sum_{q=0}^{\lfloor n/2 \rfloor} \frac{(-1)^q}{q!\,(n-2q)!\,2^q} \begin{cases} S_{n-2q,m} & odd\,(n) \\ C_{n-2q,m} & even\,(n) \end{cases}\end{aligned}$$

Combining these results yields the matrix elements of G_T in the P space.

$$\langle \vec{n}' | G_T | \vec{n} \rangle = \sum_{\vec{m}} \frac{E}{E - \lambda_{\vec{m}}} \chi_{\vec{n}',\vec{m}} \chi_{\vec{n},\vec{m}} \tag{9.1.6}$$

The representation $b^{-1}_{\vec{n}',\vec{n}}$ will be used for these matrix elements and $b_{\vec{n}',\vec{n}}$ for the inverse.

To obtain $G_{QT} |\vec{n}\rangle = b_{\vec{n},\vec{n}'} G_T |\vec{n}'\rangle$, $G_T |\vec{n}'\rangle$ is also needed, but this is easily obtained from the work above.

$$\begin{aligned}G_T(E;\ \mathbf{r}, \mathbf{r}') |\vec{n}\rangle &= \sum_{\vec{m}} \frac{E}{E - \lambda_{\vec{m}}} \phi_{\vec{m}}(\mathbf{r}) \int_{-L/2}^{L/2} d\vec{r}\,'\; \phi_{\vec{m}}(\mathbf{r}')\, H_{\vec{n}}(\vec{r}\,') \\ &= \sum_{\vec{m}} \frac{E\ \chi_{\vec{n},\vec{m}}}{E - \lambda_{\vec{m}}} \phi_{\vec{m}}(\mathbf{r})\end{aligned}$$

9.2 Kinetic Energy Matrix Elements

The kinetic energy part of the effective Hamiltonian can be written in a more convenient form for evaluation

$$\left\langle \vec{n}' \middle| G_{QT} E \left(T + T \frac{Q}{E} T \right) E G_{QT} \middle| \vec{n} \right\rangle = \langle \vec{n}' | T E G_{QT} | \vec{n} \rangle$$

Starting with this form the matrix elements can be computed in terms of E and $b_{ij} = \langle i | G_T | j \rangle^{-1}$.

$$\begin{aligned}\left\langle \vec{n}' \middle| T \frac{E}{E - QT} \middle| \vec{n} \right\rangle &= \left\langle \vec{n}' \middle| T \frac{E}{E - T} \middle| \vec{n}'' \right\rangle b_{\vec{n}'',\vec{n}} \\ &= E \left\langle \vec{n}' \middle| \left(1 - \left(1 - \frac{T}{E} \right) \right) \frac{1}{1 - T/E} \middle| \vec{n} \right\rangle b_{\vec{n}'',\vec{n}} \\ &= E \left\langle \vec{n}' \middle| \frac{E}{E - T} - 1 \middle| \vec{n}'' \right\rangle b_{\vec{n}'',\vec{n}} \\ &= E\,(\delta_{\vec{n}',\vec{n}} - b_{\vec{n}',\vec{n}})\end{aligned}$$

An interesting observation is that the effective kinetic energy operator diverges at the same values of E that $b_{\vec{n}',\vec{n}}$ does. V_δ must then have a compensating divergence at infinite order.

9.3 Matrix Elements of V_{IR}

This section first addresses some of the specific issues with evaluation of the matrix elements of $V_{IR} = V_\pi$, which is the long range potential of choice for nucleon-nucleon interactions. Afterwards, more general issues related to the computational approach for any V_{IR} are addressed. Computation of these matrix elements is the most expensive step in the construction of the effective Hamiltonian.

The general form of the required matrix elements is

$$\left\langle n', S', m'_S \left| G^\dagger_{QT}\, V_\pi\, G_{QT} \right| n, S', m'_S \right\rangle \tag{9.3.1}$$

with the local potential V_π defined as

$$\tilde{f}^2_\pi m_\pi \tau_1 \cdot \tau_2 \frac{e^{-\alpha r}}{\alpha r} \left[\sigma_1 \cdot \sigma_2 + \left(1 + \frac{3}{\alpha r} + \frac{3}{(\alpha r)^2} \right) S_{12} \right]$$

$$\alpha = m_\pi \sqrt{2}\; b/\hbar, \qquad \tilde{f}^2_\pi \sim \frac{m^2_\pi}{12\pi} \left(\frac{g_A}{\sqrt{2} f_\pi} \right)^2 \sim 0.024$$

At the physical point the values $f_\pi = 130.4$ MeV and $g_A = 1.272$ are used and in the pn channel an effective pion mass $m_\pi = 138.05$ MeV reflects the contributions from both charged and neutral pions. The usual delta function in V_π is dropped as it corresponds directly to the lowest order term in the V_δ expansion.

Quantum number m_S is included because the Cartesian basis states do not have good angular momentum. In particular, the matrix elements of the S_{12} operator in the spin basis and direction $\hat{r}$ are needed. Spherical vector components are listed in the order $(+1, 0, -1)$, so the upper right corner of the matrix below corresponds to $m' = 1,\ m = -1$.

$$S_{12} = 3\,(\sigma_1 \cdot \hat{r})\,(\sigma_2 \cdot \hat{r}) - \sigma_1 \cdot \sigma_2$$

$$\langle \hat{r}, S'{=}1, m'_S \,|S_{12}|\, \hat{r}, S{=}1, m_S \rangle =$$

$$\begin{pmatrix} 3\hat{r}_z^2{-}1 & 3\sqrt{2}\hat{r}_z\,(\hat{r}_x{-}i\hat{r}_y) & 3(\hat{r}_x{-}i\hat{r}_y)^2 \\ 3\sqrt{2}\hat{r}_z\,(\hat{r}_x{+}i\hat{r}_y) & 2\,(1{-}3\hat{r}_z^2) & -3\sqrt{2}\hat{r}_z\,(\hat{r}_x{-}i\hat{r}_y) \\ 3(\hat{r}_x{+}i\hat{r}_y)^2 & -3\sqrt{2}\hat{r}_z\,(\hat{r}_x{+}i\hat{r}_y) & 3\hat{r}_z^2{-}1 \end{pmatrix}_{m',m}$$

The matrix elements will be determined by numerical integration against V_π. However, when evaluating entries where both $\vec{n}'$ and $\vec{n}$ are edge states the number of such integrals is too large as each state expression is a sum over the momentum basis. The individual elements of S_{12} and $\sigma_1 \cdot \sigma_2$ can be computed as part of straightforward numeric integrals. In what follows $W(r)$ stands for a spin component of V_π selected by m' and m.

$$\left\langle n' \left| G^\dagger_{QT}\, W\,(r)\; G_{QT} \right| n \right\rangle = b^{-1}_{n',j} b^{-1}_{n,i} \left\langle j \left| G^\dagger_T\, W\,(r)\; G_T \right| i \right\rangle$$

Excessive computation can be avoided by rewriting the matrix elements to expose a much smaller number of integrals that can be computed via FFT. A double sum over the momentum basis will still be required but the computation per entry will be small.

$$\left\langle j \left| G_T^\dagger \; W\left(r\right) \; G_T \right| i \right\rangle = \sum_{\vec{m}',\vec{m}} \frac{E}{E-\lambda_{m'}} \frac{E}{E-\lambda_m} \left\langle j \right| m' \left\rangle \right\langle m' \left| W(\vec{x}) \right| m \left\rangle \right\langle m \right| i \left\rangle$$

$$\left\langle j \left| G_T^\dagger \; W\left(r\right) \; G_T \right| i \right\rangle = \sum_{\vec{m}',\vec{m}} \frac{E \; \chi_{j,\vec{m}'}}{E-\lambda_{\vec{m}'}} \frac{E \; \chi_{i,\vec{m}}}{E-\lambda_{\vec{m}}} \int\limits_V d\vec{x} \; \phi_{m'}\left(\vec{x}\right) \phi_{\vec{m}}\left(\vec{x}\right) W\left(\vec{x}\right)$$

Naively the number of integrals is equal to the number of lattice momentum states squared. However, the two references to ϕ can be expanded to exponentials so that the integrals correspond to sums of a few components of the FFT of the potential. This allows quick construction of the integrals. V_π can be sampled on the lattice and then a 3D FFT applied to generate the components. As an example, take $m' = 1, 2, 3$ and $m = 4, 4, 4$.

$$\phi_{m'}(x)\phi_m(x) = \cos(1 \cdot \frac{2\pi}{L_x}x)\cos(4 \cdot \frac{2\pi}{L_x}x) \cos(2 \cdot \frac{2\pi}{L_y}y)\cos(4 \cdot \frac{2\pi}{L_y}y)\cos(3 \cdot \frac{2\pi}{L_z}z)\cos(4 \cdot \frac{2\pi}{L_z}z)$$

The following expansions to the products of two cos functions (or cos and sin, etc.) can be used as a first step toward a sum of exponentials.

$$\sin(\beta x)\sin(\alpha x) = (1/2)\left(\cos\left((\alpha-\beta)x\right) - \cos\left((\alpha+\beta)x\right)\right)$$
$$\cos(\beta x)\sin(\alpha x) = (1/2)\left(\sin\left((\alpha-\beta)x\right) + \sin\left((\alpha+\beta)x\right)\right)$$
$$\cos(\beta x)\cos(\alpha x) = (1/2)\left(\cos\left((\alpha-\beta)x\right) + \cos\left((\alpha+\beta)x\right)\right)$$

This substitution results in

$$\begin{aligned}\phi_{m'}(x)\phi_m(x) = \frac{1}{8} &\left(\cos(3 \cdot \frac{2\pi}{L_x}x) + \cos(4 \cdot \frac{2\pi}{L_x}x)\right) \\ &* \left(\cos(2 \cdot \frac{2\pi}{L_y}y) + \cos(6 \cdot \frac{2\pi}{L_y}y)\right) \\ &* \left(\cos(1 \cdot \frac{2\pi}{L_z}z) + \cos(7 \cdot \frac{2\pi}{L_z}z)\right)\end{aligned} \tag{9.3.2}$$

Expanding the cos or sin functions into exponentials and expanding the product results in $4^3 = 64$ of the FFT basis functions. The integral of $W(x)$ against the product of momentum states is then a sum across the corresponding FFT components of $W(x)$. An accurate

approximation can be had by assuming that the high frequency components are 0, enabling runtime control of the computation. Details of using an FFT to compute the required integrals may be found in appendix D.

If V_{IR} is not smooth, as in a sharp potential well, then the FFT result will not converge well and direct integration will be required.

9.4 Matrix Elements of V_δ

V_δ encodes a combination of the short range difference between V and V_{IR} as well as the result of integrating out contributions from scattering through Q. The matrix elements can be split into two parts, one called V_δ^- that only involves states in P^- which omits edge states, and matrix elements that do involve edge states. P^- is the same space in both spherical and cartesian forms, which are related by a unitary transform, $\langle n, L, m|\, n_x, n_y, n_z\rangle$, between the two representations. V_δ^- is therefore also the same object in both representations. The strategy then is to create an expansion in Cartesian harmonic oscillator lowering operators by analogy to the spherical expansion and by insisting that V_δ^- represents the same object in either representation the matrix elements, the LECs of the two forms can be related and the resulting combinations of spherical LECs substituted into the Cartesian V_δ, including the matrix elements for edge states.

An important side effect of solving for Cartesian LECs as a linear combination of spherical LECs is that symmetries like rotational symmetry which limited the number of spherical operators are automatically imposed on the Cartesian form of the effective theory, which initially has many more LECs.

The matrix elements of states at the edge of P which are transformed by G_{QT}, also known as edge states, will be different because the boundary conditions used to construct the Green's functions are quite different. However, as the correspondence between the Cartesian LECs and the spherical LECs has already been established, the differential form of the 1D lowering operators can be applied to the momentum basis that G_{QT} is expressed in, substituting the equivalent combination of spherical LECs for each operator.

The details of construction of the Cartesian ET expansion are now addressed. Parity conservation tells us that ET operators must be built from an even number of lowering operators a_x, a_y or a_z. The order of the operator is the number of lowering operators divided by two. This definition matches the spherical operators.

The general form of an ET operator is some lowering operators acting to the left, a delta function and some lowering operators acting to the right. Unlike the spherical form the LEC values will not be adjusted with the matrix elements of the delta function. The effect on those matrix elements is a simple scaling of the LECs and as the Cartesian LECs will be eliminated in favor of the spherical ones there would be no useful effect.

The rules for distinguishing operators are simple. Operators that can't be transformed into each other by exchanges of directions are distinguishable, i.e. lowering the x oscillator

twice is different from lowering along x and along y. Hermiticity tells us that the same LEC governs operators where acting to the left and right is swapped.

The LEC label for an operator can be generated uniquely from the x, y, and z lowering counts to the left and right as follows. First compare the total count of left and right lowering operations. If the right hand side has more lowering operations, then swap the sets of counts. Otherwise, sort the x, y, and z lowering counts on each side with the largest first and compare the resulting 3 digit numbers. If the right hand 3 digit number is larger, then swap the counts. Next, directions are ordered by weights determined by the left and right counts (as in $left * 1000 + right$) with swapping by directions applied to both left and right sets of counts. The resulting sets of left and right counts identify the same LEC for operators that are equivalent under exchange of direction or conjugation. In what follows the LEC name begins with c to identify it as a Cartesian LEC and the ordered left and right lowering counts are used in the name. Table 9.1 illustrates the organization of the operators into groups with associated LECs and the naming of the LECs.

Table 9.1: LECs and Cartesian operators

LEC	operators
$c000d000$	$\delta(r)$
$c100d100$	$\left(a_x^\dagger \delta(r) a_x + a_y^\dagger \delta(r) a_y + a_z^\dagger \delta(r) a_z\right)$
$c100d010$	$\left(a_x^\dagger \delta(r) a_y + a_x^\dagger \delta(r) a_z + a_y^\dagger \delta(r) a_z\right) + \text{h.c.}$
$c200d000$	$\left(a_x^{\dagger 2} + a_y^{\dagger 2} + a_z^{\dagger 2}\right) \delta(r) + \text{h.c.}$
$c110d000$	$\left(a_x^\dagger a_y^\dagger + a_x^\dagger a_z^\dagger + a_y^\dagger a_z^\dagger\right) \delta(r) + \text{h.c.}$

The matrix elements of V_δ^- in either basis are related by spherical-cartesian brackets, allowing us to write the Cartesian LECs as a linear combination of spherical LECs. These expressions can then be used to express the result of applying a Cartesian operator in terms of spherical LECs.

Consider a simple example with even parity states up to $\Lambda = 2$ and an interaction that does not mix angular momentum states. In spherical and Cartesian forms this results in 7 states:

$$|n, \ell, m\rangle \quad \in \{|1,0,0\rangle, |2,0,0\rangle, |1,2,-2\rangle, |1,2,-1\rangle, |1,2,0\rangle, |1,2,1\rangle, |1,2,2\rangle\}$$
$$|n_x, n_y, n_z\rangle \in \{|0,0,0\rangle, |1,1,0\rangle, |1,0,1\rangle, |0,\ 1,\ 1\rangle, |2,0,0\rangle, |0,2,0\rangle, |0,0,2\rangle\}$$

V_δ^- is constructed in a Cartesian harmonic oscillator basis using operators as defined in table 9.1. Then V_δ^- is constructed in a spherical harmonic oscillator basis and using spherical-Cartesian brackets transformed it to a Cartesian harmonic oscillator basis. In both bases the matrix elements of V_δ^- are simple linear combinations of LECs, in one case the Cartesian LECS and in the other the original spherical or angular momentum channel LECs. Both constructions of V_δ^- must match, immediately relating the Cartesian LECs to the spherical

ones. With these constraints one can easily solve for the LEC correspondence.

$$
\begin{aligned}
c000d000 &= a_{LO}^{1S0} \\
c200d000 &= a_{NLO}^{1S0} \\
c200d200 &= a_{NNLO22}^{1S0} + (2/3)a_{NNLO}^{1D2} \\
c200d020 &= a_{NNLO22}^{1S0} - (1/3)a_{NNLO}^{1D2} \\
c110d110 &= 2a_{NNLO}^{1D2}
\end{aligned}
$$

A key point is that in establishing this correspondence that the symmetries such as angular momentum conservation imposed on the spherical V_δ^- by construction will now be imposed as linear constraints on the Cartesian LECs. The Cartesian LECs will in fact be eliminated in favor of the spherical ones, so that fitting of the Cartesian theory to observables is done in terms of spherical LECs and automatically respects the associated symmetries.

After the correspondence is established, the operators can be applied as differential operators to edge states, which are expressed as a linear combination of lattice momentum states. Table 9.2 gives the action of powers of the lowering operator evaluated at 0. When applied to momentum state $\phi_{\vec{m}}$ the derivatives produce powers of $\alpha_{\vec{m}}$ and a sign as the derivative cycles between sine and cosine, so the action is easy to compute.

Table 9.2: Powers of lowering operator simplified at $r_i = 0$ for edge states. Derivative operators have been commuted to the right and terms with remaining powers of r dropped.

Power	Expansion
n	$2^{-n/2}\left(\partial_i + r_i\right)^n$
0	1
1	$2^{-1/2}\left(\partial_i\right)$
2	$2^{-2/2}\left(1 + \partial_i^2\right)$
3	$2^{-3/2}\left(3\partial_i + \partial_i^3\right)$
4	$2^{-4/2}\left(3 + 6\partial_i^2 + \partial_i^4\right)$
5	$2^{-5/2}\left(15\partial_i + 10\partial_i^3 + \partial_i^5\right)$

The result is again a linear combination of spherical LECs. Such edge matrix elements will include the non physical mixing between angular momentum channels that are implied by the periodic box constraints.

9.5 Fitting the LECs

It is common in LQCD calculations to perform calculations in more than on volume. Because V_δ is isolated from the boundary conditions and to a lesser extent from an overly long range potential, data from all volumes can be combined in the fitting of the LECs. For each pair of energy and periodic box $H^{eff}\left(E\right)$ can now be constructed. The V_δ portion of H^{eff} has

matrix elements that are a linear combination of LECs. The fitting goal is to choose a single set of LEC values such that for all sample energies $H^{eff}(E)$ has an eigenvalue close to that energy.

The Monte-Carlo measures of the energy eigenvalues naturally have uncertainty. This uncertainty may also be correlated because because multiple measurements can be taken from a single configuration. A procedure for taking uncertainty and correlation into account in the fit may be found inSection 6.2.

The spectrum in a box will contain states belonging to different cubic representations which overlap subsets of angular momentum states. One possible strategy is to fit all the angular momentum states of a given parity up to some ℓ cutoff simultaneously. At low energy, the angular momentum barrier above that cutoff will make LEC values for high ℓ channels unimportant. With ample sample data this is a successful strategy.

If less data is available, it is possible to fit just the $\ell = 0$ channel. LQCD states can be projected onto cubic representations, only one of which, the A_1^+ representation, overlaps $\ell = 0$. More discussion of cubic representations will follow in the next chapter, but some properties of A_1^+ are relevant here. The A_1^+ representation overlaps only $\ell = 0, 4, 6$ and higher even values of ℓ. This means that $\ell = 0$ can be independently fit for moderate energies where $\ell = 4$ is unimportant.

An additional issue in fitting is that the Cartesian H_{eff} covers all the states up to the energy cutoff Λ and will be a fairly large matrix with a large number of eigenpairs, only one of which represents the Bloch-Horowitz state being fit. It is quite possible that one of the other eigenpairs with no $\ell = 0$ overlap will actually be initially closer to the sample energy than the correct eigenpair with the initial LEC values used in fitting. In such a case modest trial changes to the $\ell = 0$ LECs will not change the closest eigenvalue to the sample energy and the fitting process will not make progress. To overcome this, only eigenpairs overlapping the target channel should be considered when determining the nearest eigenvalue in the spectrum of the matrix. With this addition, the fitting process for a restricted set of LECs works well.

9.6 Determining Phase Shifts from the Effective Theory

After LECs are fit to minimize the consistency error of the Cartesian $H_{eff}(E_i)$, the LECs can be used in the spherical H_{eff} construction. Normally, the phase shifts would be an input to the process and the LECs would be unknown and fit to achieve energy consistency. In this case the reverse is true and the phase shifts are fit to achieve energy consistency with the known LEC values fixed.

The phase shifts can be found numerically by generating an initial set of phase shifts and then for each one iterating the equation $H_{eff}(E, \delta_\ell)P|\psi\rangle = EP|\psi\rangle$ until the energy $E = k^2/2$ converges. Some trial phase shift values may have no solution and should be discarded. The resulting pairs of $\left\{k^{2\ell+1}\cot(\delta_\ell), k^2\right\}$ can be used to fit an effective range

expansion.

$$k^{2\ell+1}\ \cot\left(\delta_\ell\right) = -\frac{1}{a_\ell} + r_\ell k^2 + v_\ell k^4 + \cdots \tag{9.6.1}$$

The effective range expansion is then used to estimate an initial phase shift for a selected energy, which can be refined by bisection.

Chapter 10

Demonstration of HOBET in a Box

The demonstration of HOBET in a box has two parts. The first part is an examination of the impact of periodic boundary conditions and the non-physical mixing induced by them. This establishes the context in which the effective theory is constructed and fit.

The second part uses a known potential with a one pion exchange like long range behavior to generate a spectrum in a periodic box. As an extra challenge, the potential does not die out by the edge of the box. The potential is also used to establish reference phase shifts that HOBET can be tested against. The periodic box Cartesian harmonic oscillator based effective theory is fit to the spectrum, transformed to a spherical infinite volume effective theory and then used to recover phase shifts and bound states. The recovered phase shifts are expected to match the reference values, demonstrating that the derived effective theory is a faithful representation of the full theory.

10.1 Induced Mixing via Periodic Boundary Conditions

Periodic boundary conditions lead to non physical mixing of angular momentum states. Consider a bound state in one dimension about a central potential. Outside of the range of the potential the wave function will be a linear combination of an exponentially growing part and an exponentially decaying part. In an infinite volume normalization considerations rule out the exponentially growing part. If one now imposes periodic boundary conditions about the origin of the potential, then the exponentially growing part must be reintroduced to satisfy the boundary conditions.

Generalizing to three dimensions, if one starts with an S-channel bound state and introduces periodic boundary conditions, then one not only has to re-introduce the growing exponential solution, but also higher L components are needed to establish periodicity away from the centers of the faces.

A concrete example can be constructed by solving the Schrödinger equation in an 35 fm

side length periodic volume for a simple well potential.

$$V(r) = \begin{cases} -V_0 & r \le R \\ 0 & r > R \end{cases}, \quad \begin{array}{l} R = 2.1 \text{ fm} \\ V_0 = 33.73416 \text{ MeV} \end{array}$$

This potential was tuned to produce a bound state with the binding energy of the deuteron, ≈ -2.2245 MeV.

The low lying eigenstates of this system were found on a 400^3 lattice with a solver described in Section 11.5. The side length of the volume is quite a bit larger than the range of the potential and one might think that this would reduce the mixing.

Outside the range of the potential and inside the box these eigenstates have the usual form.

$$\psi(\vec{r}) = \sum_{\ell m} Y_{\ell m}(\hat{r})\, \psi_{\ell,m}(r)$$

An assumption made by Lüsher [42] is that this is a rapidly convergent series in L. The bound state is only slightly modified by the boundary conditions, gaining only small contributions in other channels, but other low lying states are significantly affected. With this very simple example, the 3rd positive parity state with $E = 1.336$ MeV has an interesting structure shown in Fig. 10.1. The figures show the wave function on a spherical slice outside the range of the potential as a radial displacement on a unit sphere. This state has large $L = 2, 4, 6$ components and no $L = 0$ component. The higher order structure is clearly visible in the top view in the neck between the top and bottom lobes. This state would not be useful in deriving an S-channel model because it belongs to the E^+ representation of the cubic rotation group which does not overlap S.

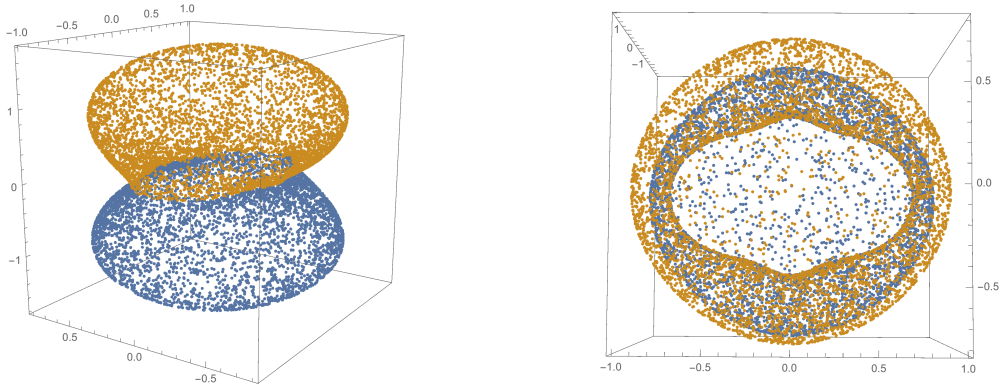

Figure 10.1: Spherical slice of the 3^{rd} positive parity eigenstate in a 35 fm box. The wave function is displayed as a radial displacement on a unit sphere. Points in the top half are gold to give a depth cue in the top view on the right.

The next state up in energy at $E = 1.692$ MeV belongs to the A_1^+ representation which has the following 3 components up to $\ell = 6$ with $m = 0$. Details on cubic representations

can be found in Luu and Savage [44] as well as Lüscher [42].

$$\begin{aligned} &|0,0\rangle \\ &\frac{1}{2}\sqrt{\frac{5}{6}}\,|4,4\rangle + \frac{1}{2}\sqrt{\frac{7}{3}}\,|4,0\rangle + \frac{1}{2}\sqrt{\frac{5}{6}}\,|4,-4\rangle \\ &\frac{\sqrt{7}}{4}\,|6,4\rangle - \frac{1}{\sqrt{8}}\,|6,0\rangle + \frac{\sqrt{7}}{4}\,|6,-4\rangle \end{aligned} \tag{10.1.1}$$

Table 10.1: Angular momentum content of the $E = 1.692$ MeV state.

ℓ	m	$\lvert Amplitude\rvert$
0	0	0.31431
4	-4	0.30036
4	0	0.49887
4	+4	0.30036
6	-4	0.45430
6	0	0.24317
6	+4	0.45430

To check this the angular momentum content of the lattice solution was extracted by numerically integrating against $Y_{\ell,m}$ on a shell inside the volume but outside the range of the potential at two closely separated radii, giving the derivative of the radial function. Using Eq.(C.0.1) the amplitude of the component can be calculated. For Table (10.1) the amplitudes were normalized ignoring states above $\ell = 6$. If this state belongs to the A_1 representation, then the amplitude ratios of the components for $\ell = 4$ as well as $\ell = 6$ should match the ratios from Eq.(10.1.1).

$$0.30036/0.49887 = 0.60208, \quad \frac{1}{2}\sqrt{\frac{5}{6}}\Big/\left(\frac{1}{2}\sqrt{\frac{7}{3}}\right) = 0.60208$$

$$0.45430/0.24318 = 1.86816, \quad \frac{\sqrt{7}}{4}\Big/\left(\frac{1}{\sqrt{8}}\right) = 1.86818$$

These results show that to high precision the ratios of the components, which are independent of the normalization, match the expected values.

When LQCD states are generated, they can be projected on to cubic representations. This is important because each cubic representation has specific angular momentum content. As an example, states in the E representation have no $L = 0$ content and should not be included in a fit unless LECs connecting to $L = 2$ states are part of the fit. The danger is that a non-physical eigenstate of the $H_{eff}(E_i)$ matrix will respond to changes in S-channel LECs, leading to an incorrect local minimum in the fitting cost function. A similar problem

can occur if a non-physical eigenstate with no $L = 0$ overlap may have the closest eigenvalue to E_i. The result is that even when trial changes to LECs move the correct eigenstate's eigenvalue closer to E_i that the even closer non-physical eigenvalue hides the improvement from the cost function. To avoid this problem the fitting program has been modified to ignore eigenstates of H_{eff} that don't match the cubic representation of the target state.

10.2 Construction of the Effective Interaction from a Spectrum

For this example he periodic volume corresponds to $m_\pi L \approx 10$, yielding $L = 14.3$ fm. This periodic volume size is large compared to typical LQCD volumes which are used with heavier pion masses.

A potential with the long range form of a one pion exchange potential was used. The Schrödinger equation with the full potential is solved in the periodic volume on a lattice sizes of N^3 with $N = 350, 400, 450$. The energy eigenvalues are expressed as a quadratic function of the lattice spacing 14.3 fm$/N$ and extrapolated to the continuum to produce a spectrum. The idea is to avoid as much as possible the introduction of error in the result due to small errors in the spectrum so that other error sources can be better analyzed. The rest of the calculations use only the IR part of the potential, the volume size and the spectrum.

$$V_{IR}(r) = -1.3 * 100.0 \frac{e^{-m_\pi r}}{m_\pi (r + 0.75 \text{ fm})} \text{ MeV}$$
$$V(r) = V_{IR}(r) + 1.3 * 138.0 e^{-4 m_\pi r} \text{ MeV}$$

The addition of 0.75 fm in the denominator avoids an infinite potential at the origin and has little impact on the OPEP like behavior at long range. The value of m_π is set to the blended value of 138.039 MeV so that the potential decays like a physical pion mass potential would. Originally, a potential with a more realistic hard core was tried, but the periodic volume Schrödinger equation solver had insufficient resolution near the origin, resulting in too much error in the generated spectrum that is input for both HOBET and Lüscher's method. The somewhat smoother potential with the long range part broken out separately is shown in Figure (10.2). The behavior of the potential near the center of a face of the periodic volume is shown in Figure (10.3). A Λ=500 calculation yields a bound state at -4.0518 MeV, which HOBET should predict.

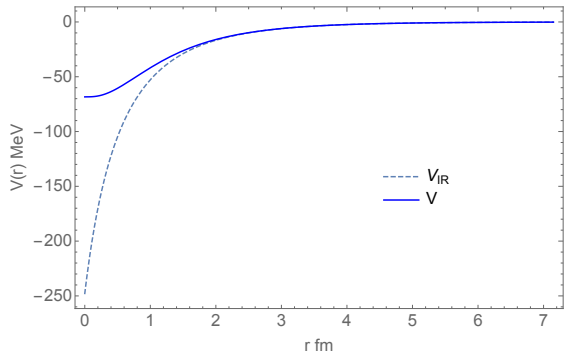

Figure 10.2: The full and long range potential V_{IR}.

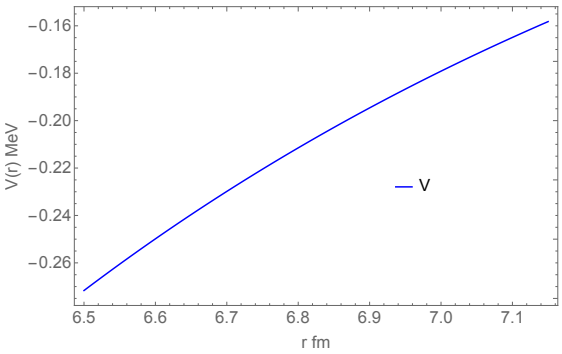

Figure 10.3: The potential at the edge of the box is not zero.

An important aspect of the chosen long range potential is that it does not completely go to 0 by the edge of the box. This violates a requirement for Lüscher's method, which relies on a free propagation region between the range of the potential and the edge of the periodic box at $L/2$. Choosing L so that the potential has some remaining effect at the edge will show the impact of a small violation on calculated phase shifts for Lüscher's method.

The set of positive parity states found with potential V and box size 14.3 fm is shown in Table (10.2). A few other states are omitted that had not converged in the allowed runtime of the solver. Only the states belonging to the A_1 representation are included in the fit as the states in the E representation have no overlap with $L = 0$.

Some selected states have a small overlap with $L = 0$ and some a large overlap, but the size of the overlap is not important as long as it is not zero. The S-channel wave function with its phase shift in a free propagation region in the box can be continued as a valid and independent infinite volume solution regardless of its relative amplitude. Lüscher's method relies on the existence of the free propagation region to obtain the phase shift. HOBET does not have this requirement as the phase shifts are determined later from V_δ.

Table 10.2: Spectrum of $H = T + V$ in a periodic volume with $L = 14.3$ fm plus the overlap with angular momentum states.

Rep	MeV	L=0	L=2	L=4	L=6
A_1^+	-4.4428	0.5	0	0.866	0
A_1^+	2.0314	0.155	0	0.988	0
E^+	7.5995	0	0.424	0.361	0.830
E^+	15.2980	0	0.474	0.393	0.788
A_1^+	21.6167	0.326	0	0.265	0.908
E^+	23.2423	0	0.468	0.597	0.651
A_1^+	29.4041	0.521	0	0.853	0.023
E^+	30.9457	0	0.567	0.428	0.704
A_1^+	35.2449	0.655	0	0.189	0.732
E^+	38.4043	0	0.882	0.176	0.437
A_1^+	45.1402	0.526	0	0.576	0.625

Effective Hamiltonians with $\Lambda = 8$ and $b = 0.8$ fm were constructed for the 6 indicated states, parameterized by a full set of LECs up to N3LO. The effective Hamiltonian is represented as a matrix with the dimension of the P space and has a full set of eigenvectors with different angular momentum content. Only eigenvectors that do not overlap D(L=2) were considered in the fitting process, which was in other respects standard. At N3LO, there are no LECs for G state operators, so the fitting was restricted to S-channel LECs. A tight fit was found with the LEC's shown in Table (10.3).

Table 10.3: S-channel LECs from fit to 6 states in $L = 14.3$ fm box.

LEC	Value
a_{LO}^{S}	70.0274
a_{NLO}^{S}	10.2596
$a_{NNLO}^{40,S}$	1.94882
$a_{NNLO}^{22,S}$	3.12887
$a_{N3LO}^{60,S}$	0.13716
$a_{N3LO}^{42,S}$	0.10177

Based on these LECs, a self consistent infinite volume bound state energy of -4.066 MeV was found by iteration which should be compared to the -4.0518 MeV value found in a large basis.

Reference phase shifts can be computed straight from the full potential using Eq.(7.4.1). A sample of phase shifts from 1 to 20 MeV is shown in Table (10.4).

For comparision, Lüscher's method was used to compute the phase shifts corresponding to the 6 states and an effective range expansion up to k^6 was fit to the data. The formula

for the $L = 0$ phase shift with $\tilde{k} = kL/(2\pi)$ is found in reference [44].

$$k \cot \delta_0 = \frac{2}{\sqrt{\pi} L} \mathcal{Z}_{0,0}\left(1; \tilde{k}^2\right) + \frac{12288\pi^7}{7L^{10}} \frac{\mathcal{Z}_{4,0}\left(1; \tilde{k}^2\right)^2}{k^9 \cot \delta_4} + \mathcal{O}\left(\tan^2 \delta_4\right) \tag{10.2.1}$$

A common assumption is that the second term is small because the $L = 4$ phase shifts are expected to be small and also that the term is suppressed by a high power of k. There is a more complex way to solve for $\cot \delta_0$ and $\cot \delta_4$ at the same time, but in this case δ_4 is easily obtained from the known potential so both the leading and next to leading calculations are displayed.

HOBET phase shifts are computed by searching for a phase shift that makes the equation $H_{eff}(E_i)P\left|\psi_i\right\rangle = \varepsilon_i \left|\psi_i\right\rangle$ self consistent, meaning that $E_i = \varepsilon_i$.

Table 10.4: Phase shifts in degrees from the potential, HOBET, and Lüscher's method from a $L = 14.3$ fm periodic volume.

E MeV	V	HOBET	Leading Lüscher	Next Order Lüscher
1	142.023	141.931	142.552	142.751
2	128.972	128.860	129.571	129.823
4	113.602	113.464	114.205	114.403
8	96.919	96.752	97.575	97.3135
10	91.473	91.296	92.228	91.6403
15	81.672	81.480	82.852	81.3184
20	74.876	74.691	76.667	74.0936

The HOBET phase shifts are clearly better than those from Lüscher's method, so some discussion of the sources of error is appropriate.

One common source of error for both HOBET and Lüscher's method is the accuracy of the solutions with the full potential of the Schrödinger equation in a periodic box. By computing the spectrum at 3 lattice spacings and performing a continuum extrapolation the expected residual quantization error is very small. For each eigenstate the 3 values have a consistent behavior, increasing slightly and consistently as the the lattice spacing shrinks.

Two columns for Lüscher's method have been included in the table, showing that the next order correction is not insignificant. The root cause is that the zeta function has many $\tilde{k}$ values at which it diverges and at values near those points it becomes quite large, raising the importance of the second term. Because the slope of the zeta function is very large near these points, small uncertainties in energy are magnified to large uncertainties in $k \cot \delta_0$.

An additional potential source of error for HOBET is the cutoff on the momentum basis which ends at $N = 30$ for this demonstration. The impact of the cutoff can be measured by examining the matrix elements $\langle j \left| G_{TQ} V_{IR} G_{QT} \right| i \rangle$ because G_{QT} is implemented as a sum over the momentum basis. When i and j correspond to non-edge states the matrix element

can be simplified to $\langle j \left| V_{IR} \right| i \rangle$. Calculating this matrix element both ways for all non-edge j, i the largest error found was 0.0059 on a value of -9.91251, resulting in an error of about 0.06%, which is much smaller than the observed error in the phase shifts.

One more possible source of error for HOBET is the harmonic oscillator length scale which has been set here to $b = 0.8$ fm so that basis functions are very close to 0 at the edge of the box. If b were much larger, then images of the harmonic oscillator potential would disturb the basis states and the overlap calculation between the states and the momentum basis used in many of the calculations.

The most important error source comes from the fact that the potential is not 0 at the edge of the box and will lead to a poorly quantified error in Lüscher's method. In a periodic volume the neighboring images of the potential also contribute to a total potential V_{image}. For HOBET an overly long range V_{imag} will enter in first power in the direct matrix elements of V_{IR} and with two powers of V_{image} in V_δ. So the impact on V_δ of the images of the potential will be suppressed by an extra power making it much less sensitive. In this case the ratio of $V_{imag}/V(0) = 0.32/68.4 \approx 0.005$ so the square will have a small impact on V_δ.

To summarize what has been accomplished here: An effective theory for the interaction was constructed from a spectrum in a periodic box plus a one-pion like long range potential, without knowledge of the short range part of the interaction. The effective theory was transformed into an infinite volume spherical form with LECs fixed, but without knowledge of the phase shifts. Subsequently, the phase shifts were derived from the effective theory by demanding energy consistency of the Bloch-Horowitz equation. The resulting phase shifts are significantly more accurate than Lüscher's method. And finally, HOBET produces not just phase shifts but an effective interaction that can be used to perform additional calculations.

Chapter 11

Computation

The work in this dissertation is a combination of theory and computation. This chapter is devoted to an overview of the software constructed to implement, test, and demonstrate the concepts. It is surprising how often an actual implementation can detect an error or reveal a new concept.

Much of the code is organized in a library that is shared by all the applications. All of this software was written in C++ in parallel form using both OpenMP for shared memory computations as well as MPI for message passing based distribution of work across nodes in a supercomputer. C++ code written for this project totals about 32K lines of code.

11.1 Library

Most of the code written in support of this dissertation is in a shared library. Like any other substantial project, it relies in turn on substantial code written by others who deserve credit for their useful software. Prerequisites for the library include:

- GSL - The GNU scientific library.
- GMP - An arbitrary precision integer package.
- MPFR - An arbitrary precision floating point package.
- Cubature - A simple N-dimensional numerical integration package written by Steven G. Johnson.
- LAPACK - A linear algebra package [46].
- FFTW - A fast Fourier transform package [47].

The library itself has the following subcomponents:

- Vector and matrix support with direct, sparse graph, sparse compressed and one-the-fly evaluation. Arithmetic operations are implemented with simultaneous use of both OpenMP and MPI for parallelism. Matrix operations include inversion and eigenpair generation.
- A parallel implementation of the Lanczos algorithm for computing low lying eigenpairs of extremely large sparse matrices. Both OpenMP and MPI are used to achieve high levels of parallelism.
- Special Functions: Lüscher's zeta function, Laguerre polynomial, Legendre polynomial, Hermite polynomal, spherical harmonics, spherical Bessel functions of complex arguments.
- Harmonic oscillator functions for the 1D case and the radial function of the spherical harmonic oscillator for large n.
- Various transform coefficients: Clebsch-Gordan, 3J/6J/9J symbols, Moshinsky brackets, and spherical Cartesian harmonic oscillator brackets.
- Cubic spline for interpolation.
- A uniform spherical random point generator for sampling the 2D surface.
- Binary input/output with cross platform support.

11.2 Hobfit - Fitting LECs

Hobfit solves an inverse eigenvalue problem. The input is a list of pairs of a target eigenvalue and a parameterized matrix. Additional input describes the mapping from matrix indices to states for either a Cartesian or spherical harmonic oscillator basis. The target eigenvalue is the energy at which H_{eff} was built. The parameterized matrix is $H_{eff}(E)$ with the contributions of the LECs represented symbolically.

The problem is to pick a set of LEC values such that all input matrices have an eigenvalue as near as possible to their target eigenvalue, and in the case of a Cartesian basis with the appropriate angular momentum content for the associated eigenvector.

A control file specifies an initial set of LEC values and the set of LECs to be involved in the fit. The control file also specifies the energy range or cost function options such as enabling variance estimation by measuring derivatives of the fitting cost with respect to LECs above the included order of LECs. Two fitting strategies are alternated in fitting.

The first strategy is to fit a quadratic surface to the cost function and then to solve for the optimal location on this surface. The resulting point is used to define a line in LEC space along which to search for an improvement. The job of generating and evaluating points near the line is divided up over processes connected with MPI. The points to evaluate are independently generated in each process beginning with a different pseudo random seed.

The number of points in each process is chosen to obtain a target density of sampling. If more MPI processes are used then the number of points tested in each process is reduced.

The second strategy is to attach to each LEC a distribution parameter that controls the range of values generated for the LEC. The distribution parameters are independent and are updated after each major iteration based on the change from the previous value. If the motion is less than the distribution parameter then the distribution parameter is reduced to the amount of motion with a minimum of 0.5 times the old value. Each MPI process independently generates points around the last best point following these distributions. A typical number of points for an N3LO or N4LO fit is 400,000 divided up over the MPI processes.

The first strategy loses some effectiveness at higher LEC order, but is cheap. The problem seems to be that higher order derivatives become important and the direction found on the quadratic surface is valid for shorter and shorter distances. The second strategy continues to be effective in high order fits and has some ability to recover from poor starting points such as is shown in Figure (6.1).

11.3 Hoblat - HOBET in a box

The program name hoblat was originally meant to indicate a connection to LQCD, but hoblat is really aimed at forming a H_{eff} in a Cartesian harmonic oscillator basis in a periodic box.

Refering to Eq.(5.0.2), the most expensive parts of the computation are the matrix elements of V_{IR} for edge states.

$$\langle j\,|G_{TQ}V_{IR}G_{QT}|\,i\rangle = \sum_{m',m,s,t} b_{js}\frac{E}{E-\lambda_{m'}}\,\langle s|\,m'\rangle\,\langle m'\,|V_{IR}|\,m\rangle\,\langle m|\,t\rangle\,\frac{E}{E-\lambda_m}b_{ti} \qquad (11.3.1)$$

In the summation, m and m' range over the momentum basis and s and t range over the Cartesian harmonic oscillator basis. The inner part, $\langle m'\,|V_{IR}|\,m\rangle$ is independent of E and is calculated once and reused for production of $H_{eff}(E)$ at multiple energies. Results are saved to disk as they are produced and the computation is restartable. The choice of an FFT based calculation or direct numerical integration is an option. For the demonstration the momentum basis was cut off at $N = 30$, yielding 4951 matrix elements.

When hoblat is run for a specific E it first produces Eq.(11.3.1) and saves it to disk. A last run computes other parts of H_{eff} and the result is saved to disk in the format expected by hobfit. Part of this last run is the construction of V_δ. The construction is done symbolically in terms of LECs in both Cartesian and spherical forms. The spherical form with the same Λ cutoff is transformed to Cartesian form using an implementation of spherical-Cartesian brackets from Appendix A.6. Insisting that both forms represent the same object results in a set of linear constraints between the two sets of LECS. Hoblat solves this set of equations by repeatedly finding a constraint equation expressing a single Cartesian LEC in as a linear combination of spherical LECs and substituting into all the other constraints. This simple

strategy works because the next order of matrix elements introduces a single LEC in both V_δ forms so the substitutions ripple up in order.

Hoblat produces matrices in Mathematica format representing the contributions of T, V_{IR}, and V_δ to $H_{eff}(E)$. V_δ is rendered as list of terms each of which is product of an LEC and a matrix. Additionally the energy E at which H_{eff} was built and a mapping of matrix indices to Cartesian harmonic oscillator states is included in the output. This enables the fitting process in hobfit to evaluate the angular momentum content of eigenvectors of H_{eff} to aid in filtering out non-physical states.

A general testing strategy is that non-edge matrix elements are computed both directly in the Cartesian harmonic oscillator basis and with the insertion of a resolution over the identity with the momentum basis. Too small a cut off on the momentum basis or a coding error results in a significant difference between the two calculations.

11.4 Hobme - Solving the Schrödinger Equation in a large spherical harmonic oscillator basis

Hobme takes the matrix elements of $H = T + V$ in a large harmonic oscillator basis. Matrix elements of T are easily had using Eq.(A.4.1). V is more arbitrary so matrix elements must in general be determined by numeric integration. For large nodal number n the harmonic oscillator basis is difficult to evaluate because the terms in the required Lagaurre polynomial become large and of opposite sign, canceling to leave a small result. An arbitrary precision implementation of the radial function was constructed to obtain the required accuracy. This makes the individual numerical integrations slow, so OpenMP was used to parallelize the computation of V matrix elements, producing reasonable runtimes. In hindsight, MPI would have been a better choice as the calculations are independent and could have been spread over more cores.

Once the matrix is produced, the eigenpairs are found with LAPACK and reported. If the harmonic oscillator length scale is chosen to match the one used for the effective theory then the lower components of the eigenvectors form a useful reference to test the effective theory against.

A additional important use of this program is to implement a direct construction of non-edge state matrix elements of V_δ. With a given energy E and matrix elements of T and V one can simply compute

$$\left\langle j \left| H \frac{1}{E - QH} QH \right| i \right\rangle \tag{11.4.1}$$

yielding a matrix of simple numbers. By doing this is a very large basis, say $\Lambda >= 500$, the error associated with scattering through states left out of the calculation can be made insignificant. If one then asserts that the matrix elements lying in P^- equal the matrix elements generated for V_δ in P^- by Eq.(5.4.18) the result is a set of easily solvable linear

equations for the LECs. This process was used in analysis of the energy dependence of LECs shown in Figure (7.4).

11.5 Hobeig - Solving the Schrödinger Equation in a Periodic Box

HOBET in a periodic volume requires a spectrum for the interacting particles. In it's eventual use with LQCD the spectrum will come from the energy eigenvalues or effective mass of the two nucleon propagator on the lattice. For testing purposes, the spectrum generated by a potential in a periodic volume has the advantage that the same potential can be used in infinite volume to generate bound states, phase shifts, and wave functions that are good references to compare the effective theory results to.

Numerically solving the 3D Schrödinger equations for an arbitrary potential is a surprisingly challenging problem. Two methods usually in use for the problem are DMC (Diffusion Monte-Carlo) and the FDTD (Finite Difference Time Domain) method [48]. Because of the need for the determination of excited states the DMC method is not useful for testing HOBET. The FDTD method is based on the same Euclidian time concept used in LQCD. An initial state is evolved in Euclidian time with a discrete space time lattice, eventually leaving only the ground state. The ground state can then be projected out of wave functions saved at earlier times, exposing the excited states at the cost of numerical noise.

Because of the need for an accurate spectrum a decision was made to investigate an alternative solver that solves the stationary Schrödinger equation on a discrete lattice. A matrix is constructed where each row corresponds to a statement of the local correctness at a lattice point of the Schrödinger equation with the Laplacian approximated by a difference operator acting on the lattice point and 6 neighbors and the potential evaluated at the lattice point.

The next step is to find the low lying eigenstates of the matrix. A related situation happens in nuclear structure calculations where a very large sparse matrix representation of the Hamiltonian is constructed over an M-scheme basis discussed previously in Section 4. There, the Lanczos method is commonly used to find the low lying eigenstates of the Hamiltonian, requiring a few hundred iterations to converge 10 or so states for large problems. In operation, the Lanczos method repeatedly applies the matrix to an initial usually random state. At each step the new result is expressed as a linear combination of the previous state, the current state, and a new state and all new states are mathematically orthogonal to the previous ones, forming a basis reflecting the strongest moments of the matrix and matrix elements in that new basis. Eigenstates of the new, smaller dimension matrix quickly converge to the extreme eigenstates of the original very large matrix.

One reason the Lanczos method works well for the nuclear structure problem is that a modest number of applications of the Hamiltonian connects any two states in the basis that are not protected from each other by a symmetry of the Hamiltonian. In the lattice case,

each row of the matrix only connects immediate neighbors on the lattice. The resulting convergence is known to be very poor for 1D problems and the lore is that it is also poor for 2D and 3D problems. Initial experiments backed this notion up, taking a large number of iterations to converge to inaccurate results for simple problems that could be solved more directly as a reference. Before abandoning the method, the dependence on the lattice spacing was investigated and found to be responsible for for the inaccurate results. Decreasing the lattice spacing produced a working method, but with a very long runtime due to requiring even more iterations. An alternative to decreasing the lattice spacing is to improve the operators. The potential evaluation at the lattice point was replaced by an integration over the volume associated with the lattice point. For rapidly changing potentials such as a sharp edged spherical potential well the error is obviously reduced. A more important change is the conversion from a 7 point stencil Laplacian to a 27 point stencil Laplacian [49]. This change dramatically improves the rotational symmetry of the operator and the new operator also connects lattice points that are farther away, reducing the number of iterations of the Lanczos algorithm. An even larger stencil may continue the improvement, but at the cost of substantially more matrix entries.

Hobeig implements the algorithm described above. For the demonstration problems several thousand iterations, which can be thought of as 10 or so transits across the lattice, are required to converge roughly 30 eigenstates on a 450^3 lattice, which is more than 10 times the number of iterations required for the same dimension nuclear structure problem. At completion each state is checked and the maximum error at any lattice point is reported to measure the convergence of the state. The resulting eigenstates and program options are saved to a large database for later analysis. This separation is made because large problems will need to run on a many-node system, but the post run analysis is less demanding and can be run on a desktop. The database is saved in a binary format that can be written and read on different computer architectures such as IBM and Intel processors.

The post processing determines the angular momentum content of the states by numerically integrating against spherical harmonics near the edge on two closely placed shells and using C.0.1 to compute the associated amplitude of the component.

The most important future improvement to hobeig is to support a variable lattice spacing to more accurately model fast changing potentials such as the hard core of a realistic nuclear potential and to accurately compute the Laplacian where the wave function has large curvature. Using a dense lattice only in these regions will reduce the size of the matrix dramatically and improve both runtime and memory consumption.

Chapter 12

Conclusions

The last component of the bridge from LQCD to nuclear structure is the construction of an A-body effective Hamiltonian for use in the configuration interaction shell model. Included below is a sketch of that final construction. Questions of convergence and evaluation of some remaining terms in the expansion remain as a future project.

In the last section, with the A-body sketch in hand, the results and contributions of this work are summarized.

12.1 Next Step - A Sketch of the A-body Effective Hamiltonian

A last part of the bridge between LQCD and nuclear structure is the construction of an A-Body effective Hamiltonian from the two-body effective interaction constructed in prior chapters. There will also be three- and four-body contributions eventually, so in the construction from a two-body interaction we can defer contributions that involve a nucleon interacting with multiple other nucleons.

A sketch of a possible construction follows. Most contributions have been evaluated in terms of the two-body interaction, but a few interesting ones remain. It also remains to be demonstrated that the expansion is well behaved with higher order contributions making smaller contributions in a controlled way.

A-body HOBET refers to a rigorous application of effective theory to A nucleons. This sketch concerns itself with connecting that two-body interaction to a consistent A-body one. One key factor is the definition of an included space. For translation invariance the proper way to cut off the included space is to limit the total excitation quanta for all particles. With this definition of P a two body interaction in a A-body context will become sensitive to the excitation of nucleons not directly included in the interaction. Nucleons not participating in the interaction are known as spectators and the excitation of spectators limits the two-body P space for interacting pairs of particles.

It will also be seen that beginning with a two-body interaction that H^{eff} naturally grows 3, 4, and N-body interactions.

12.1.1 A-Body Formulation

P is defined as a projection operator from the full Hilbert space to a subspace where the total excitation quanta for all particles is limited to Λ. Such a consistent energy cutoff is required to maintain translation invariance. As usual the complementary projection operator $Q = 1 - P$ is defined for the excluded space.

To begin, the assumption is that H may be decomposed into a sum of two body contributions.

$$H = \sum_{i<j} H_{ij} = \sum_{a} H_a \tag{12.1.1}$$

Here each ordered pair $\{i, j\}$ has been given a label a. The effective Hamiltonian can be written in a slightly compressed way.

$$H^{eff} = P\left[H\frac{E}{E-QH}\right]P = P\left[\left(\sum_a H_a\right)\frac{E}{E-QH}\right]P \tag{12.1.2}$$

The operator equation $1/(A-B) = 1/A + (1/A)B(1/(A-B))$ is used to reorganize H^{eff}.

$$H^{eff} = P\left[\sum_{a\neq b} H_a \frac{E}{E-QH_a}\left(1 + \frac{1}{E}Q\left(\sum_{b\neq a} H_b \frac{E}{E-QH}\right)\right)\right]P \tag{12.1.3}$$

$H_a^{eff} = H_a\left(E/\left(E-QH_a\right)\right)$ is used to denote the two-body part of the effective Hamiltonian. Performing the obvious repeated expansion on the right results the following expansion.

$$H^{eff} = P\left[\sum_a H_a^{eff} + \frac{1}{E}\sum_{a\neq b} H_a^{eff} Q H_b^{eff} + \frac{1}{E^2}\sum_{a\neq b, b\neq c} H_a^{eff} Q H_b^{eff} Q H_c^{eff} + \cdots\right]P \tag{12.1.4}$$

Now evaluation of H^{eff} needs to be understood. Q and P in the definition refer to the total quanta for all particles. If one examines the interaction of a specific pair of particles, say 1 and 2, then the excitations of the uninvolved particles will be unaffected. The P space can then be described as a sum over the possible total excitation value of the uninvolved spectator particles Λ_S.

$$P = \sum_{\Lambda_S=0}^{\Lambda} |\Lambda_S\rangle\langle\Lambda_S| \quad P_{12}\left(\Lambda - \Lambda_S\right) \tag{12.1.5}$$

This simply says that the P space for the pair 1,2 is reduced by the sum of the excitations of the other particles. One should interpret $|\Lambda_S\rangle\langle\Lambda_S|$ as a projection operator for the subspace

where the other particles total excitation is equal to Λ_S, in other words, the excitation of the spectators. In a two body contribution for the pair a

$$H_a^{eff} = H_a \frac{E}{E - QH_a} \tag{12.1.6}$$

there is the complication that the Q is the three body Q. Otherwise, this is the known 2 body effective Hamiltonian. The total excitation of the other particles can range from 0 to Λ, the maximum excitation for the system. H_a^{eff} can now be written as a sum over the spectator quanta Λ_S.

$$\left[H_a \frac{E}{E - QH_a} \right] = \left[\sum_{\Lambda_S=0}^{\Lambda} H_a \frac{E}{E - Q_a \left(\Lambda - \Lambda_S\right) H_a} P_a(\Lambda - \Lambda_S) \left|\Lambda_S\right\rangle \left\langle\Lambda_S\right| \right] \tag{12.1.7}$$

$$H_a^{eff} = \left[\sum_{\Lambda_S=0}^{\Lambda} \left|\Lambda_S\right\rangle \left\langle\Lambda_S\right| P_a(\Lambda - \Lambda_S) H_a \frac{E}{E - Q_a \left(\Lambda - \Lambda_S\right) H_a} P_a(\Lambda - \Lambda_S) \left|\Lambda_S\right\rangle \left\langle\Lambda_S\right| \right] \tag{12.1.8}$$

The interpretation of this equation is straightforward. The usual two body H^{eff} must be constructed for a range of P spaces determined by the spectator excitation. With this understanding the first term in Eq.(12.1.4) is easily evaluated.

To understand the evaluation of other terms it is helpful to decompose H_a^{eff} into kinetic and potential parts using the Haxton-Luu form of the Bloch-Horowitz equation.

$$\begin{aligned} H_a^{eff} &= T_a^{eff} + V_a^{eff} \\ T_a^{eff} &= G_{T_a Q} \left(T_a + T_a \frac{Q}{E} T_a \right) = G_{T_a Q} T_a = T_a G_{Q T_a} \\ V_a^{eff} &= G_{T_a Q} \left(V_a + V_a \frac{1}{E - QH_a} Q V_a \right) G_{Q T_a} \end{aligned}$$

A subset of the terms in Eq.(12.1.4) are pure sequences of T_x^{eff} which can be removed and implemented globally. Their sum must be equivalent to pure kinetic energy scattering of the A-body state. The replacement is

$$\left\langle n' \left| T^{eff} \right| n \right\rangle = E \left(\delta_{n',n} - \left\langle n' \left| \frac{E}{E - T} \right| n \right\rangle \right) \tag{12.1.9}$$

where n' and n label A-body states in P. This expression may be evaluated by insertion of states in a Jacobi basis in which T is diagonal [50].

The second term $PH_a^{eff} Q H_b^{eff} P$ can now be evaluated with the restriction that $a \not\subset b$. If there is an intersection, then a single particle is involved with two other particles and we can classify the interaction as a 3-body interaction, to be considered later. With that restriction

$$PH_a^{eff} Q H_b^{eff} P = P P_a H_a^{eff} P_a Q_{ab} P_b H_b^{eff} P_b P \tag{12.1.10}$$

where the quanta limits for the labled projectors are set by the quanta associated with the state of spectators to the 4 involved particles. The central P_b projectors inserted next to Q_{ab} states that the pair labeled b may not exceed the quanta limit for the 4 particles on it's own. If it did, then the total quanta for a and b could not be corrected by application of H_a^{eff}. The two parts on the right are complete 2-body interactions wrapped in projection operators and are easily evaluated. Arbitrary sequences of H_x^{eff} where the x do not overlap can be evaluated in the same way.

Sequences of three H_x^{eff} do produce a new situation that requires more study where each particle interacts with at most one other particle. In the following, a does not intersect b.

$$PH_a^{eff}QH_b^{eff}QH_a^{eff}P = PP_aH_a^{eff}QP_bH_b^{eff}P_bQH_a^{eff}P_aP \tag{12.1.11}$$

P_a can't be inserted on both sides of H_a^{eff} because the second instance of H_a^{eff} can couple an arbitrary state of pair a back to the P space. With a known potential such terms are easily calculated in a large basis, the problem is to express the result in terms of the 2-body effective interaction. Summing such higher order terms, showing their convergence, and the inclusion of three+ body interactions in the A-body effective Hamiltonian will require more investigation.

12.1.2 Reducing $H_{eff}^{(\Lambda)}$ to a Smaller P Space

In the formulation of the A-body H_{eff} a need was found to produce the two body $H_{eff}^{(x)}$ for all $x \in \{0, \ldots, \Lambda\}$. As one would hope, the smaller $P(x)$ space H_{eff} can be determined from the $P(\Lambda)$ one. Let $S(y)$ be a projection operator for states with exactly y quanta, then $P(\Lambda) = P(\Lambda - 1) + S(\Lambda)$ and $Q(\Lambda) = 1 - P(\Lambda - 1) - S(\Lambda)$. This enables a rewrite of $H_{eff}^{(\Lambda)}$ in the following way.

$$H\frac{E}{E - Q(\Lambda)H} = H\frac{E}{E - (1 - P(\Lambda - 1) - S(\Lambda))\,H} = H\frac{E}{E - Q(\Lambda - 1)H + S(\Lambda)H}$$

This form is suitable for expansion by the operator equation 2.0.6 with $A = E - Q(\Lambda - 1)H$ and $B = -S(\Lambda)H$.

$$P(\Lambda)H\frac{E}{E - Q(\Lambda)H}P(\Lambda) = P(\Lambda)H\frac{E}{E - Q(\Lambda - 1)H}P(\Lambda)\left(1 - S(\Lambda)H\frac{E}{E - Q(\Lambda)H}\right)P(\Lambda)$$

The equation is wrapped in $P(\Lambda)$ to complete the two body effective interaction, and $P(\Lambda)$ has also been propagated from the $P(\Lambda)$ on the right to the middle position, yielding two $P(\Lambda)$ space matrices. Solving for the first matrix on the right yields a matrix including the desired smaller $\Lambda - 1$ effective interaction.

$$P(\Lambda)H\frac{E}{E - Q(\Lambda - 1)H}P(\Lambda) = H_{eff}^{(\Lambda)}\left\{P(\Lambda)\left(1 - S(\Lambda)H_{eff}^{(\Lambda)}\right)P(\Lambda)\right\}^{-1}$$

Finally, using $P(\Lambda-1)P(\Lambda) = P(\Lambda-1)$ the left hand side is restricted to the $\Lambda-1$ two body effective interaction.

$$\begin{aligned} H_{eff}^{(\Lambda-1)} &= P(\Lambda-1)H\frac{E}{E-Q(\Lambda-1)H}P(\Lambda-1) \\ &= P(\Lambda-1)H_{eff}^{(\Lambda)}\ \left\{P(\Lambda)\left(1-S(\Lambda)H_{eff}^{(\Lambda)}\right)P(\Lambda)\right\}^{-1}P(\Lambda-1) \end{aligned} \tag{12.1.12}$$

Only the largest P space two body interaction need be constructed or fit, all smaller ones are easily generated from the larger ones.

12.2 Summary

Building on the prior work by Haxton, Song, and Luu on HOBET in which they demonstrated the construction of a convergent harmonic oscillator based effective theory from a known UV potential, this work directly derives the effective theory from a sample of the spectrum and associated wave function boundary conditions. In one case the boundary conditions are the familiar phase shifts and mixing angles.

The construction of the effective Hamiltonian is directly from observables with a single cutoff in the harmonic oscillator basis avoids a common pitfall in other effective theory work, a first cutoff in a momentum basis followed by a second cutoff in the harmonic oscillator basis. The pitfall manifests as increasing errors when matrix elements in a large harmonic oscillator basis are reduced to a small one and the violation of symmetries such as translation invariance, which allows the center of mass oscillations to contaminate the spectrum. The root cause of the problem is an overlap between the included harmonic oscillator basis and the cut off part of the momentum basis. HOBET avoids this problem by directly constructing the effective theory in the harmonic oscillator basis.

In testing of the resulting effective theory against known potentials the relationship between scattering observables and energy was reproduced with constant LECs, including the continuation to bound states and showing the continuity with energy achieved with HOBET.

As was argued, the residual energy dependence of the LECs is small, manifesting only in the sensitive S-D channel as a small variation in the D and S channel wave function. A heuristic was demonstrated to determine the LECs as a function of energy, but it should be put on a more formal basis.

A second application of HOBET described here makes the connection to ongoing work in LQCD which aims to measure the spectrum of two and eventually three-body scattering in a periodic volume. In this second case, called HOBET in a box, the periodicity of the wave function replaces the phase shifts and mixing angles and the spectrum is necessarily discrete. A key result is that the Cartesian effective theory in the periodic volume can be described in terms of the LECs of the spherical infinite volume effective theory. If the range of the interaction R is smaller than $L/2$, the distance to the edge of the volume, then the finite volume effects are sequestered in Green's functions. In the transition to an infinite volume effective theory the Green's function boundary conditions are changed to phase shifts which are determined by energy consistency of the infinite volume effective theory. The result is an effective interaction.

Of interest to the LQCD community, HOBET in a box gives a new way to determine phase shifts from a spectrum in a periodic volume that is demonstrated to be more accurate than the commonly used Lüscher's method when the potential actually has longer range than $L/2$. The effective interaction constructed in the periodic volume is parameterized in terms of the spherical infinite volume LECs and then fit to the spectrum. The LECs are then used to construct the infinite volume spherical form of the interaction, automatically removing finite volume effects from the construction of the infinite volume interaction. Phase shifts are then easily determined as a consequence of energy self consistency of the Bloch-Horowitz

equation.

The effect of neighboring images of the potential is first absorbed in matrix elements of V_{IR}, leaving the kernel of the effective theory expansion V_δ isolated from the effect of the periodic images. The degree to which the interaction goes to 0 at the edge is quantified by the product $m_\pi L$, with common values in calculations for this product from 4-8 and with next generation calculations a bit larger. The comparison in this work had $m_\pi L = 10$, larger than in current use, and still had 1% errors from Lüscher's method.

The connection to A-body HOBET was explored, sketching out how a 2-body effective interaction generates an A-body effective interaction with 3 and higher body terms. The inclusion of a fundamental 3-body interaction has not yet been investigated. Integration into configuration interaction shell model code is straightforward but more time consuming to run than the usual energy independent interactions because the algorithm will have to be iterated to energy self consistency for each state. The prospect of an effective theory correct shell model code is exciting. Many persistent issues in nuclear physics are most likely due to oversimplified treatment of operators, often involving the evaluation of bare operators against distorted and cut off wave functions. A rigorous construction of H^{eff} offers the possibility of renormalizing operators in a matching way [14].

Improved 2-nucleon scattering data from LQCD will be coming in the next few years and it is exciting to apply HOBET to that data in order to calculate the low lying states of light nuclei. It has been a long term goal in nuclear physics to connect nuclear structure to the fundamental theory of QCD [51]. In this dissertation much of a formal effective theory bridge has been constructed from a 2-nucleon spectrum generated by LQCD in a periodic volume to an effective interaction used in the construction of an A-body nucleon effective interaction, suitable for nuclear structure calculations, which will be an answer to the goal.

Bibliography

[1]E. Berkowitz, T. Kurth, A. Nicholson, B. Joó, E. Rinaldi, M. Strother, P. M. Vranas, and A. Walker-Loud, "Two-nucleon higher partial-wave scattering from lattice QCD", Physics Letters B **765**, 285–292 (2017).

[2]H. Fritzsch, M. Gell-Mann, and H. Leutwyler, "Advantages of the color octet gluon picture", Physics Letters B **47**, 365–368 (1973).

[3]M. Creutz, *Quarks, gluons and lattices*, Vol. 8 (Cambridge University Press, 1983).

[4]E. Berkowitz, A. Nicholson, C. C. Chang, E. Rinaldi, M. A. Clark, B. Joó, T. Kurth, P. Vranas, and A. Walker-Loud, "Calm Multi-Baryon Operators", in 35th International Symposium on Lattice Field Theory (Lattice 2017) Granada, Spain, June 18-24, 2017 (2017).

[5]M. G. Mayer, "Nuclear Configurations in the Spin-Orbit Coupling Model. I. Empirical Evidence", Physical Review **78**, 16–21 (1950).

[6]A. deShalit and H. Feshbach, *Theoretical Nuclear Physics Vol. 1: Nuclear Structure* (John Wiley & Sons, Inc., 1974), p. 979.

[7]B. R. Barrett and M. W. Kirson, "Higher-order terms and the apparent non-convergence of the perturbation expansion for the effective interaction in finite nuclei", Nuclear Physics A **148**, 145–180 (1970).

[8]T. Schucan and H. Weidenmüller, "The effective interaction in nuclei and its perturbation expansion: An algebraic approach", Annals of Physics **73**, 108–135 (1972).

[9]T. H. Schucan and H. A. Weidenmüller, "Perturbation theory for the effective interaction in nuclei", Annals of Physics **76**, 483–509 (1973).

[10]S. D. Głazek and K. G. Wilson, "Renormalization of hamiltonians", Physical Review D **48**, 5863 (1993).

[11]S. K. Bogner, R. J. Furnstahl, and R. J. Perry, "Similarity renormalization group for nucleon-nucleon interactions", Physical Review C - Nuclear Physics **75**, 1–5 (2007).

[12]P. Navrátil, J. Vary, and B. Barrett, "Large-basis ab initio no-core shell model and its application to 12C", Physical Review C **62**, 1–14 (2000).

[13]S. Weinberg, "Phenomenological Lagrangians*", Physica A: Statistical Mechanics and its Applications, 327–340 (1979).

[14]W. C. Haxton and C. L. Song, "The Canonical Nuclear Many-Body Problem as a Rigorous Effective Theory", ArXiv Nuclear Theory e-prints, nucl-th/9906082 (1999).

[15]T. C. Luu, S. Bogner, W. C. Haxton, and P. Navrátil, "Effective interactions for the three-body problem", Physical Review C **70**, 014316 (2004).

[16]D. Phillips, "Building light nuclei from neutrons, protons, and pions", Czechoslovak Journal of Physics **52**, B49–B101 (2002).

[17]K. Suzuki and S. Y. Lee, "Convergent Theory for Effective Interaction in Nuclei", Progress of Theoretical Physics **64**, 2091–2106 (1980).

[18]B. K. Jennings, "Projection operator formalisms and the nuclear shell model", Europhysics Letters (EPL) **72**, 211–215 (2005).

[19]R. Machleidt and D. R. Entem, "Chiral effective field theory and nuclear forces", Physics Reports **503**, 1–75 (2011).

[20]D. Lee, "Lattice simulations for few- and many-body systems", Progress in Particle and Nuclear Physics **63**, 117–154 (2009).

[21]C. Bloch and J. Horowitz, "Sur La Détermination Des Premiers États D'un Système de Ferminons dans le Case Dégénéré", Nuclear Physics B **8**, 91–105 (1958).

[22]W. Haxton and T. Luu, "The canonical nuclear many-body problem as an effective theory", Nuclear Physics A **690**, 15–28 (2001).

[23]R. Klomp, J. de Swart, T. Rijken, C. Terheggen, R. Timmermans, V. Stoks, J. Rubio-Melón, and W. Vink, *NN-OnLine, http://nn-online.org*.

[24]K. M. Case and A. A. Pais, "On spin-orbit interactions and nucleon-nucleon scattering", Physical Review **80**, 203 (1950).

[25]R. B. Wiringa, V. G. J. Stoks, and R. Schiavilla, "Accurate nucleon-nucleon potential with charge-independence breaking", Physical Review C **51** (1995).

[26]R. Whitehead, A. Watt, B. Cole, and I. Morrison, *Computational Methods for Shell-Model Calculations, Advances in Nuclear Physics Volume 9*, edited by M. Baranger and E. Vogt (Springer US, Boston, MA, 1977) Chap. 2, pp. 123–176.

[27]C. W. Johnson, W. E. Erich Ormand, and P. G. Krastev, "Factorization in large-scale many-body calculations", Computer Physics Communications **184**, 2761–2774 (2013).

[28]H. Shan, S. Williams, C. Johnson, K. McElvain, and W. E. Ormand, "Parallel implementation and performance optimization of the configuration-interaction method", in Proceedings of the International Conference for High Performance Computing, Networking, Storage and Analysis on - SC '15 (2015), pp. 1–12.

[29]W. C. Haxton and C.-L. Song, "Morphing the shell model into an effective theory", Physical review letters **84**, 5484 (2000).

[30]M. Moshinsky, "Transformation brackets for harmonic oscillator functions", Nuclear Physics **13** (1959).

[31]D. H. Gloeckner and R. D. Lawson, "Spurious center-of-mass motion", Physics Letters B **53**, 313–318 (1974).

[32]T. C. Luu, "Effective Interactions within an Oscillator Basis", PhD thesis (University of Washington, 2003).

[33]P. Lepage, "How to Renormalize the Schrodinger Equation", in Nuclear physics. Proceedings, 8th Jorge Andre Swieca Summer School, Sao Jose dos Campos, Campos do Jordao, Brazil, January 26-February 7, 1997 (June 1997), pp. 135–180.

[34]B. Mihaila, "Matrix elements of the Argonne v18 potential", ArXiv e-prints, nucl-th/1111.4018 (2011).

[35]M. Abramowitz and I. A. Stegun, *Handbook of mathematical functions: with formulas, graphs, and mathematical tables*, Vol. 55 (Courier Corporation, 1964).

[36]M. Moshinsky, *The Harmonic Oscillator in Modern Physics: From Atoms to Quarks* (Gordon and Breach, Inc., New York, 1969), pp. 4–41.

[37]J. M. Blatt and L. C. Biedenharn, "Neutron-Proton Scattering with Spin-Orbit Coupling. I. General Expressions", Physical Review **86**, 399–404 (1952).

[38]W. C. Haxton, "Form of the effective interaction in harmonic-oscillator-based effective theory", Physical Review C **77**, 034005 (2008).

[39]M. Chu and G. Golub, *Inverse eigenvalue problems: theory, algorithms, and applications*, Vol. 13 (Oxford University Press, 2005).

[40]I. C. F. Ipsen, "Computing an eigenvector with inverse iteration", SIAM review **39**, 254–291 (1997).

[41]F. Calogero, *Variable Phase Approach to Potential Scattering*, Vol. 35 (Elsevier, 1967).

[42]M. Lüscher, "Two-particle states on a torus and their relation to the scattering matrix", Nuclear Physics B **354**, 531–578 (1991).

[43]E. J. Weniger, "The Spherical Tensor Gradient Operator", Collection of Czechoslovak chemical communications **70**, 1225–1271 (2005).

[44]T. Luu and M. J. Savage, "Extracting scattering phase shifts in higher partial waves from lattice QCD calculations", Physical Review D **83**, 114508 (2011).

[45]T. Inoue, S. Aoki, T. Doi, T. Hatsuda, Y. Ikeda, N. Ishii, K. Murano, H. Nemura, and K. Sasaki, "Two-baryon potentials and H-dibaryon from 3-flavor lattice QCD simulations", Nuclear Physics A **881**, 28–43 (2012).

[46]E. Anderson, Z. Bai, J. Dongarra, A. Greenbaum, A. McKenney, J. Du Croz, S. Hammarling, J. Demmel, C. Bischof, and D. Sorensen, "LAPACK: A Portable Linear Algebra Library for High-performance Computers", in Proceedings of the 1990 ACM/IEEE Conference on Supercomputing, Supercomputing '90 (1990), pp. 2–11.

[47]M. Frigo and S. Johnson, "The Design and Implementation of FFTW3", Proceedings of the IEEE **93**, 216–231 (2005).

[48]M. Strickland and D. Yager-Elorriaga, "A parallel algorithm for solving the 3d Schrödinger equation", Journal of Computational Physics **229**, 6015–6026 (2010).

[49]R. C. O'Reilly and J. M. Beck, "A Family of Large-Stencil Discrete Laplacian Approximations in Three Dimensions", International Journal for Numerical Methods in Engineering, 1–16 (2006).

[50]W. Haxton and T. Luu, "Perturbative Effective Theory in an Oscillator Basis?", Physical Review Letters **89**, 182503 (2002).

[51]R. E. Tribble, L. Trache, and S. Stoica, "The Frontiers of Nuclear Science: A New Long Range Plan for the United States", in AIP Conference Proceedings, Vol. 972 (2008), pp. 17–27.

[52]R. Alvarez-Nodarse, J. L. Cardoso, and N. R. Quintero, "On recurrence relations for radial wave functions for the N-th dimensional oscillators and hydrogenlike atoms: analytical and numerical study", Electronic Transactions on Numerical Analysis **24**, 7–23 (2006).

[53]Y. Liu and J. Zeng, "Four kinds of raising and lowering operators of n-dimensional hydrogen atom and isotropic harmonic oscillator", Science in China Series A: Mathematics **40**, 1110–1115 (1997).

[54]K. T. R. Davies and S. J. Krieger, "Harmonic-oscillator transformation coefficients", Canadian Journal of Physics **69**, 62–69 (1991).

[55]B. Buck and A. C. Merchant, "A simple expression for the general oscillator bracket", Nuclear Physics A **600**, 387–402 (1996).

[56]J. D. Jackson, *Classical Electrodynamics*, 3rd ed. (John Wiley & Sons, 1998), p. 832.

[57]A. R. Edmonds, *Angular momentum in quantum mechanics*, 4th ed. (Princeton University Press, 1996), p. 146.

Appendix A

The Harmonic Oscillator Basis

Much of the development of this thesis depends on the rich theory of the harmonic oscillator in both 1D and 3D forms. This appendix will specify conventions and assemble and organize the relevant facts and formulas about quantum harmonic oscillators. A list of conventions used here are specified in Appendix E.

The base reference on the theory of 1D and 3D harmonic oscillators used here is Moshinsky's book on the topic [36]. A notational difference is that he used nodal quantum numbers for the spherical harmonic oscillator starting with 0, instead of 1, which is used here. Also, his η_i and ξ_i correspond to $\eta_i^\dagger$ and η_i here.

It should be emphasized that the harmonic oscillator basis is used for calculation and the harmonic oscillator Hamiltonian plays no other role than defining the properties of that basis.

A.1 The Harmonic Oscillator Hamiltonian and Units

The harmonic oscillator basis is defined by a Hamiltonian and a choice of coordinate basis, spherical or Cartesian. Letting M be twice the reduced mass μ of a two nucleon system.

$$H_\rho^{ho} = \frac{P^2}{M} + \frac{M}{4}\omega^2\rho^2 = -\frac{\hbar^2}{M}\nabla_\rho^2 + \frac{M\omega^2}{4}\rho^2$$

Dimensionless energy values $E = \text{Energy}/\hbar\omega$ and radial coordinate $r = \rho/\left(\sqrt{2}b\right)$ are adopted with harmonic oscillator length scale $b^2 = \hbar/\left(M\omega\right)$. Equivalently, one can adopt units where $\hbar = 1$, $\mu = 1$ and $\omega = 1$. Substituting this into the harmonic oscillator Hamiltonian yields

$$H^{ho} = -\frac{1}{2}\nabla_r^2 + \frac{1}{2}r^2 \tag{A.1.1}$$

An advantage of this choice of energy and length units is that the wave number for a free wave is very simply related to the dimensionless energy. Substituting $\hbar = \mu = 1$ into the usual relationship gives

$$k^2 = 2E \tag{A.1.2}$$

$E < 0$ results in $k = i\sqrt{2\,|E|} = i\kappa$ where $\kappa = \sqrt{2\,|E|}$.

A.2 3D Cartesian Harmonic Oscillator

In the Cartesian basis there are independent oscillators in the x, y and z directions. Three dimensional states are described by a vector of excitations counts $\vec{n} = (n_x, n_y, n_z)$ for 1D harmonic oscillators in the three basis directions. These excitation counts begin with 0.

The 1D eigenfunctions are given for the x direction below and are known as Hermite functions, a product of a Gaussian and a Hermite polynomial.

$$\begin{aligned} \psi_n(x) &= \frac{1}{\pi^{1/4}\sqrt{2^n n!}}\, e^{-\frac{1}{2}x^2} H_n(x) \\ H_n(x) &= n! \sum_{q=0}^{\lfloor n/2 \rfloor} \frac{(-1)^q 2^{n-2q}}{q!\,(n-2q)!} x^{n-2q} \end{aligned} \tag{A.2.1}$$

These states have lowering and raising differential operators

$$\eta_i = \frac{1}{\sqrt{2}}(x_i + ip_i) = \frac{1}{\sqrt{2}}(r_i + \partial_i) \quad \text{and} \quad \eta_i^\dagger = \frac{1}{\sqrt{2}}(x_i - ip_i) = \frac{1}{\sqrt{2}}(r_i - \partial_i) \tag{A.2.2}$$

The operators can be organized as vectors $\vec{\eta} = (\eta_x, \eta_y, \eta_z)$. They satisfy the commutation relations

$$\left[\eta_i, \eta_j^\dagger\right] = \delta_{ij}, \quad [\eta_i, \eta_j] = \left[\eta_i^\dagger, \eta_j^\dagger\right] = 0$$

Angular momentum can be expressed in terms of the raising and lowering operators as

$$\vec{L} = (L_x, L_y, L_z) = -i\,\vec{\eta}^\dagger \times \vec{\eta} \tag{A.2.3}$$

As vectors, they also have representation as spherical vectors

$$\eta_m = \begin{cases} \eta_1 &= -\dfrac{1}{\sqrt{2}}(\eta_x - i\eta_y) \\ \eta_0 &= \eta_z \\ \eta_{-1} &= \dfrac{1}{\sqrt{2}}(\eta_x + i\eta_y) \end{cases} \qquad \eta_m^\dagger = \begin{cases} \eta_1^\dagger &= -\dfrac{1}{\sqrt{2}}\left(\eta_x^\dagger + i\eta_y^\dagger\right) \\ \eta_0^\dagger &= \eta_z^\dagger \\ \eta_{-1}^\dagger &= \dfrac{1}{\sqrt{2}}\left(\eta_x^\dagger - i\eta_y^\dagger\right) \end{cases}$$

The angular momentum operators can be expressed in terms of spherical operators as

$$\begin{aligned} L_z &= \left(\eta_1^\dagger \eta_1 - \eta_{-1}^\dagger \eta_{-1}\right) \\ L_+ &= L_x + iL_y = \sqrt{2}\left(\eta_1^\dagger \eta_0 + \eta_0^\dagger \eta_{-1}\right) \\ L_- &= L_x - iL_y = \sqrt{2}\left(\eta_{-1}^\dagger \eta_0 + \eta_0^\dagger \eta_1\right) \end{aligned} \tag{A.2.4}$$

The operator $\eta_m^\dagger$ as well as the new operator $\tilde{\eta}_m = (-1)^m \eta_{-m}$ both transform as rank-1 spherical tensors with magnetic projection m, e.g.,

$$\begin{aligned}
&\left[L_+, \eta_1^\dagger\right] = 0 \quad \left[L_+, \eta_0^\dagger\right] = \sqrt{2}\eta_1^\dagger \quad \left[L_+, \eta_{-1}^\dagger\right] = \sqrt{2}\eta_0^\dagger \\
&\left[L_z, \eta_m^\dagger\right] = m\eta_m^\dagger \\
&\left[L_-, \eta_1^\dagger\right] = \sqrt{2}\eta_0^\dagger \quad \left[L_-, \eta_0^\dagger\right] = \sqrt{2}\eta_{-1}^\dagger \quad \left[L_-, \eta_{-1}^\dagger\right] = 0
\end{aligned}$$

An important scalar operator that will find use as a nodal lowering operator is $\vec{\eta} \cdot \vec{\eta} = \tilde{\eta} \cdot \tilde{\eta}$. The dot product for spherical vectors results in a scalar and is defined as

$$\vec{x} \cdot \vec{y} = \sum_{m=-1}^{1} (-1)^m x_m y_{-m} \tag{A.2.5}$$

and is equivalent to the Cartesian vector dot product.

Any state of the 3D Cartesian Harmonic oscillator can be constructed by application of the raising operators to the ground state.

$$|n_x, n_y, n_z\rangle = [n_x! n_y! n_z!]^{-1/2} \eta_x^{n_x\dagger} \eta_y^{n_y\dagger} \eta_z^{n_z\dagger} |0,0,0\rangle$$

A.3 3D Spherical Harmonic Oscillator

The basis has the usual decomposition into a radial part parameterized by a nodal quantum number $n \in 1 \ldots \infty$, and a Y_ℓ^m.

$$\begin{aligned}
&\Psi_{n,\ell,m}(r,\theta,\phi) = h_{n,\ell}(r)\, Y_\ell^m(\hat{r}) \\
&h_{n,\ell}(r) = r H_{n,\ell}(r) = \sqrt{\frac{2\Gamma(n)}{\Gamma(n+\ell+1/2)}} r^{\ell+1} e^{-r^2/2} L_{n-1}^{\ell+1/2}\left(r^2\right)
\end{aligned} \tag{A.3.1}$$

$$L_{n-1}^{\ell+1/2}\left(r^2\right) = \sum_{j=0}^{n-1} \frac{(-1)^j\, \Gamma(n+\ell+1/2)}{(n-j-1)!\, \Gamma(j+\ell+3/2)\, j!} r^{2j} \tag{A.3.2}$$

where L is the associated Laguerre polynomial of Abramowitz and Stengun [35], which also happens to match the convention followed in Mathematica. In a large basis, evaluation of Eq.(A.3.1) can become quite expensive, requiring high precision (100's of digits) to compute. A recurrence relation given by Alvarez-Nodarse, et al. [52] can be used to compute a set of basis state values at a given r, dramatically speeding up the process, though high precision arithmetic will still be required.

$$\sqrt{(n-1)(n+\ell-1/2)} H_{n-1,\ell}(r) + \left(r^2 - (2n+\ell-1/2)\right) H_{n,\ell}(r) + \sqrt{n\,(n+\ell+1/2)} H_{n+1,\ell}(r) = 0 \tag{A.3.3}$$

The spherical states can be manipulated with raising and lower operators as well. In particular, an arbitrary state may be generated as

$$\begin{aligned} |n,\ell,m\rangle &= A_{n\ell}\left(\vec{\eta}^{\,\dagger}\cdot\vec{\eta}^{\,\dagger}\right)^n \mathcal{Y}_{\ell m}\left(\vec{\eta}^{\,\dagger}\right)|1,0,0\rangle \\ A_{n\ell} &= (-1)^n\left[\frac{4\pi}{(2n+2\ell-1)!!(2n-2)!!}\right]^{1/2} \end{aligned} \tag{A.3.4}$$

Exploiting the fact that $|n=1,\ell=0,m=0\rangle = |n_x=0,n_y=0,n_z=0\rangle$ can be used to construct brackets relating the Cartesian states to the spherical states.

$\mathcal{Y}_{\ell m}(\vec{r}) = r^\ell Y_{\ell m}(\hat{r})$ is a solid harmonic and $\mathcal{Y}_{\ell m}\left(\vec{\eta}^{\,\dagger}\right)$ is a harmonic polynomial in the Cartesian raising operators. This suggests correctly that the nodal lowering and raising operators are $(\vec{\eta}\cdot\vec{\eta})$ and $\left(\vec{\eta}^{\,\dagger}\cdot\vec{\eta}^{\,\dagger}\right)$. Moshinsky gives an easy way to see this by pointing out that $\eta_i^\dagger$ and η_j have the same commutation relations as x_i and ∂_j. Given this correspondence, $(\vec{\eta}\cdot\vec{\eta})$ will act on $\left(\vec{\eta}^{\,\dagger}\cdot\vec{\eta}^{\,\dagger}\right)^n\mathcal{Y}_{\ell m}\left(\vec{\eta}^{\,\dagger}\right)$ in precise analogy to the action of ∇^2 on $r^{2(n-1)}\mathcal{Y}_{\ell,m}(r) = r^{2(n-1)}r^\ell Y_{\ell,m}(\hat{r})$, yielding

$$\nabla^2 r^{2(n-1)+\ell}Y_{\ell,m}(\hat{r}) = 2(n-1)(2n+2\ell-1)r^{2(n-2)+\ell}Y_{\ell,m}(\hat{r}) \tag{A.3.5}$$

Applying this reasoning to both raising and lowering operators and combining this result with the change in normalization constant $A_{n\ell}$ between the starting and ending state results one finds

$$\begin{aligned} (\vec{\eta}\cdot\vec{\eta})\,|n,\ell,m\rangle &= -2\sqrt{(n-1)\,(n+\ell-1/2)}\,|n-1,\ell,m\rangle \\ \left(\vec{\eta}^{\,\dagger}\cdot\vec{\eta}^{\,\dagger}\right)|n,\ell,m\rangle &= -2\sqrt{n\,(n+\ell+1/2)}\,|n+1,\ell,m\rangle \end{aligned} \tag{A.3.6}$$

A raising operator for ℓ will also be needed. $\eta^\dagger$ is a rank one spherical operator meaning that the tensor product of $\eta^\dagger$ with $|n,\ell,m\rangle$ will generate overlap with angular momentum values $\ell+1$, ℓ, and $\ell-1$. The raised part can be projected out.

$$\left[\eta^\dagger\otimes|n,\ell\rangle\right]_m^{\ell+1} = \sqrt{\frac{2\,(\ell+1)\,(n+\ell+1/2)}{2\ell+3}}\,|n,\ell+1,m\rangle \tag{A.3.7}$$

The scaling must be independent of m, so the coefficient may most easily be determined by raising $|n,\ell,\ell\rangle$ to $|n,\ell+1,\ell+1\rangle$ which will have a single contribution to the tensor product. To declutter the notation raising and lowering operators are defined.

$$\hat{a}^\dagger\,|n,\ell,m\rangle = \left(\vec{\eta}^{\dagger}\cdot\vec{\eta}^{\dagger}\right)|n,\ell,m\rangle = -2\sqrt{n\,(n+\ell+1/2)}\,|n+1,\ell,m\rangle \tag{A.3.8}$$

$$\hat{a}\,|n,\ell,m\rangle = (\vec{\eta}\cdot\vec{\eta})\,|n,\ell,m\rangle = -2\sqrt{(n-1)\,(n+\ell-1/2)}\,|n-1,\ell,m\rangle \tag{A.3.9}$$

$$\hat{c}^\dagger\,|n,\ell,m\rangle = \left[\eta^\dagger\otimes|n,\ell\rangle\right]_m^{\ell+1} = \sqrt{\frac{2\,(\ell+1)\,(n+\ell+1/2)}{2\ell+3}}\,|n,\ell+1,m\rangle \tag{A.3.10}$$

The corresponding ℓ lowering operator scaling can be determined by insisting that $\left\langle n,\ell+1,m\left|\hat{c}^\dagger\right|n,\ell,m\right\rangle = \langle n,\ell,m\,|\hat{c}|\,n,\ell+1,m\rangle$ and assuming that $|m|\leq\ell-1$.

$$\hat{c}\,|n,\ell,m\rangle = \sqrt{\frac{2\ell\,(n+\ell-1/2)}{2\ell+1}}\,|n,\ell-1,m\rangle \tag{A.3.11}$$

The iterated ℓ raising operator is used in producing matrix elements of V_δ.

$$\hat{c}^{\dagger\ell}\left|n,0,0\right\rangle = 2^{\frac{\ell}{2}}\sqrt{\frac{\ell!}{(2\ell+1)!!}}\sqrt{\frac{\Gamma\left(n+\ell+1/2\right)}{\Gamma\left(n+1/2\right)}}\left|n,\ell,m\right\rangle \tag{A.3.12}$$

A useful property of these operators that can be found by application to an arbitrary state is that

$$[\hat{c},\hat{a}] = 0 \tag{A.3.13}$$

Both lowering operations can also be implemented by differential operators on the radial part of the position space wave function. This is useful for evaluating effective theory operators on the infinite superpositions of harmonic oscillator states used for HOBET edge states.

A.4 Kinetic Energy Operator T

The kinetic energy operator, $T = -(1/2)\nabla^2$, acting on SHO states is a hopping operator in label $n \in 1\ldots\infty$, mapping state n to a superposition of neighboring states with the same ℓ. See Moshinsky eqn 3.10 [36] for a derivation.

$$T\left|n,\ell,\alpha\right\rangle = \frac{1}{2}\left[\begin{array}{cc} \sqrt{n\left(n+\ell+1/2\right)} & \left|n+1,\ell,\alpha\right\rangle + \\ \left(2n+\ell-1/2\right) & \left|n,\ell,\alpha\right\rangle + \\ \sqrt{\left(n-1\right)\left(n+\ell-1/2\right)} & \left|n-1,\ell,\alpha\right\rangle \end{array}\right] \tag{A.4.1}$$

An important property of T is that its application leaves angular momentum quantum numbers unaffected. This property propagates to $(E-T)$, $1/(E-T)$ and $1/(E-QT)$ as well.

A.5 Differential Forms of Raising and Lowering Operators

The effective theory expansion will require the application spherical lowering operators to arbitrary radial wave functions. One method would be to decompose the wave function into the SHO basis and then apply Eq.(A.3.9). This would be computationally expensive. A more efficient approach is the use of differential operators to implement the lowering. The operators can depend on ℓ because separate the angular momentum channels, but may not depend on the nodal quantum number.

These operators can be constructed from the following first order operators described by Lui and Zeng in [53] with the first up/down arrow referring to ℓ and the second to $N = 2(n-1)+\ell$, which describes the energy $E = (N+3/2)$. These differential operators

should be applied to the radial wave function in the form of $h_{n\ell}(r) = rH_{n\ell}(r)$.

$$\begin{aligned}
\hat{d}_{\uparrow\uparrow} h_{n,\ell}(r) &= (\partial_r - (\ell+1)/r - r)\, h_{n,\ell}(r) = -2\sqrt{n+\ell+1/2}\; h_{n,\ell+1}(r) \\
\hat{d}_{\uparrow\downarrow} h_{n,\ell}(r) &= (\partial_r - (\ell+1)/r + r)\, h_{n,\ell}(r) = -2\sqrt{n-1}\; h_{n-1,\ell+1}(r) \\
\hat{d}_{\downarrow\uparrow} h_{n,\ell}(r) &= (\partial_r + \ell/r - r)\, h_{n,\ell}(r) = 2\sqrt{n}\; h_{n+1,\ell-1}(r) \\
\hat{d}_{\downarrow\downarrow} h_{n,\ell}(r) &= (\partial_r + \ell/r + r)\, h_{n,\ell}(r) = 2\sqrt{n+\ell-1/2}\; h_{n,\ell-1}(r)
\end{aligned} \tag{A.5.1}$$

For example, the nodal quantum number differential lowering operator $\hat{a}$ which is equivalent to $(\vec{\eta}\cdot\vec{\eta})$ is defined as

$$\begin{aligned}
\hat{a}\; h_{n,\ell}(r) &= \frac{1}{2}\hat{d}_{\downarrow\downarrow}\hat{d}_{\uparrow\downarrow} h_{n,\ell}(r) = -2\sqrt{(n-1)\,(n+\ell-1/2)}\, h_{n-1,\ell}(r) \\
\hat{a} &= \frac{1}{2}\left(\partial_r^2 - \frac{\ell(\ell+1)}{r^2} + 2r\partial_r + r^2 + 1\right) \\
\hat{a} &= -T + \frac{1}{2}\left(1 + r^2 + 2r\partial_r\right)
\end{aligned} \tag{A.5.2}$$

The operator can also be cast in a form useful for operating on $H_{n\ell}(r)$ instead of $h_{n\ell}(r)$.

$$\hat{a}\; H_{n,\ell}(r) = \left[-T + \frac{1}{2}\left(3 + r^2 + 2r\partial_r\right)\right]\; H_{n,\ell}(r) \tag{A.5.3}$$

The forms expressed in terms of T will be useful when applying the lowering operator to edge states formed in part by the application of the Green's function $E/(E-T)$

A last required operator is $\hat{c}$, which lowers ℓ by 1 while holding n constant to implement the nuclear tensor interaction.

$$\hat{c}\; h_{n,\ell}(r) = \sqrt{\frac{2\ell}{2\ell+1}}\;\frac{1}{2}\;\left(\partial_r + \frac{\ell}{r} + r\right)\; h_{n,\ell}(r) = \sqrt{\frac{2\ell}{2\ell+1}}\sqrt{(n+\ell-1/2)}\; h_{n,\ell-1}(r) \tag{A.5.4}$$

The operator can also be written for $H_{n,\ell}$ as

$$\hat{c}\; H_{n,\ell}(r) = \sqrt{\frac{2\ell}{2\ell+1}}\;\frac{1}{2}\left(\partial_r + \frac{\ell+1}{r} + r\right) H_{n,\ell} = \sqrt{\frac{2\ell}{2\ell+1}}\sqrt{(n+\ell-1/2)} H_{n,\ell-1}(r) \tag{A.5.5}$$

A.6 Spherical Cartesian Brackets

The states of the 3D harmonic oscillator can also be expressed in Cartesian form as the simple product of 3 1D harmonic oscillator states $|n_x, n_y, n_z\rangle$ where n_x indicates the number of quanta in the oscillator along the x-axis. Expressed either way, there are the same number of states for each energy eigenvalue. The unitary transform $\langle n, \ell, m|\, n_x, n_y, n_z\rangle$ for $m \geq 0$

is given by Davies and Krieger in [54]. Modified to match the conventions used here the bracket is

$$\begin{aligned}
&\delta_{2(n-1)+\ell,n_x+n_y+n_z}\,(-1)^{(2(n-1)+n_x+n_y-m)/2}\,i^{n_y}\left[\frac{(2\ell+1)\,(\ell-m)!\,(n-1+\ell)!}{2^\ell\,(\ell+m)!\,n!\;(2(n-1)+2\ell+1)!}\right]^{1/2}\\
&\qquad\times\left(\frac{n_x+n_y+m}{2}\right)!\;\left[n_x!\,n_y!\,n_z!\right]^{1/2}\left[\frac{1+(-1)^{(n_x+n_y+m)}}{2}\right]\\
&\qquad\times\sum_{s=s_{min}}^{s_{\max}}\frac{(-1)^s\,(2\ell-2s)!\,(n-1+s)!}{s!\;(\ell-s)!\;(\ell-2s-m)!\;(n-1+s-(n_x+n_y-m)/2)!}\\
&\qquad\times\sum_{p=p_{\min}}^{p_{\max}}\frac{(-1)^p}{p!\;(n_x-p)!\;(p+(n_y-n_x-m)/2)!\;((n_x+n_y+m)/2-p)!}
\end{aligned}\tag{A.6.1}$$

with the understanding that the factorial of a negative value is to be treated as 0 and limits are set by

$$\begin{aligned}
s_{\min}&=\begin{cases}0 & n>(n_x+n_y-m)/2\\ (n_x+n_y-m)/2 & n\leqslant(n_x+n_y-m)/2\end{cases}\\
s_{\max}&=\begin{cases}(\ell-m)/2 & (\ell-m)\ \textit{odd}\\ (\ell-m-1)/2 & (\ell-m)\ \textit{even}\end{cases}\\
p_{\min}&=\begin{cases}0 & n_y>n_x+m\\ (n_x-n_y+m)/2 & n_y\leqslant n_x+m\end{cases}\\
p_{\max}&=\begin{cases}n_x & n_x<n_y+m\\ (n_x+n_y+m)/2 & n_x\geqslant n_y+m\end{cases}
\end{aligned}$$

For negative m the bracket can be transformed as

$$\langle n,L,-m|\,n_x,n_y,n_z\rangle=(-1)^m\,\langle n,L,m|\,n_x,n_y,n_z\rangle^*\tag{A.6.2}$$

This expression can be found by inserting the operator $1=\hat{T}^\dagger\hat{T}$ acting to the right where $\hat{T}$ is the time reversal operator and then reversing the direction of $\hat{T}^\dagger$, noting that $\hat{T}\,|n,L,-m\rangle=(-1)^m\,|n,L,m\rangle$. Conjugation is the result of the change of direction of the anti-linear operator $\hat{T}^\dagger$.

A.7 Brody-Moshinsky Brackets

Brody-Moshinsky brackets [30] implement a unitary transform between the states of a pair of independent harmonic oscillators and a pair of relative and center of mass oscillators. A common use of these brackets is in the implementation of integrals of functions of relative coordinates in a basis of independent oscillators. Buck and Merchant [55] developed a useful generalization, which is used here, to the case where the two oscillators labeled x and y have

different length scales $b_i^2 = \hbar/(\mu_i\omega_i)$ and $\tan\beta = b_y/b_x$ characterizes the relationship of the oscillator parameters. The states of the independent oscillators are specifed with n_x, ℓ_x and n_y, ℓ_y. The relative and center of mass oscillator states are specified with n, ℓ and N, L. N is not to be taken as an energy quantum number in this section. On both sides of the bracket the oscillator angular momentums are coupled to total angular momentum Λ and the result is independent of the z component of total angular momentum which must be conserved. Their expression for the bracket connecting independent oscillators to the relative and CM oscillators with nodal numbers n and N is

$$n_4 = n-1,\ \ell_4 = \ell, \quad n_3 = N-1,\ \ell_3 = L, \quad n_2 = n_y,\ \ell_2 = \ell_y, \quad n_1 = n_x - 1,\ \ell_1 = \ell_x$$

$$\langle N, L,\ n, \ell : \Lambda |\, n_x, \ell_x,\ n_y, \ell_y : \Lambda \rangle = \prod_{k=1}^{4} i^{-\ell_k} \sqrt{n_k!\,(2\,(n_k+\ell_k)+1)!!\,/2^k}$$

$$\times \sum_{\substack{abcd \\ \ell_a\ell_b\ell_c\ell_d}} \left[(-1)^{\ell_d} (\sin\beta)^{2a+\ell_a+2d+\ell_d} (\cos\beta)^{2b+\ell_b+2c+\ell_c} \begin{Bmatrix} \ell_a & \ell_b & \ell_1 \\ \ell_c & \ell_d & \ell_2 \\ \ell_3 & \ell_4 & \Lambda \end{Bmatrix} \right.$$

$$\left. \times \prod_{p=a}^{d} \frac{(-1)^{\ell_p}\sqrt{2^{\ell_p}}\,(2\ell_p+1)}{p!\ \ (2\,(p+\ell_p)+1)!!} \langle \ell_a 0 \ell_b 0 |\, \ell_1 0 \rangle \langle \ell_c 0 \ell_d 0 |\, \ell_2 0 \rangle \langle \ell_a 0 \ell_c 0 |\, \ell_3 0 \rangle \langle \ell_b 0 \ell_d 0 |\, \ell_4 0 \rangle \right]$$

The inner product over p should be read as p takes on the 4 labels a, b, c, d. The summation over 8 variables above is constrained by

$$\begin{aligned} 2a + \ell_a + 2b + \ell_b &= 2n_1 + \ell_1 \\ 2c + \ell_c + 2d + \ell_d &= 2n_2 + \ell_2 \\ 2a + \ell_a + 2c + \ell_c &= 2n_3 + \ell_3 \\ 2b + \ell_b + 2d + \ell_d &= 2n_4 + \ell_4 \end{aligned}$$

The new relative and center of mass coordinates are

$$\begin{aligned} r &= r_x \cos\beta - r_y \sin\beta \\ R &= r_x \sin\beta + r_y \cos\beta \end{aligned}$$

As long as $\omega_x = \omega_y$ R will be the center of mass coordinate.

Appendix B

Spherical Green's Function and Action on Harmonic Oscillator States

This appendix collects together technical details about the the Green's function for $E/(E-QT)$ in spherical coordinates, which plays a central role in HOBET. The use of phase shifts as boundary conditions for the Green's functions creates a kind of basis transform of P for the effective Hamiltonian that restores the IR behavior of the full wave function from the truncated harmonic oscillator basis. It is what makes HOBET IR-correct, enabling an analytic sum of the impact of repeated scattering through the excluded Q space by the kinetic energy operator T and also implements a large part of the renormalization of the potential.

The sections below begin with the decomposition of $E/(E-QT)$ to separate the effect of Q, which complicates the construction of the Green's function. Next, analytic expressions for matrix elements of the Green's function with phase shift boundary conditions in a harmonic oscillator basis are derived. And last, the action of the Green's function on harmonic oscillator states is also computed in analytic form.

Numerical calculations are often much simpler to implement, but because effective operators involve high order derivatives the results are noisy and damage results. However, numerical calculations have been an essential crosscheck of the analytic forms below.

B.1 E/(E-QT) Decomposition

The presence of the operator Q in the resolvent greatly complicates the construction of a Green's function. Fortunately the decomposition for $E/(E-QT)$ can be found in Luu's thesis [32].

$$\frac{E}{E-QT}P = \frac{E}{E-T}\left\{P\frac{E}{E-T}P\right\}^{-1}P \tag{B.1.1}$$

This is such a central result that it is worth including a derivation with some additional commentary. First a supporting lemma is needed that comes immediately from application

of Eq.(2.0.6).

$$\frac{E}{E-T} = 1 + T\frac{1}{E-T} \tag{B.1.2}$$

Letting $A = E - T$ and $B = -PT$ then $E - QT = A - B$ the same operator equation can be used again to isolate $1/(E - QT)$ inside a pair of P projection operators.

$$\frac{1}{E-QT}P = \frac{1}{E-T}\left(1 - PT\frac{1}{E-QT}\right)P \tag{B.1.3}$$

This is already a win as the part isolated in the pair of projection operators is simply a matrix. Next a simpler way to evaluate the matrix is needed . Substituting Eq.(B.1.3) into the matrix will allow a solution for the matrix in terms of $1/(E - T)$.

$$PT\frac{1}{E-QT}P = PT\frac{1}{E-T}P - PT\frac{1}{E-T}PT\frac{1}{E-QT}P$$

$$P\left(1 + T\frac{1}{E-T}\right)P\ PT\frac{1}{E-QT}P = P\ T\frac{1}{E-T}P \tag{B.1.4}$$

Re-writing with Eq.(B.1.2) results in an equation involving P space matrices.

$$\left\{P\frac{E}{E-T}P\right\}\ PT\frac{1}{E-QT}P = P - \left\{P\frac{E}{E-T}P\right\}P$$

Multiplying through by the inverse of the left hand matrix the desired result is obtained.

$$PT\frac{1}{E-QT}P = \left\{P\frac{E}{E-T}P\right\}^{-1}P - P$$

Substitution into Eq.(B.1.3) and multiplication by E yields Eq.(B.1.1). Often the equation is written using index notation with an implied summation over j.

$$\frac{E}{E-QT}P_i = \frac{E}{E-T}\left\{P\frac{E}{E-T}P\right\}^{-1}_{i,j}P_j \tag{B.1.5}$$

In this form it is clear that one can apply the linear operator $E/(E - T)$ directly to all the basis states in P and then sum over the matrix elements, which for a given value of E are just constants.

This equation gives a direct way to numerically evaluate $E/(E-QT)\ P_i$ using a differential equation solver. The wavefunctions produced in this way are useful for testing, but will be too noisy for application of effective operators. Instead, analytic forms are pursued so that the higher order derivatives used in the effective operators can be accurately evaluated for edge states.

The remaining issue in computing $E/(E - QT)\ P_i$ is the implementation of a Green's function for $E/(E - T)$, which is covered in the following sections.

B.2 The Free Green's Function G_0

Two representations are needed of the Green's function for $G_0 = 1/(k^2 + \nabla^2)$ where $E/(E - T) = k^2 G_0$. The first representation is expressed in $\vec{x} = (\vec{r}\,' - \vec{r})$ and will be used in section B.5 to take matrix elements of $E/(E - T)$. The second is decomposed into angular momentum channels with a radial Green's function for each channel and is used everywhere else.

Applying the operator to the Fourier representation of $G_0(\vec{x})$ yields

$$\left(k^2 + \nabla^2\right) \frac{1}{(2\pi)^3} \int d^3p \, G_0\left(\vec{k}\right) e^{-i\vec{p}\cdot\vec{x}} = \delta^{(3)}\left(\vec{r}\right)$$

$$\frac{1}{(2\pi)^3} \int d^3p \, \left(k^2 - p^2\right) G_0\left(\vec{k}\right) e^{-i\vec{p}\cdot\vec{x}} = \delta^{(3)}\left(\vec{r}\right)$$

To form a delta function one must have $G_0\left(\vec{k}\right) = 1/\left(k^2 - p^2\right)$. The next step is to convert to a position space form and change to more convenient spherical coordinates with the z-axis aligned with $\vec{x}$. Now only the magnitude $|x|$ of $\vec{x}$ is needed.

$$G_0\left(\vec{x}\right) = \frac{1}{(2\pi)^3} \int d^3p \, \frac{1}{k^2 - p^2} e^{-i\vec{p}\cdot\vec{x}} = \frac{1}{(2\pi)^3} \int d\phi d\theta dp \, p^2 \sin\theta \frac{1}{k^2 - p^2} e^{-ip|x|\cos\theta}$$

ϕ can be immediately integrated out and the substitution $u = -\cos\theta$ is made.

$$G_0\left(\vec{x}\right) = \frac{1}{4\pi^2} \int_0^\infty dp \, p^2 \int_{-1}^{1} du \, \frac{1}{k^2 - p^2} e^{ip|x|u} = -\frac{i}{4\pi^2 |x|} \int_0^\infty dp \, p \frac{e^{ip|x|} - e^{-ip|x|}}{k^2 - p^2 \pm i\varepsilon}$$

The final integration of the two terms can be completed by contour integration where the $\pm i\varepsilon$ selects between two options for avoiding the poles at $p = \pm k$. e^{ipx} should be closed in the upper half plane and e^{-ipx} in the lower plane. The two resulting options for a Green's function are

$$G_0\left(\vec{x}\right) = -\frac{i}{4\pi^2 |x|} 2\pi i \left(-\frac{\pi}{2}\right) e^{\pm ik|x|} = -\frac{e^{\pm ik|x|}}{4\pi |x|}$$

These Green's functions can be averaged to produce a real Green's function which is more convenient.

$$G_0\left(\vec{r} - \vec{r}\,'\right) = -\frac{\cos k \left|\vec{r} - \vec{r}\,'\right|}{4\pi \left|\vec{r} - \vec{r}\,'\right|} \tag{B.2.1}$$

This Green's function is known as a "free" green's function.

B.3 G_0 With Phase Shifts

For other uses of G_0 a decomposition into angular momentum channels is needed with a phase shift in each channel. A related development of a different Green's function may be

found in Jackson[56], page 427. As before, the first step is the application of the operator $(k^2 + \nabla^2)$ to the Green's function, but producing a spherical coordinate delta function.

$$\left(k^2 + \nabla^2\right) G_0\left(\vec{r}, \vec{r}\,'\right) = \frac{1}{r^2}\delta\left(r - r'\right)\delta\left(\hat{r} - \hat{r}'\right)$$

The completeness theorem gives us an angular delta function representation.

$$\sum_{\ell=0}^{\infty}\sum_{m=-\ell}^{\ell} Y_{\ell m}^{*}\left(\hat{r}\right) Y_{\ell m}\left(\hat{r}'\right) = \delta\left(\hat{r} - \hat{r}'\right)$$

This suggests that the solution can be found as a linear combination of these terms

$$G_0\left(\vec{r}, \vec{r}\,'\right) = \sum_{\ell=0}^{\infty}\sum_{m=-\ell}^{\ell} G_{0\ell}\left(r, r'\right) Y_{\ell m}\left(\hat{r}\right) Y_{\ell m}^{*}\left(\hat{r}'\right)$$

Using $\nabla^2\left(f\left(r\right) Y_{\ell}^{m}\left(\hat{r}\right)\right) = \left[\left(\partial_r^2 + \left(2/r\right)\partial_r - \ell\left(\ell+1\right)/r^2\right) f\left(r\right)\right] Y_{\ell}^{m}\left(\hat{r}\right)$ the gradient operator can be applied to G_0.

$$\left(k^2 + \nabla^2\right) G_0\left(\vec{r}, \vec{r}\,'\right) = \sum_{\ell=0}^{\infty}\sum_{m=-\ell}^{\ell}\left[\left(\partial_r^2 + \frac{2}{r}\partial_r + k^2 - \frac{\ell\left(\ell+1\right)}{r^2}\right) G_{\ell}\left(r, r'\right)\right] Y_{\ell m}\left(\hat{r}\right) Y_{\ell m}^{*}\left(\hat{r}'\right)$$

For this to work, the bracketed expression must generate radial part of the delta function, separating G_0 into a radial Green's function per angular momentum channel.

$$\left(\partial_r^2 + \frac{2}{r}\partial_r + k^2 - \frac{\ell\left(\ell+1\right)}{r^2}\right) G_{\ell}\left(r, r'\right) = \frac{1}{r^2}\delta\left(r - r'\right) \tag{B.3.1}$$

Multiplying both sides on the left by $r\,r'$ and then commuting over the differential operator allows reexpressing the equation in terms of $g_\ell(r, r') = rr'G_\ell(r, r')$.

$$\left(\partial_r^2 + k^2 - \frac{\ell\left(\ell+1\right)}{r^2}\right) g_{\ell}\left(r, r'\right) = \delta\left(r - r'\right) \tag{B.3.2}$$

The solutions to the homogeneous part are known to be the spherical Bessel functions $rj_\ell(r)$ and $r\eta_\ell(r)$. One can construct a radial Green's function from a linearly independent pair of solutions of the homogeneous part of the above differential equation above. The pair consists of an inner and an outer solution which meet boundary conditions at the origin and infinity respectively. The constructed Green's function with constant K to be determined later is:

$$g_{\ell}\left(r, r'\right) = K\begin{cases} u_{\ell,in}(r)\, u_{\ell,out}(r') & r \leq r' \\ u_{\ell,in}(r') u_{\ell,out}(r) & r > r' \end{cases}$$

The crossing of r' and r yields a derivative discontinuity, producing a delta function when acted on by the differential operator.

The inner solution must go to 0 at the origin, so the only choice is $u_{in,\ell}(r) = rj_\ell(r)$. To constrain the outer solution one observes that the Green's function will be applied to wave functions in a truncated harmonic oscillator basis. Such wave functions are bounded to some range R and for $r > R$ results in

$$\psi(r) = \int_0^\infty dr' g_\ell(r,r') h_{n,\ell}(r') = K u_{\ell,out}(r) \left(\int_0^R dr' u_{\ell,in} h_{n,\ell}(r') \right)$$

The parenthesized expression is simply a constant, and at large r it is seen that $\psi(r)$ is a constant times a linear combination of $j_\ell(r)$ and $\eta_\ell(r)$. This combination will need to reproduce the target phase shift δ_ℓ as $r \to \infty$, so the outer solution must have the form.

$$u_{\ell,out}(r) = r\left(-\cot(\delta_\ell) j_\ell(kr) + \eta_\ell(kr)\right)$$

Which at large r reduces the expected form.

$$\begin{aligned} u_{\ell,out}(r) &\underset{r\to\infty}{\to} -\frac{1}{\sin(\delta_\ell)} \left(\cos(\delta_\ell) \sin(kr - \ell\frac{\pi}{2}) + \sin(\delta_\ell)\cos(kr - \ell\frac{\pi}{2}) \right) \\ &= \quad -\frac{1}{\sin(\delta_\ell)} \sin(kr + \delta_\ell - \ell\frac{\pi}{2}) \end{aligned}$$

There are two important points. First, this outer solution remains correct for bound states where $\cot(\delta) = i$. Second, the form of the long range wave function is independent of the bounded wave function to which the Green's function is applied. Only the amplitude of the long range wave function is affected by the source.

A last step in the construction of the radial Green's function is the determination of K, which is essentially a normalization value for the bend at $r = r'$. As the differential equation is of a Sturm-Liouville form, K is a constant easily determined from the Wronkskian of the inner and outer solutions.

$$K = \frac{1}{u'_{\ell,out}(r) u_{\ell,in}(r) - u'_{\ell,in}(r) u_{\ell,out}(r)} = k$$

The final radial Green's function is then

$$rr' G_\ell(r,r') = g_\ell(r,r') = krr' \begin{cases} j_\ell(kr)\ (-\cot(\delta_\ell) j_\ell(kr') + \eta_\ell(kr')) & r \le r' \\ j_\ell(kr')\,(-\cot(\delta_\ell) j_\ell(kr) + \eta_\ell(kr)) & r > r' \end{cases} \qquad \text{(B.3.3)}$$

The free Green's function from the previous section is related to G_ℓ with $cot(\delta) = 0$.

$$G_{0free}(\vec{r}, \vec{r}\,') = \sum_{\ell,m} G_\ell(r,r') Y_{\ell,m}(\hat{r}) Y_{\ell,m}(\hat{r}'), \qquad \cot(\delta_\ell) = 0$$

B.4 Applying $E/(E-T)$ to Harmonic Oscillator States

Numerical results are much better if the Green's function from Eq.(B.3.3) is applied analytically.

$$\begin{aligned}\int_0^\infty dr'\; g_\ell(r,r')\, h_{j\ell}(r') =& kr\left(-\cot\delta_\ell\; j_\ell(kr)+\eta_\ell(kr)\right)\int_0^r dr' r' j_\ell(kr')\, h_{j\ell}(r') \\ &- k\cot\delta_\ell\; r j_\ell(kr)\int_r^\infty dr' r' j_\ell(kr')\, h_{j\ell}(r') \\ &+ kr j_\ell(kr)\int_r^\infty dr' r' \eta_\ell(kr')\, h_{j\ell}(r')\end{aligned} \tag{B.4.1}$$

The harmonic oscillator wave function expands to terms that are a Gaussian times a power of r. The key building block integral, with $m > \ell$ is:

$$\begin{aligned}\int dr\; e^{-r^2/2} r^m j_\ell(kr) &= \int dr\; e^{-r^2/2} r^m (-kr)^\ell \left(\frac{1}{kr}\frac{d}{d(kr)}\right)^\ell j_0(kr) \\ &= \int dr\; e^{-r^2/2} r^{m+\ell-1}(-k)^{\ell-2}\frac{d}{dr}\left(\frac{1}{kr}\frac{d}{d(kr)}\right)^{\ell-1} j_0(kr)\end{aligned} \tag{B.4.2}$$

In which the spherical Bessel function has been expanded using Rayleigh's formula. The result can be integrated by parts.

$$\begin{aligned}&= (-k)^{-1} e^{-r^2/2} r^m (-kr)^{\ell-1}\left(\frac{1}{kr}\frac{d}{d(kr)}\right)^{\ell-1} j_0(kr) \\ &\quad +(-k)^{-1}\int dr\; e^{-r^2/2} r^{m+1}(-kr)^{\ell-1}\left(\frac{1}{kr}\frac{d}{d(kr)}\right)^{\ell-1} j_0(kr) \\ &\quad -(m+\ell-1)(-k)^{-1}\int dr\; e^{-r^2/2} r^{m-1}(-kr)^{\ell-1}\left(\frac{1}{kr}\frac{d}{d(kr)}\right)^{\ell-1} j_0(kr)\end{aligned} \tag{B.4.3}$$

By restoring the Bessel functions one obtains a simple recursion relation for the integral.

$$= -\frac{1}{k}\left[e^{-r^2/2} r^m j_{\ell-1}(kr) + \int dr\; e^{-r^2/2} r^{m+1} j_{\ell-1}(kr) - (m+\ell-1)\int dr\; e^{-r^2/2} r^{m-1} j_{\ell-1}(kr)\right]$$

The recursion relation can be repeatedly applied until all terms requiring integration contain the Gaussian, j_0 and a positive power of r. The same steps apply to integrals involving η_ℓ. The base integrals can be constructed by taking derivatives with respect to k.

$$\int dr\; e^{-r^2/2} r^{2n+1} j_0(kr) = \frac{1}{k}\int dr\; e^{-r^2/2} r^{2n}\sin(kr) = \frac{(-1)^n}{k}\left(\frac{d}{dk}\right)^{2n}\int dr\; e^{-r^2/2}\sin(kr)$$

$$\int dr\; e^{-r^2/2} r^{2n+2} j_0(kr) = \frac{1}{k}\int dr\; e^{-r^2/2} r^{2n+1}\sin(kr) = \frac{(-1)^{n+1}}{k}\left(\frac{d}{dk}\right)^{2n+1}\int dr\; e^{-r^2/2}\cos(kr)$$

To complete the process the base cases of the integral of a Gaussian and sin or cos are needed and can be obtained by expanding the sin or cos to exponentials, followed by completing the square of the resulting exponents.

$$\int dr e^{-r^2/2}\sin(kr) = -\sqrt{\frac{\pi}{2}}e^{-\frac{k^2}{2}}\left(\operatorname{erf}\left(\frac{r+ik}{\sqrt{2}}\right)-\operatorname{erf}\left(\frac{r-ik}{\sqrt{2}}\right)\right)/(2i)$$
$$\int dr e^{-r^2/2}\cos(kr) = \sqrt{\frac{\pi}{2}}e^{-\frac{k^2}{2}}\left(\operatorname{erf}\left(\frac{r+ik}{\sqrt{2}}\right)+\operatorname{erf}\left(\frac{r-ik}{\sqrt{2}}\right)\right)/2$$

For real k, this result can be transformed to eliminate complex values.

$$\int dr\ e^{-r^2/2}\sin(kr) = -\sqrt{\frac{\pi}{2}}e^{-\frac{k^2}{2}}\operatorname{Im}\left(\operatorname{erf}\left(\frac{r+ik}{\sqrt{2}}\right)\right) = -\sqrt{\frac{\pi}{2}}e^{-\frac{k^2}{2}}\operatorname{Imerf}\left(\frac{r}{\sqrt{2}},\frac{k}{\sqrt{2}}\right)$$
$$\int dr\ e^{-r^2/2}\cos(kr) = \sqrt{\frac{\pi}{2}}e^{-\frac{k^2}{2}}\operatorname{Re}\left(\operatorname{erf}\left(\frac{r+ik}{\sqrt{2}}\right)\right) = \sqrt{\frac{\pi}{2}}e^{-\frac{k^2}{2}}\operatorname{Reerf}\left(\frac{r}{\sqrt{2}},\frac{k}{\sqrt{2}}\right)$$

Two new functions Reerf and Imerf are defined above. These functions have simple derivatives which can be specified to symbolic mathematics packages such as Mathematica.

$$\partial_x \operatorname{Reerf}(x,y) = (2/\sqrt{\pi})e^{y^2-x^2}\cos(2xy)$$
$$\partial_y \operatorname{Reerf}(x,y) = (2/\sqrt{\pi})e^{y^2-x^2}\sin(2xy)$$
$$\partial_x \operatorname{Imerf}(x,y) = -(2/\sqrt{\pi})e^{y^2-x^2}\sin(2xy)$$
$$\partial_y \operatorname{Imerf}(x,y) = (2/\sqrt{\pi})e^{y^2-x^2}\cos(2xy)$$

For imaginary k, the argument of the $\operatorname{erf}(z)$ function will be real. The integrals can be restated in terms of $\kappa = -ik$.

$$\frac{1}{k}\int dr\ e^{-r^2/2}\sin(kr) = \frac{1}{\kappa}\int dr\ e^{-r^2/2}\sinh(\kappa r) = -\frac{1}{\kappa}e^{\frac{\kappa^2}{2}}\sqrt{\frac{\pi}{2}}\left(\operatorname{erf}\left(\frac{r+\kappa}{\sqrt{2}}\right)-\operatorname{erf}\left(\frac{r-\kappa}{\sqrt{2}}\right)\right)/2$$
$$\frac{1}{k}\int dr\ e^{-r^2/2}\cos(kr) = \frac{1}{i\kappa}\int dr\ e^{-r^2/2}\cosh(\kappa r) = -\frac{i}{\kappa}e^{\frac{\kappa^2}{2}}\sqrt{\frac{\pi}{2}}\left(\operatorname{erf}\left(\frac{r+\kappa}{\sqrt{2}}\right)+\operatorname{erf}\left(\frac{r-\kappa}{\sqrt{2}}\right)\right)/2$$

Again it is convienient to define a special function for the combination of erf functions.

$$\left(\operatorname{erf}\left(\frac{r+\kappa}{\sqrt{2}}\right)-\operatorname{erf}\left(\frac{r-\kappa}{\sqrt{2}}\right)\right)/2 = \operatorname{Aerf}\left(r/\sqrt{2},\kappa/\sqrt{2}\right)$$
$$\left(\operatorname{erf}\left(\frac{r+\kappa}{\sqrt{2}}\right)+\operatorname{erf}\left(\frac{r-\kappa}{\sqrt{2}}\right)\right)/2 = \operatorname{Aerf}\left(\kappa/\sqrt{2},r/\sqrt{2}\right)$$

This combination also has simple derivatives.

$$\partial_x \operatorname{Aerf}(x,y) = -\frac{2}{\sqrt{\pi}}e^{-\left(x^2+y^2\right)}\sinh(2xy)$$
$$\partial_y \operatorname{Aerf}(x,y) = \frac{2}{\sqrt{\pi}}e^{-\left(x^2+y^2\right)}\cosh(2xy)$$

The last step for imaginary k is to replace spherical Bessel functions of imaginary arguments, resulting in an even power of i in all terms, eliminating imaginary values.

$$\begin{aligned} j_\ell(iz) &= \sqrt{\frac{\pi}{2z}} i^\ell I_{\ell+1/2}(z) \\ \eta_\ell(iz) &= \sqrt{\frac{\pi}{2z}} i^{\ell+1} \left(I_{\ell+1/2}(z) + (-1)^\ell \frac{2}{\pi} K_{\ell+1/2}(z) \right) \end{aligned}$$

Finally, the resulting analytic integrals can be combined with the matrix elements of $E/(E-T)$ to give $\langle \vec{r} \,| \frac{E}{E-QT} | n\,\ell\,m \rangle$ for edge states, enabling simple generation of edge state matrix elements of V.

B.5 E/(E-T) Matrix Elements

The matrix elements $\left\langle n_a \ell_a m_a \left| \frac{1}{E-T} \right| n_b \ell_b m_b \right\rangle$ can be computed analytically. First, the free Green's function can be written either in Cartesian form or decomposed across angular momentum states. It will be convenient to use the Cartesian form for matrix elements of the free Green's function. This equivalence is valid for both real and imaginary k.

$$\frac{E}{E-T} = k^2 G_0 = -k^2 \frac{\cos k\,|\mathbf{r}-\mathbf{r}'|}{4\pi\,|\mathbf{r}-\mathbf{r}'|} = k^3 \sum_{\ell m} \left\{ \begin{array}{ll} j_\ell(kr)\,\eta_\ell(kr') & r<r' \\ \eta_\ell(kr)\,j_\ell(kr') & r>r' \end{array} \right\} Y_{\ell m}(\Omega)\, Y^*_{lm}(\Omega) \tag{B.5.1}$$

The phase shift requirement is satisfied with a homogeneous term scaled by $\cot\delta_\ell$ to produce the right long range linear combination of $j_\ell(kr)$ and $\eta_\ell(kr)$. For bound states $cot\delta_\ell = i$, yielding a cancelation of imaginary parts and a an exponentially decaying wave function. The product of two copies of $j_\ell(kr)$ is real for imaginary k as is $kcot\delta_\ell$. See Eq.(B.5.5) below.

$$G_{hom} = -k\cot\delta_\ell \sum_{\ell m} j(kr)\, j(kr')\, Y_{\ell m}(\Omega)\, Y^*_{lm}(\Omega) \tag{B.5.2}$$

Some expansions and integrals necessary for computation of the matrix elements are summarized here. The harmonic oscillator basis, with nodal quantum number n=1,2,... is

$$H_{n\ell}(r) = \sqrt{\frac{2\Gamma(n)}{\Gamma(n+\ell+1/2)}} e^{-r^2/2} r^\ell L^{\ell+1/2}_{n-1}\left(r^2\right) \tag{B.5.3}$$

$$L^{\ell+1/2}_{n-1}(r) = \sum_{i=0}^{n-1} \left(\begin{array}{c} n+\ell-1/2 \\ n-i-1 \end{array} \right) \frac{(-1)^i}{i!} r^i \tag{B.5.4}$$

This tells us how complex arguments affect j_ℓ.

$$j_n(iz) = \sqrt{\frac{\pi}{2z}} i^{-1/2} J_{n+1/2}(iz) = \sqrt{\frac{\pi}{2z}} i^n I_{n+1/2}(z) \tag{B.5.5}$$

Important integrals generated by Mathematica follow.

$$\int_0^\infty dr\; e^{-r^2/2} r^{\ell+2i+2} j_\ell(kr) = 2^{i-\frac{1}{2}} k^\ell \sqrt{\pi} \frac{\Gamma\left(i+\ell+\frac{3}{2}\right)}{\Gamma\left(\ell+\frac{3}{2}\right)}\, {}_1F_1\left(i+\ell+\frac{3}{2}, \ell+\frac{3}{2}, -\frac{k^2}{2}\right) \tag{B.5.6}$$

$$\int_0^\infty d\rho\; e^{-\rho^2/2} \cos\left(k\sqrt{2}\rho\right) \rho^{2j+1} = 2^j j!\; {}_1F_1\left(j+1,\; 1/2,\; -k^2\right) \tag{B.5.7}$$

For the following one expands the Laguerre polynomial in H_{N0} and sums the resulting terms.

$$\int_0^\infty dR\; R^2\; H_{N0}(R) = (-1)^{N-1} 2\sqrt{\Gamma(N+1/2)/\Gamma(N)} \tag{B.5.8}$$

The free Green's function contribution is computed first and the homogeneous part is done separately.

$$\left\langle n_a \ell_a m_a \left| \frac{E}{E-T} \right| n_b \ell_b m_b \right\rangle_{free} = -k^2 \delta_{\ell_a \ell_b} \delta_{m_a, m_b} \int dr\; r^2 H_{n_a \ell_a}(r) \int dr'\; r'^2 \frac{\cos k\,|\mathbf{r}-\mathbf{r}'|}{4\pi\,|\mathbf{r}-\mathbf{r}'|} H_{n_b \ell_b}(r') \tag{B.5.9}$$

Brody-Moshinsky brackets [30] can be used to to perform a coordinate transform on the input and output harmonic oscillator states from independent oscillator coordinates to relative and center of mass oscillator coordinates. An analytic expression suitable for implementation on a computer was provided by Davies and Krieger [54] and can be found in Appendix A.7.

For the coordinate transform the key notion is that the operator $E/(E-T)$ is a scalar, so the ket and conjugated bra state must couple to an $\ell = 0$, $m = 0$ state which is then coupled via the Brody-Moshinksy brackets to the relative and center of mass harmonic oscillator states. Because the result is not dependent on orientation, the magnetic quantum numbers can be set to 0, $m_a = m_b = 0$. Given that $\ell_a = \ell_b$ following equations will use ℓ for the common value.

$$\langle \ell, 0, \ell, 0 |\, 0, 0 \rangle = \frac{(-1)^\ell}{\sqrt{2\ell+1}} \tag{B.5.10}$$

The new coordinates after the transform will be $\boldsymbol{\rho} = (\mathbf{r}-\mathbf{r}')/\sqrt{2}$ and $\mathbf{R} = (\mathbf{r}+\mathbf{r}')/\sqrt{2}$ with Jacobian 1. In making the transformation the sum is over the compatible nodal numbers for the center of mass and relative oscillators. The energy constraint $N+n = n_a+n_b+\ell$ gives the range of the sum over n and determines N from n. The 4π is absorbed into the constant $\ell = 0$ spherical harmonics that are immediately integrated away, leaving only radial coordinates.

$$\begin{aligned}\left\langle n_a \ell_a m_a \left| \frac{E}{E-T} \right| n_b \ell_b m_b \right\rangle_{free} &= -\delta_{\ell_a \ell_b} \delta_{m_a, m_b} k^2 \frac{(-1)^\ell}{\sqrt{2\ell+1}} \\ &\sum_{n=1}^{n_a+n_b+\ell-1} \langle n0N0 : 0 \mid n_a \ell n_b \ell : 0 \rangle \int\int d\rho dR\; \rho^2 R^2 \frac{\cos k\sqrt{2}\rho}{\sqrt{2}\rho} H_{N0}(R) H_{n0}(\rho)\end{aligned} \tag{B.5.11}$$

The resulting integrals over ρ and R are now separable. The key integral can be had by expanding the Laguerre polynomial in the harmonic oscillator basis function and summing over the terms in the polynomial. The final integral in this expansion is Eq.(B.5.7).

$$\int d\rho\ \rho^2 \frac{\cos k\sqrt{2}\rho}{\rho} H_{n0}(\rho) = \sqrt{\frac{\Gamma(n)}{\Gamma\left(n+\frac{1}{2}\right)}} \sum_{j=0}^{n-1} \begin{pmatrix} n-\frac{1}{2} \\ n-j-1 \end{pmatrix} \frac{(-1)^j}{j!} \int_0^\infty d\rho e^{-\frac{\rho^2}{2}} \cos\left(k\sqrt{2}\rho\right) \rho^{2j+1} \tag{B.5.12}$$

The integral over R is Eq.(B.5.8). Combining all pieces results in:

$$\begin{aligned} \left\langle n_a \ell_a m_a \left| \frac{E}{E-T} \right| n_b \ell_b m_b \right\rangle_{free} &= \delta_{\ell_a \ell_b} \delta_{m_a, m_b} \frac{(-1)^\ell 2k^2}{\sqrt{2\ell+1}} \\ \sum_{n=1}^{\ell+n_a+n_b-1} &\left[\sqrt{\frac{\Gamma(N+1/2)\Gamma(n)}{\Gamma(N)\Gamma(n+1/2)}} \langle n0N0 : 0 \mid n_a \ell n_b \ell : 0 \rangle (-1)^N \right. \\ &\left. \sum_{j=0}^{n-1} \begin{pmatrix} n-1/2 \\ n-j-1 \end{pmatrix} (-2)^j\ {}_1F_1\left(j+1,\ 1/2,\ -k^2\right) \right] \end{aligned} \tag{B.5.13}$$

The next part is the homogeneous contribution that is responsible for matching boundary conditions. For scattering states $\cot\delta_\ell$ is real. Bound states result in $\cot\delta_\ell = i$. The negative energy finite volume lattice states which are extrapolated to infinite volume result in a pure imaginary $\cot\delta_\ell$. The following form works uniformly in all three cases.

$$\begin{aligned} \left\langle n_a \ell_a m_a \left| \frac{E}{E-T} \right| n_b \ell_b m_b \right\rangle_{hom} &= -\delta_{\ell_a \ell_b} \delta_{m_a m_b} k^3 \cot\delta_\ell \\ &\times \int_0^\infty dr\ r^2 H_{n_a \ell}(r)\, j_\ell(kr) \int_0^\infty dr'\ r'^2 H_{n_b \ell}(r')\, j_\ell(kr') \end{aligned}$$

There are two identical integrals to compute. The next step is expanding the Laguerre polynomial and summing over the integrals of the terms. The remaining integral in the expansion is Eq.(B.5.6).

$$\int_0^\infty dr\ r^2 H_{n,\ell}(r)\, j_\ell(kr) = \sqrt{\frac{2\Gamma(n)}{\Gamma\left(n+\ell+\frac{1}{2}\right)}} \sum_{i=0}^{n-1} \begin{pmatrix} n+\ell-\frac{1}{2} \\ n-i-1 \end{pmatrix} \frac{(-1)^i}{i!} \int_0^\infty dr\ e^{-\frac{r^2}{2}} r^{\ell+2+2i} j_\ell(kr)$$

Finally, the pieces are substituted.

$$\left\langle n_a \ell_a m_a \left| \frac{E}{E-T} \right| n_b \ell_b m_b \right\rangle_{hom} = -\delta_{\ell_a \ell_b} \delta_{m_a m_b} \pi k^{2\ell+3} \cot \delta_\ell$$
$$\sqrt{\frac{\Gamma(n_a)\,\Gamma(n_b)}{\Gamma(n_a+\ell+1/2)\,\Gamma(n_b+\ell+1/2)}} \left[\frac{1}{\Gamma(\ell+3/2)}\right]^2$$
$$\sum_{i,j=0}^{n_a-1,n_b-1} \frac{(-2)^{i+j}}{i!j!} \Gamma\left(i+\ell+\frac{3}{2}\right) \Gamma\left(j+\ell+\frac{3}{2}\right) \begin{pmatrix} n_a+\ell-1/2 \\ n_a-i-1 \end{pmatrix} \begin{pmatrix} n_b+\ell-1/2 \\ n_b-j-1 \end{pmatrix}$$
$${}_1F_1\left(i+\ell+\frac{3}{2},\ \ell+\frac{3}{2}, -\frac{k^2}{2}\right)\ {}_1F_1\left(j+\ell+\frac{3}{2},\ \ell+\frac{3}{2}, -\frac{k^2}{2}\right) \tag{B.5.14}$$

Summing the free Green's function matrix elements, Eq.(B.5.13), and the homogeneous term, Eq.(B.5.14), matrix elements produces the complete result.

Appendix C

Measuring the Angular Momentum Content of a Free Wave

When a free wave is represented in a form other than a decomposition over spherical harmonics there is often a need to extract the amplitudes of the asymptotic wave functions in the different angular momentum states. Two representations used in this dissertation where this applies are wave function values on a lattice in a periodic box and a decomposition over a harmonic oscillator basis. The measurement should be done outside the radius of a potential, but close enough to the origin to avoid the edge of the box or the truncation of the harmonic oscillator expansion.

The radial wave function is assumed to have the following standard form.

$$u_\ell(r) = A_\ell\, kr\left(\sin\delta_\ell\, \eta_\ell(kr) - \cos\delta_\ell j_\ell(kr)\right)$$

Then

$$u'_\ell(r) = \frac{u(r)}{r} + A_\ell kr \begin{pmatrix} \sin\delta_\ell \left[\frac{\ell}{r}\eta_\ell(kr) - k\eta_{\ell+1}(kr)\right] \\ -\cos\delta_\ell \left[\frac{\ell}{r} j_\ell(kr) - k j_{\ell+1}(kr)\right] \end{pmatrix} \tag{C.0.1}$$

$$u'_\ell(r) = (\ell+1)\frac{u(r)}{r} - A_\ell k^2 r\left[\sin\delta_\ell \eta_{\ell+1}(kr) - \cos\delta_\ell j_{\ell+1}(kr)\right]$$

Terms are isolated using two intermediates X and Y constructed from known values.

$$X_\ell = \frac{1}{kr}u_\ell(r) \qquad = \qquad A_\ell\left(\eta_\ell(kr),\ -j_\ell(kr)\right)\cdot\begin{pmatrix}\sin\delta_\ell\\ \cos\delta_\ell\end{pmatrix}$$

$$Y_\ell = \frac{1}{k^2 r}\left((\ell+1)\frac{u(r)}{r} - u'_\ell(r)\right) = \quad A_\ell\left(\eta_{\ell+1}(kr),\ -j_{\ell+1}(kr)\right)\cdot\begin{pmatrix}\sin\delta_\ell\\ \cos\delta_\ell\end{pmatrix}$$

The result is assembled as a matrix equation.

$$\begin{pmatrix} X_\ell \\ Y_\ell \end{pmatrix} = A_\ell \begin{pmatrix} \eta_\ell(kr) & (-j_\ell(kr)) \\ \eta_{\ell+1}(kr) & (-j_{\ell+1}(kr)) \end{pmatrix} \begin{pmatrix} \sin\delta_\ell \\ \cos\delta_\ell \end{pmatrix}$$

Isolate A_ℓ.

$$Z_\ell = \begin{pmatrix} \eta_\ell(kr) & (-j_\ell(kr)) \\ \eta_{\ell+1}(kr) & (-j_{\ell+1}(kr)) \end{pmatrix}^{-1} \begin{pmatrix} X_\ell \\ Y_\ell \end{pmatrix} = A_\ell \begin{pmatrix} \sin\delta_\ell \\ \cos\delta_\ell \end{pmatrix}$$
$$A_\ell^2 = Z_\ell \cdot Z_\ell$$

The calculation is finished by dividing the HO components of the state by A_ℓ. The low order components are then the overlaps with the P space.

In the two uses cases mentioned at the beginning, the derivative of the radial function is computed by repeating the integration of the wave function against a $Y_{\ell,m}$ at two closely space radii.

Appendix D

FFT Based Matrix Elements of $\left\langle j \left| G_{TQ} V G_{QT} \right| i \right\rangle$ in a Periodic Volume

In Section 9.3 the matrix elements of V_π were reduced to computing a large set of integrals of the form

$$\int_V d\vec{x}\; e^{\pm i\vec{m}\cdot\vec{x}} W(\vec{x})$$

An inexpensive way to compute these integrals is an FFT. Following the convention used in FFTW [47] the backward FFT is defined as:

$$I_{\vec{k}} = \sum_{\vec{j}\in V} W_{\vec{j}} e^{\frac{2\pi i}{n}\vec{k}\cdot\vec{j}}$$

V is the set of integer positions with $0 \le j_i < N$ for each component i. Position N corresponds to wrapping back to position 0 in a periodic volume. Discrete positions are described by an integer vector $\vec{m}, m_i \in \{-N/2+1 \ldots N/2\}$ so that $\vec{x} = (L/N)\,\vec{m}$. Letting $\vec{N} = (N, N, N)$, the position x can be related to the index $\vec{j}$ used in the definition of $I_{\vec{k}}$ as

$$\begin{aligned}
\vec{m} &= \vec{j} - \vec{N}/2 + \vec{1} \\
\vec{x} &= (L/N)\,\vec{m} = (L/N)\,\vec{j} + \vec{L}\,(1/N - 1/2) \\
(L/N)\,\vec{j} &= \vec{x} - \vec{L}\,(1/N - 1/2) \\
\vec{j} &= (N/L)\,\vec{x} - \vec{N}\,(1/N - 1/2) \\
\vec{j} &= (N/L)\,\vec{x} + \vec{N}/2 - \vec{1}
\end{aligned}$$

The definition of $I_{\vec{k}}$ is rewritten in terms of $\vec{m}$ and $\vec{x}$.

$$\begin{aligned}
I_{\vec{k}} &= \sum_{\vec{j}} W_{\vec{j}} e^{\frac{2\pi i}{N}\vec{k}\cdot\vec{j}} = e^{\frac{2\pi i}{N}\vec{k}\cdot\left(\vec{N}/2-\vec{1}\right)} \sum_{\vec{m}} W_{\vec{m}} e^{\frac{2\pi i}{N}\vec{k}\cdot(N/L)\vec{x}} \\
I_{\vec{k}} &= e^{\left(1-\frac{2}{N}\right)\pi i \sum k_i} e^{-\frac{2\pi i}{N}k} \sum_{\vec{m}} W_{\vec{m}} e^{\frac{2\pi i}{L}\vec{k}\cdot\vec{x}}
\end{aligned}$$

The final sum is of course an approximation to an integral.

$$\begin{aligned} I_{\vec{k}} &\approx e^{\left(1-\frac{2}{N}\right)\pi i\sum k_i}\left(\frac{N}{L}\right)^3 \int\limits_V d^3x\; W\left(\vec{x}\right) e^{\frac{2\pi i}{L}\vec{k}\cdot\vec{x}} \\ \int\limits_V d^3x\; W\left(\vec{x}\right) e^{\frac{2\pi i}{L}\vec{k}\cdot\vec{x}} &\approx \qquad\qquad \exp\left(\left(\frac{2}{N}-1\right)\pi i\sum k_i\right)\left(\frac{L}{N}\right)^3 I_k \end{aligned} \tag{D.0.1}$$

Note that frequency $-\vec{k}$ is equivalent to $\vec{N}-\vec{k}$.

Appendix E

Conventions

To spare the reader from guessing about conventions the choices are detailed here.

E.1 External

- The constants $\hbar$, ω (the oscillator frequency), and μ (the oscillator mass) are all set to 1.
- The spherical harmonic oscillator basis nodal quantum number begins with $n = 1$. Many authors, including several referenced here, begin with $n = 0$. For Cartesian harmonic oscillators the nodal index begins with $n = 0$.
- Laguerre Polynomials follow the convention of Abramowitz and Stengun [35], which is also the convention followed in Mathematica.
- Jacobi coordinates are used beginning with the 2 body problem.

$$\vec{\rho} = \frac{1}{\sqrt{2}}(\vec{\rho}_1 - \vec{\rho}_2) \qquad \vec{\rho}_{cm} = \frac{1}{\sqrt{2}}(\vec{\rho}_1 + \vec{\rho}_2) \tag{E.1.1}$$

  Relative and CM two-body coordinates are often done with different scaling, but this treatment is consistent with the more general Jacobi coordinate transformations of simple rotations.
- The notation $\vec{r}$ will be used instead of $\mathbf{r}$ because the author's eyes don't pick out the bolding.
- The reference of choice for manipulation of angular momentum states and matrix elements is Edmonds' "Angular Momentum in Quantum Mechanics" [57]. When formulae are used from this book they will be referenced as Edmonds (7.1.6), where 7.1.6 is the equation number in the book.

E.2 Internal

An attempt has been made to consistently use the same variables and terms with the same meaning. The most commonly used are listed here.

b is used as the length scale for the harmonic oscillator before setting $\hbar = \omega = \mu = 1$.

T is the kinetic energy operator. In dimensionless form $T = -(1/2)\nabla^2$.

P is the projection operator from the full Hilbert space to the included space with $P^2 = P$.

P^- is the projection operator P minus edge states which T couples to Q.

Q is the complementary projection operator to P, $Q = 1 - P$.

$|e\rangle$ is an HO state in P such that $QT|e\rangle \neq 0$, also known as an edge state.

G_0 is shorthand for $1/(k^2 + \nabla^2)$. $G_T = k^2 G_0$.

G_T is shorthand for $E/(E - T)$.

G_{QT} is shorthand for $E/(E - QT)$.

G_{QH} is shorthand for $E/(E - QH)$.

$b_{i,j}$ is the inverse of the matrix elements of G_T, indexed by abstract state indices.

$b^{\ell,m}_{n',n}$ is the inverse of the matrix elements of G_T, indexed by nodal quantum numbers and in the ℓ, m subblock.

k is the wave number. In dimensionless form $k^2 = 2E$.

m is the magnetic quantum number for $Y_{\ell m}$, or momentum index in a periodic box.

n is used for SHO nodal label, or for Cartesian nodal number.

ρ represents the nucleon separation in fm. The use of ρ is minimized.

r is used for the dimensionless separation between nucleons.

V is a potential.

V_{IR} is a simplified potential, correct long range but missing short range detail.

V_π is a one pion exchange potential, or OPEP.